NUCLEAR MAGNETIC RESONANCE STUDIES OF BIOLOGICAL SYSTEMS

Thesis by

William G. Antypas, Jr.

In Partial Fulfillment of the Requirements

for the Degree of Doctor of Philosophy

California Institute of Technology

Pasadena, California

1988

(Submitted October 2, 1987)

Acknowledgements

I would like to express my deepest appreciation for the guidance and support of John H. Richards, my thesis advisor. His academic insight, patience, and advice have been invaluable. He is also responsible for assembling a group that is stimulating in its diversity, reflecting his broad range of interests.

I wish to thank the members of the Richard's group for many conversations, many of which involved science. In particular, I am grateful to Jim Neitzel, Rob Kaiser, and Gloria McFarland for the particular perspective each brought to the scientific pursuit. I would like to thank Sheila Iverson and Tom Chang for the many hours that we spent discussing their projects, allowing me to broaden my horizons just a little.

I would also like to thank Carmen Visser and Ann Baker for making sure I had something else to do when I wasn't at the bench.

The NIH through Training Grant GM07616 and Research Grant HL15162 provided financial support.

Abstract

Chapter 1: pH Homeostasis in Human Red Blood Cells

The intracellular pH of normal and homozygous sickle cell red blood cells was measured in cell suspensions in plasma by NMR. Freshly drawn, metabolically active red cells maintain a transmembrane pH gradient that differs significantly from the expected Donnan equilibrium proton distribution. In the physiologically important extracellular pH range of 7.12 to 7.57 the intracellular pH is maintained within the narrow range of 7.20 to 7.37. Outside of this range, the intracellular pH is linearly dependent on the extracellular pH. Thus, red cells maintain an intracellular pH that is closer to 7.3 over the entire extracellular pH range than is expected from the Donnan equilibrium ion distribution. The ligation state of cellular hemoglobin shifted the position of the intra- vs extra-cellular pH relationship, but did not alter the ability of the cells to regulate intracellular pH. Deoxygenation of normal red blood cells resulted in an intracellular pH increase of 0.05 ± 0.02 compared to oxygenated cells over the extracellular pH range 7.00 to 7.80. Metabolically depleted cells are unable to maintain a non-Donnan equilibrium proton distribution. The regulation of intracellular pH was regained by restoring cellular ATP

levels. Sickle cell blood demonstrated the same ability to regulate intracellular pH as was observed in normal blood. Deoxygenation of sickle cell blood also resulted in a net increase in intracellular pH. However, gelation of the sample prevented accurate intracellular pH measurements of completely deoxygenated sickle cell samples.

Chapter 2: Measurements of Cell Volume by Nuclear Magnetic Resonance

The Mean Hemoglobin Concentration (MHC) of red blood cells was measured non-invasively and non-destructively by NMR. The difference between intracellular and extracellular proton relaxation rates provides the basis for the determination of the MHC in red blood cells. T_1 relaxation times were measured at a proton frequency of 200 MHz. The T_1 relaxation time for water protons in serum is 2.20 $\pm$ 0.20 seconds. The T_1 relaxation time of water protons in red blood cell pellets is 0.64 $\pm$ 0.15 seconds. In red blood cell lysate, the T_1 relaxation time is 0.77 $\pm$ 0.11 seconds. The observed water T_1 relaxation data from red blood cell samples under various conditions were fit to the complete equation for the time-dependent decay of magnetization for a two-compartment system including

chemical exchange. The MHC for each sample was calculated from the hematocrit and the intracellular water fraction as determined by NMR. MHC values obtained in this manner ranged from 25% to 29% by volume for normal red blood cells in serum, in agreement with published values. The use of proton NMR to determine MHC values directly and non-destructively provides a method to evaluate the effect of various agents on the MHC in viable cells and has wide applicability to the study of antisickling agents in intact cells. The ability to monitor cell volume and to follow the effect of agents known to affect ion transport (valinomycin, nystatin, amiloride, etc.) on cell volume has enormous experimental potential.

Chapter 3: ^{31}P NMR Studies of the Binding Site of anti-Phosphorylcholine Antibodies

The binding of the phosphorylcholine (PC) analogue, 2-(trimethylphosphonio)-ethylphosphate (phosphoryl-phosphocholine, PPC) to the PC binding myeloma proteins TEPC-15, McPC 603, and MOPC 167 was studied by ^{31}P NMR. Binding of PPC to each of the proteins results in an observed phosphate chemical shift that is identical to the shift observed when PC is bound. Thus, the specific binding interactions of the phosphate subsite of the proteins with

PC are maintained when PPC is bound. The chemical shift and titration behavior of the phosphonium resonance of PPC was studied as a probe of the choline subsite of these proteins. PPC bound to TEPC-15 or MOPC 167 exhibits a +0.1 ppm upfield shift from the free hapten. In contrast, PPC binding to McPC 603 results in a +2.7 ppm upfield shift that titrates with a pK_a of 3.6. The shape of the titration curve indicates that the ionizations of 2 protons of equal pK_a are responsible for the observed titration. Three acidic residues provide the major contribution to the choline subsite in both TEPC-15 and MOPC 167. The amino acid substitution Asp_{99H}--> Asn in the third hypervariable region of McPC 603 destroys the spatial symmetry of the choline subsite in McPC 603. The symmetry of the charge distribution of the choline subsite that is lost by this substitution is restored at low pH by titrating the negative charges of Glu_{35H} and Glu_{59H}.

Table of Contents

Chapter 3:

List of Figures

Chapter 1

Chapter 2

Chapter 3

Table Title **Page**

List of Abreviations

Abreviation	Name
AA	Cells homozygous for hemoglobin A
A_{760}	Absorbance measured at 760 nanometers
CC	Cells homozygous for hemoglobin C
DMMP	dimethyl-methylphosphonate
DMO	5,5 dimethyl-2,4 oxazolidenedione
DNP	Dinitrophenyl
$F_{ab'}$	Single binding domain of an antibody
FID	Free induction decay
BBS	Borate buffered saline
HBS	HEPES buffered saline
L_2H_2	Basic antibody unit composed of 2 light chains and 2 heavy chains
LLC-PK_1	Renal epithelial cell line
k_i	Rate constant for i --> j
MEP	Methyl phosphonate
MHC	Mean hemoglobin concentration
NMR	Nuclear Magnetic Resonance
p_i	Fractional population of site i
PC	Phosphorylcholine
PPC	Phosphorylphosphocholine
RBC	Red blood cells
SITS	4-acetamido-4'-isothiocyanostilbene-2,2' disulphonic acid
SS	Cells homozygous for hemoglobin S

T_1	Spin-lattice relaxation time
T_2	Spin-spin relaxation time
2,3-DPG	2,3-diphosphoglycerate

Chapter 1

pH Homeostasis in Human Red Blood Cells

INTRODUCTION

Intracellular pH, widely studied in a variety of cell systems (1, 2, 3, 4), regulates, initiates or mediates a wide variety of cellular functions (for a review, see 5). For example, the pH gradient across the inner mitochondrial membrane is a key factor in the phosphorylating activity of mitochondria (6). In fibroblasts (7) and renal epithelial cells (8) growth factors activate a Na^+/H^+ antiporter, resulting in cytoplasmic alkalinization, triggering initiation of S phase in quiescent cells. As a protective mechanism, hepatocytes regulate intracellular pH within a very narrow range against extreme extracellular pH variations (9).

In all mammalian cells, with the possible exception of human erythrocytes, intracellular pH is actively regulated (5). In a wide variety of cells, a membrane-bound Na^+/H^+ antiporter mediates the exchange of internal protons for external Na^+. Kinetic evidence suggests that a second cytoplasmic H^+ binding site acts as an effector site, altering the affinity of the cation transport site towards different monovalent cations, thus providing a possible mechanism of intracellular pH control (10). Chaillet et al. (11) demonstrated that LLC-PK_1 (renal epithelial) cells possess a Na^+ independent Cl^-/HCO_3^- exchanger and that anion exchange plays a significant role in intracellular pH regulation. They further demonstrated Na^+/H^+ exchange in

the same cells and postulated that both transporters play important roles in intracellular pH regulation. Thus, both regulated cation and anion exchange play central roles in the regulation of intracellular pH, control of cellular volume, and initiation of cell growth and proliferation.

In erythrocytes, intracellular pH has been studied extensively. Maintenance of intracellular pH plays a crucial role in many of the biological processes of red blood cells (12). These include the oxygen affinity of hemoglobin, the efficiency of glycolysis, the rate of 2,3-diphosphoglycerate (2,3-DPG) synthesis, and the regulation of cell volume (and, hence, hemoglobin concentration). Canine red blood cells, the only mammalian cells that do not show Na^+/K^+ ATPase activity, are able to regulate cell volume in response to changes in extracellular pH by a Na^+/H^+ transporter (13). Since these cells lack a Na^+/K^+ ATPase, any transport of Na^+ causes a change in ion concentration and hence in osmolarity of the red blood cell (RBC) resulting in changes in cell volume in response to changes in pH (14).

It has long been supposed that the H^+ gradient across the red cell membrane was solely determined by the transmembrane ion gradient generated as a result of the Donnan equilibrium ion distribution. Van Slyke and McLean (15) were the first to apply the Gibbs-Donnan formalism to red cell electrolyte distribution and showed

that the proton gradient across the cell membrane closely followed the ion gradient predicted by the Donnan equilibrium condition. Following their pioneering work, much study has focused on the applicability of the Donnan equilibrium condition with respect to the transmembrane proton ratio in erythrocytes.

The formation of tactoid rods is the primary molecular event in the vaso-occlusive pathology of sickle cell anemia. The rate of polymerization of deoxyhemoglobin S is dependent on hemoglobin concentration (16), pH (17), ionic strength (18), extent of ligation (19), and concentration of 2,3-DPG (18). In the cellular environment, changes in any one of these factors often lead to detrimental, cascading effects on other conditions. For example, decreasing plasma pH directly promotes sickling through the concomitant decrease in intracellular pH (17), in addition to indirectly promoting tactoid rod formation by decreasing the oxygen saturation at a given pO_2 (the Bohr effect) (18). Consequently, changes in cell volume and/or pH have a profound influence on the pathology of sickle cell disease. Recently, Brugnara et al. (20) demonstrated a K^+/H^+ exchange mechanism in SS red blood cells that results in pH-dependent volume changes similar to those seen in canine red blood cells. In response to decreased extracellular pH, SS red blood cells import protons in exchange for potassium, resulting in a decrease in cell volume (hence an

increase in cellular hemoglobin concentration (MHC)). This change in volume in response to a change in extracellular pH is independent of the oxygenation state of cellular hemoglobin and occurs readily in both oxygenated and deoxygenated cells. As a result, a decrease in extracellular pH results in a higher MHC, in addition to a lower intracellular pH. These conditions promote tactoid rod formation and thereby further exacerbate the increase in the rate of formation of tactoid rods caused by the primary effect of pH.

The recent demonstration of H^+/K^+ or H^+/Na^+ exchange in CC and SS red blood cells (20, 21), and the observation that canine red blood cells maintain osmotic equilibrium in the absence of Na^+/K^+ ATPase by a Na^+/H^+ transporter, coupled with observations that 4-acetamido-4′-isothiocyanostilbene-2,2′ disulphonic acid (SITS) is able to inhibit proton equilibration in normal red blood cells (22), provide indirect evidence that proton gradients in red blood cells are affected by conditions other than just the intracellular concentration of non-diffusible anions. Since the rate of formation of tactoid rods of SS hemoglobin during gelation and the resulting sickling of red blood cells is intimately dependent on pH, the ability of SS red blood cells to regulate intracellular pH is important in the development of possible treatments for this disease.

There are three techniques commonly used to measure intracellular pH in erythrocytes. The first method measures intracellular pH by direct immersion of a combination pH electrode in the lysate resulting from repeated freeze-thaw cycles of pelleted cells. This method is subject to artifacts resulting from the lysis procedure (23), and depends upon the accuracy of the response of a glass electrode in a concentrated protein solution, as well as an indeterminate liquid-junction potential (4). The second technique utilizes the pH dependence of the distribution of weak organic acids across the cell membrane (24). The permeability of the membrane, compartmentalization within the cell, or interaction of the weak acid with cellular components can affect the pH as measured by this technique (25). The third method utilizes the pH dependence of the NMR chemical shift of certain cellular constituents. The utility of this method was demonstrated for measurement of intracellular pH in carbon monoxygenated rabbit red blood cells by observing the ^{31}P signals of 2,3-DPG (26). Because 2,3-DPG binds preferentially to deoxyhemoglobin, the ^{31}P NMR signals of 2,3-DPG are sensitive to the ligation state of hemoglobin (27), such that under conditions of incomplete ligation of hemoglobin, they are less reliable indicators of intracellular pH.

This shortcoming of physiologically occurring compounds may be overcome by employing modified amino acids

such as difluro-methylalanine (28) or non-physiologic phosphate esters such as methyl phosphonate (MEP) (29) as markers of intracellular pH. Improved sensitivity, decreased effects from exogenous compounds, and the inherent resolution of NMR techniques make it possible to reexamine the role of extracellular pH. The recent use of MEP (29, 30) as a non-perturbing probe of intracellular pH allows a further, more accurate determination of intracellular pH regulation in red blood cells. The work reported in this chapter suggests that the red blood cell membrane maintains a pH differential that is significantly different from that expected only from the Donnan equilibrium; in general, these non-Donnan effects act to maintain a more constant intracellular pH. But when the extracellular pH falls below about pH 7.1, the Donnan equilibrium dominates, resulting in a steep decrease in intracellular pH that can greatly exacerbate the formation of tactoid rods within SS erythrocytes even at pO_2 values such that 50-60% of the hemoglobin is present as oxyhemoglobin.

MATERIALS and METHODS

Chemicals and Buffers

Methyl phosphonic acid (MEP), purchased from Alfa Products (Davenport, MA), was used without further purification. All other chemicals were obtained from standard sources. Citrate, bicarbonate and HEPES buffer solutions were prepared by adding the appropriate buffering compound to a final concentration of 50 mM in a physiologic saline solution (total osmolarity 300 mOsm, 110 mM NaCl, 0.15 mM KCl) and adjusting the pH to 7.40. Blood plasma was isolated from whole blood provided by the Red Cross Blood Bank. Erythrocytes and white blood cells were removed by centrifugation, the pH adjusted to 7.40 by slow addition of concentrated NaOH, and the plasma stored at 4°C until just prior to use. A stock solution of 100 mM MEP, pH 7.40 in physiologic bicarbonate (0.004 M $NaHCO_3$, 0.14 M NaCl) buffer was prepared and used in all experiments.

Red Blood Samples

Normal whole blood (10 - 15 ml) was obtained from adult volunteers by venous puncture into vacutainers containing either heparin, citrate, or EDTA as anticoagulant. SS Blood collected at the USC Sickle Cell Center was drawn from patients not in crisis and not currently receiving drug treatment. The SS samples (15 - 20 ml) were obtained by venous puncture into

vacutainers containing either heparin or citrate. All samples were stored on ice at 4°C and used as soon as possible.

Preparation of Blood Samples for NMR Studies

Blood samples were fully oxygenated by passing a steady stream of humidified gas (95% O_2, 5% CO_2, by volume) at room temperature over the sample with gentle agitation. MEP was added to the whole blood sample to a final concentration of 10 mM, and the sample was either used immediately to measure cellular MEP uptake or incubated at 37°C for 1 hour to allow equilibration of MEP across the cell membrane.

NMR Spectra

^{31}P NMR spectra were recorded on a Varian XL-200 spectrometer operating in the Fourier transform mode at 80.95 MHz, using quadrature detection and broadband gated proton heteronuclear decoupling. A typical NMR experiment consisted of a 5 - 10 minute FID accumulation into 4K data points with a 45 - 90 degree pulse, and a 0.300 second signal acquisition with proton decoupling, followed by a 0.100 to 1.000 second decoupler off delay to allow dissipation of decoupler energy and to minimize cellular damage due to localized temperature increases during decoupling. The decoupler off delay and pulse width were

chosen to allow complete relaxation of the intracellular MEP ^{31}P signal. The FID was zero-filled to 8K data points and weighted with a Gaussian convolution difference function and 10 Hz line broadening to improve signal to noise prior to Fourier transformation. For measurements of pH_i vs degree of hemoglobin ligation, a special NMR tube was constructed by fusing a 10 mm diameter NMR tube to a 20 mm diameter equilibration chamber topped by a 1 mm path length cuvette. Other experiments were conducted in 10 mm diameter NMR tubes (Wilmad). A concentric 2 mm capillary tube containing methylene diphosphonic acid in D_2O provided field frequency lock and chemical shift reference. Samples were capped by a Teflon plug to minimize gas exchange, and to prevent vortexing of the sample. To reduce field inhomogeneity caused by red blood cells in suspension, the sample was spun at 5 to 10 Hz. Spinning the sample also reduced the sedimentation of the red blood cells during FID acquisition. The probe temperature was maintained at $37^{o} \pm 2^{o}C$ whenever the sample was in the instrument.

MEP Uptake by Red Cells

The dependence of the rate of MEP uptake by red blood cells upon the type and concentration of anticoagulant was measured by oxygenating freshly drawn blood and adding MEP to a final concentration of 10 mM to a suspension of cells in plasma. The sample was placed in the NMR tube and spectra

recorded at 30 minute intervals for 12 hours. The integrated intensity of the signals representing internal and external MEP was compared and used to calculate the time course of MEP uptake. Alternatively, after recording the initial spectrum to quantitate the total MEP signal intensity, $MnCl_2$ at a final concentration of 10^{-4} M was added to suppress the extracellular MEP signal. At 30 minute intervals spectra were recorded and the integrated intensity of the observed MEP signal compared with the initial signal intensity to determine the rate of MEP uptake.

Intracellular pH Dependence

Packed red blood cells were washed by centrifugation three times in the appropriate buffer at pH 7.40, followed by continued washes in buffer at the desired extracellular pH of the experiment. Equilibrating washes were continued until the measured pH of the cell suspension did not change during centrifugation of the red cells. After equilibration of the red blood cells at the appropriate extracellular pH, the cells were suspended in plasma (with or without added glucose) to a final hematocrit of 50. The cells were completely oxygenated, the pH of the suspension measured, and NMR spectra recorded. The pH of the cell suspension was measured with a Radiometer GK2322C combination electrode directly in the NMR tube immediately prior to FID accumulation and immediately upon completion of the

acquisition. Samples that deviated by more than 0.05 pH were repeated.

Determination of Hemoglobin Ligation State

The per cent ligation of cellular hemoglobin was determined by measuring the absorbance at 760 nm of the sample. The absorbance was measured as the sample was continuously oxygenated (95% O_2, 5% CO_2 by volume, humidified); when A_{760} reached a minimum, oxygenation was assumed to be complete. A_{760} was recorded as the sample was deoxygenated (95% N_2, 5% CO_2 by volume, humidified); when further deoxygenation produced no change in A_{760}, complete deoxygenation was assumed. The per cent ligation of the intermediate samples was determined by linear extrapolation between the end points.

Dependence of pH_i on Hemoglobin Ligation State

Packed red blood cells (20 ml) were washed three times in plasma at pH 7.40, followed by incubation with 10 mM MEP in plasma (pH 7.40) for 30 minutes. The cells were washed in plasma and then suspended in plasma containing 5 mg/ml glucose at a final hematocrit of 50. The sample was fully oxygenated and placed in the special NMR tube previously described. Oxygenation of the sample was continued while monitoring A_{760} until there was no change in the absorbance. An aliquot was withdrawn from the tube and the suspension pH

measured by glass electrode. The ^{31}P spectrum was recorded and the extracellular pH as determined by the MEP phosphate chemical shift was compared to the pH measured by glass electrode. The sample was partially deoxygenated by injection of 95% N_2, 5% CO_2 by volume (humidified), followed by gentle agitation until equilibrium (as measured by A_{760}) was reached and additional spectra recorded. The extracellular pH of the sample was monitored by observing the MEP signal. If the pH began to change, the sample was replaced and the experiment repeated. Following complete deoxygenation, the sample was completely reoxygenated and the spectra recorded and compared to the initial spectra as a final control.

Measurement of Intracellular pH

Intracellular pH was determined by measuring the ^{31}P chemical shift of MEP (Figure 1). A standard titration curve was constructed by measuring the chemical shift of MEP as a function of pH in a variety of buffer systems and at several MEP concentrations (Figure 2). The chemical shift of MEP is not sensitive to MEP concentration, ionic strength, or protein concentration. MEP does not compete for the DPG effector site and does not affect the dissociation behavior of hemoglobin.

Between pH 6.80 and 7.80 the resulting titration curve was linear and described by:

$$\delta = -0.465(pH) + 18.40.$$

Between pH 6.80 and 7.80, intracellular pH was calculated from the observed chemical shift of intracellular MEP and the above linear relationship. Outside of this range, pH was calculated by extrapolation of this standard titration curve. The accuracy of these pH measurements was limited to the reproducibility of the NMR spectra, which gives $\pm$ 0.02 ppm. This translates to a precision of 0.01 pH unit.

Analysis of Results

Triplicate measurements of pH_i at each pH_e value were recorded for each red blood cell sample. The triplicate data points were averaged, and the resulting mean pH_i values used in further computations. The data from each blood sample were analyzed separately in order to fully differentiate between sample variation and random error. The best fit to the full data set for each sample was obtained by multiple non-linear polynomial least-squares analysis. The best fit was defined as the lowest order polynomial. Significance of each order was established by Chi square analysis. Linear sections of the full curves were identified by stepwise elimination of end points followed by linear least-squares analysis of the remaining data points. Sections of the full curves were considered linear when the correlation coefficient exceeded 0.97.

RESULTS

The effect of the type and concentration of anticoagulant on the rate of uptake of methyl phosphonic acid (MEP) by oxygenated red blood cells in normal whole blood is shown in Figure 3. Cellular uptake of MEP in whole blood that had been treated with citrate as anticoagulant is complete in approximately 90 minutes. The concentration of citrate does not have a significant effect on the rate of MEP uptake over the range of citrate concentrations studied. In contrast, the rate of MEP uptake by red blood cells in whole blood samples treated with heparin as anticoagulant is dependent upon the heparin concentration and is considerably slower than the observed rate of MEP uptake in blood treated with citrate. At high concentrations of heparin (5 mg/ml, 450 iu/ml), the uptake of MEP is completely inhibited during the course of the NMR experiments (12 hrs). Heparin is known to inhibit anion transport by the anion exchanger; this result suggests that MEP is transported by the anion exchanger. Based on these results, citrate or EDTA was used as anticoagulant in all subsequent blood samples for NMR experiments.

Figure 4 shows the relationship between extracellular pH (pH_e) and intracellular pH (pH_i) of fully oxygenated normal red blood cells. The data clearly demonstrate that intracellular pH is a polyphasic function of extracellular pH. Below an extracellular pH of 7.12, the intracellular pH

is a linear function of the extracellular pH, and may be expressed as:

$$pH_i = 0.68(pH_e) + 1.90. \quad (1)$$

At extracellular pH values between 7.12 and 7.50, the intracellular pH is much less sensitive to changes in the extracellular pH. The intracellular pH is maintained between 7.20 and 7.37 in this range of extracellular pH. Linear regression analysis of the pH_i vs pH_e values in this range gives:

$$pH_i = 0.52(pH_e) + 3.40. \quad (2)$$

The reduced value of the slope of Equation (2) (0.52) as compared to the value of the slope of Equation (1) (0.68) is indicative of the reduced sensitivity of intracellular pH to changes in extracellular pH in this physiologically important pH range. Above an extracellular pH of 7.50, the intracellular pH regains its linear dependence upon the extracellular pH; however, pH_i is more sensitive to changes in pH_e in this pH domain than in the domain below pH 7.12. This is demonstrated by the increased value of the slope obtained from linear regression of pH_i vs pH_e values in this range:

$$pH_i = 0.72(pH_e) + 2.01. \quad (3)$$

Changing the buffering agent from bicarbonate to phosphate, citrate or HEPES while maintaining physiological osmolarity and physiological concentrations of Na^+, K^+ and Cl^- produces the same intracellular pH dependence as is observed in

plasma. However, phosphate buffered saline, citrate buffered saline, and HEPES buffered saline all display considerably less buffering power than plasma. Thus, actively metabolizing red cell suspensions in physiologic saline buffers showed considerable pH changes (> 0.1) over the course of the NMR experiments. All subsequent experiments were performed in plasma to minimize extracellular pH changes during NMR data acquisition, and to simulate more realistically in vivo conditions.

Figure 4 also demonstrates the variability of intracellular pH control between different subjects and even between samples drawn from the same subject at different times. In all cases, the shape of the experimental curves is comparable, the major difference being the offset along the abscissa of each curve. Linear regression analysis was performed on the linear regions of each curve. Each linear segment gives the same slope within experimental error, the difference being the y intercept of the curves.

Also shown in Figure 4 is the pH relationship that would be expected if protons were distributed across the red cell membrane according to the chloride ion Donnan equilibrium. The curve was calculated using the known Cl^- distribution as a function of pH (31). This relationship is second order in pH_e and is given by:

$$pH_i = - 0.06(pH_e^2) + 1.77(pH_e) - 2.06. \quad (4)$$

If the second-order term is neglected, regression analysis yields a linear function with a correlation coefficient of 0.997:

$$pH_i = 0.76(pH_e) + 1.66. \quad (5)$$

The slope and intercept of the pH curve generated using the Donnan equilibrium relationship are experimentally identical to the observed pH_i dependence for pH_e greater than 7.50. At pH_e values less than 7.50, the experimentally observed intracellular pH shifts significantly towards neutrality compared to the intracellular pH expected from the Donnan equilibrium.

Figure 5 shows the effect of different ligation states and different metabolic states on the ability of normal red blood cells to maintain a non-Donnan equilibrium transmembrane proton distribution. Relative to fully oxygenated red blood cells, fully deoxygenated normal red blood cells exhibit a slight increase in intracellular pH over the entire extracellular pH range. The pH_i vs pH_e curve maintains the same triphasic shape, with the three linear segments of the curve being described by

$$pH_i = 0.64(pH_e) + 2.21 \qquad pH_e < 7.15 \quad (6)$$

$$pH_i = 0.52(pH_e) + 3.56 \qquad 7.22 < pH_e < 7.55 \quad (7)$$

$$pH_i = 0.77(pH_e) + 2.25 \qquad 7.70 < pH_e < 8.45. \quad (8)$$

The slope of each section of the curve corresponds well to the slope of the comparable regions of the curve for fully oxygenated cells, while the intercept of each linear

section has increased. The increase is most noticeable in the pH_e range between 7.70 and 8.45. As was observed in fully oxygenated samples, there is considerable variation between samples; however, all samples exhibited similar triphasic pH_i vs pH_e behavior, the major difference being the offset along the pH_i axis.

In their ability to maintain a transmembrane pH gradient, normal red blood cells with metabolically depleted levels of ATP differ significantly from cells that have normal ATP levels. Oxygenated red blood cells that have depleted levels of ATP do not exhibit the triphasic transmembrane pH gradient, but rather a linear intracellular vs extracellular pH relationship over the entire range between pH 6.8 and 8.1 described by:

$$pH_i = 0.85(pH_e) + 1.70. \qquad (9)$$

This relationship is close to that expected if a Donnan equilibrium were the only contribution to the transmembrane hydrogen ion distribution (compare Equation 9 and Equation 5). The ability of cells to maintain a non-Donnan equilibrium proton distribution may be restored by the addition of glucose to the cell suspension. After normal levels of intracellular ATP are obtained, the triphasic pH_i vs pH_e curve is again observed. This cycle can be repeated as long as the cells maintain their viability. Red blood cells that have been aged at 4^oC for 30 days (ATP depleted as a result of storage) exhibit a Donnan

equilibrium proton distribution. Active regulation of the intracellular pH is restored in aged blood by addition of glucose to the cell suspension. Active pH_i regulation is concomitant with return of normal ATP levels in the cells and is not substantially reduced or impaired in aged red blood cells. The addition of fluoride, which completely inhibits glycolysis, along with the addition of glucose to ATP depleted cells results in no increase in the cellular ATP level and no recovery of the ability to actively regulate the transmembrane proton gradient by the cells is observed.

The pH profile of sickle cell blood samples is shown in Figure 6. The cells exhibit the same ability to regulate intracellular pH as is seen in normal red blood cells. The range of sample variability, as determined by the standard deviation, is larger for sickle cell samples. The average of all samples exhibits an intracellular pH shift of 0.07 towards alkalinity over the entire extracellular pH range studied. Carbon monoxygenation of sickle cell samples results in no experimentally observable deviation from the behavior seen in oxygenated blood. Deoxygenation of sickle cell suspensions results in an alkaline pH shift in the observed intracellular pH, but does not interfere with the active regulation of intracellular pH.

Figure 7 shows the effect of the extent of hemoglobin ligation on intracellular pH in both normal red blood cells

and sickle cell cells. At an extracellular pH of 7.36, fully oxygenated red blood cells maintain an intracellular pH of 7.22. Upon deoxygenation, the intracellular pH increases monotonically to a final pH of 7.28 at complete deoxygenation. The intracellular pH increase is completely reversible; reoxygenation of the sample restores the initial intracellular pH of 7.22.

At an extracellular pH of 7.04, the intracellular pH of fully oxygenated red blood cells is 7.06. Deoxygenation of the sample produces an intracellular pH of 7.13, resulting in an alkaline shift of 0.07. This is within experimental error of the alkaline shift of 0.06 seen at pH_e of 7.36. Reoxygenation of the sample restores the intracellular pH to 7.06. Furthermore, the intracellular pH changes caused by deoxygenation at pH_e 7.04 parallel the changes seen at pH_e 7.36. Thus, the intracellular pH changes caused by deoxygenation are the same whether extracellular pH is 7.04 or 7.36.

At an extracellular pH of 7.36, the intracellular pH of fully oxygenated SS blood is 7.28. This intracellular pH increase of 0.06 compared to the normal red blood cell sample is consistent with the average difference between AA and SS blood shown earlier. As the SS blood sample is deoxygenated, the intracellular pH increases to 7.31 at 18% O_2 saturation. This compares to an intracellular pH of 7.25 at 18% saturation in the normal red blood cell sample.

Extrapolating to complete deoxygenation, the intracellular pH of the SS sample would be 7.33. This is an increase of 0.05 pH, which is within experimental error of the increase of 0.06 pH seen in normal red blood cells.

At an extracellular pH of 7.04, deoxygenation of SS red blood cells results in radically different changes in intracellular pH. Between a hemoglobin ligation of 100% and 65% the intracellular pH increases monotonically as the sample is deoxygenated. However, below a saturation of 65%, intracellular pH decreases to 7.00 at complete deoxygenation. Microscopic examination of the completely deoxygenated sample shows a significant number of sickled cells, while measured hematocrit decreases, indicating approximately 30% cell lysis. Significant broadening of the ^{31}P MEP resonance (in excess of that seen in deoxygenated AA blood) is also observed.

DISCUSSION

Active Maintenance of pH Gradient

The results demonstrate that normal red blood cells actively maintain a transmembrane pH gradient that differs significantly from the gradient predicted from the Donnan equilibrium chloride ion distribution. While the intracellular proton concentration predicted from the Cl^- ion distribution between pH 6.8 and pH 8.0 is a linear function of extracellular pH (33), the actual observed intracellular pH is a triphasic function of the extracellular pH. The net effect of the non-Donnan proton distribution is to maintain an intracellular pH that is "buffered" in the physiologically important range 7.20 to 7.45.

The triphasic relationship between extracellular pH and intracellular pH indicates the complex interaction of several distinct proton translocation mechanisms. Above an extracellular pH of 7.50, the Donnan equilibrium and cellular regulation of intracellular pH work in concert to minimize intracellular pH increases in response to extracellular pH increases. Below pH_e 7.20, active pH regulation mitigates against the decrease in intracellular pH (resulting from the Donnan equilibrium) expected from a decrease in extracellular pH. In both of these pH_e ranges, the mechanism that regulates intracellular pH is not able to completely nullify the change in pH_i predicted from the

Cl^- ion Donnan equilibrium distribution; however, regulation of pH_i does reduce the effect of pH_e changes on pH_i.

In the physiologically important pH range 7.20 to 7.45, the cell is able to ameliorate the effect of extracellular pH changes. While extracellular pH changes by 0.25, intracellular pH changes by only 0.13. In the same pH_e range, the Donnan equilibrium pH_i changes by 0.19. Thus, regulation of pH_i minimizes the effect of the Donnan equilibrium on intracellular pH and hence on many cellular functions that depend directly or indirectly on pH.

In addition to the NMR study of intracellular pH in erythrocytes presented here, the intracellular pH of red blood cells has been studied extensively by freeze-thaw lysis (33, 34) and equilibrium distribution of 5,5 dimethyl-2,4 oxazolidinedione (DMO) (34, 35). The proton gradient reported in these earlier studies was also not equivalent to the Cl^- ion gradient. However, the discrepancy was attributed to differences between Cl^- ion activity in the cytosol and plasma, or to experimental error, and mechanisms other than passive distribution of protons according to the Donnan equilibrium were not considered necessary.

If the observed discrepancy between the Cl^- ratio and the proton ratio were to be caused by differences in activity coefficients, a 33% difference in Cl^- ion activity between cytosol and plasma would be necessary (37). However,

since hemoglobin provides the major charged, titratable, impermeable species (36), one would expect the pH dependence of all passively distributed ions to follow linearly the titration curve of hemoglobin, regardless of differences in activity coefficients. A difference in activity coefficients would explain a consistent difference between Cl^- and H^+ ratios, but is insufficient to explain the difference in the shape of the two curves.

Role of Metabolic Activity

In metabolically active cells impermeable phosphate esters, such as 2,3-DPG, fructose 1,6 phosphate, and ATP will contribute to the Donnan equilibrium and the resulting diffusible ion gradients. Since phosphate esters generally have pK_a values less than 4.0, at physiologic pH these esters are negatively charged, enhancing the Donnan effect of hemoglobin. Furthermore, they will not titrate in the pH range studied here; thus, their contribution to the Donnan equilibrium will remain essentially constant within this important pH range. Measurements of the proton ratio as a function of phosphate ester concentration (38) gives $pH_i=pH_e$ at 6.4 when extrapolated to 0 concentration of any phosphate esters. If the Donnan equilibrium were the only contributor to intracellular pH regulation, one would expect $pH_i=pH_e$ at the pI of hemoglobin, 6.85. These observations provide

corroborating evidence for active pH regulation by red blood cells.

The depletion of ATP results in the collapse of the proton gradient, further demonstrating that pH homeostasis by red blood cells is an active function. The subsequent restoration of the gradient upon addition of glucose to the cells is an additional argument for an active mechanism of proton translocation in red blood cells. At an extracellular pH of 7.45, the oxygenated red blood cell intracellular pH is 7.37. From the Donnan equilibrium Cl^- ion distribution at the same extracellular pH, the predicted intracellular pH is approximately 7.37, and thus no energy is required to maintain this difference. As the extracellular pH is lowered to 7.20, the observed intracellular pH is 7.25. The expected Donnan equilibrium intracellular pH is calculated from the Cl^- ratio to be 7.12, resulting in a concentration gradient of $10^{-0.13}$. This gradient requires 0.2 kcal/mol to maintain.

Possible Mechanism of Proton Translocation

Intracellular pH regulation is known to result from the regulation of a Na^+/H^+ antiporter in many cell types (39). Proton translocation also occurs as a by-product of divalent anion transport in red blood cells (22). Regulation of intracellular pH might be a by-product of regulation of the anion affinity of the Cl^-/HCO_3^- anion exchanger by cytoplasmic factors such as hemoglobin (40) or other pH

sensitive components. Both of these mechanisms have been implicated in intracellular pH homeostasis in mammalian cells (5). In fibroblasts the Na^+/H^+ antiporter is the primary agent in pH regulation (7), while in LLC PK_1 cells, the anion exchanger provides the mechanism for intracellular pH regulation (11).

In red blood cells, our data strongly suggest that intracellular homeostasis is a result of active transport of protons driven by the Na^+ gradient. The relatively narrow range where proton pumping is effective in reducing the effect of extracellular pH changes is indicative of a mechanism that is easily saturated. The estimate of 200,000 to 300,000 copies of an antiporter is consistent with this assumption. Additionally, the observed energy requirement for pH homeostasis is met by the proton antiporter's requirement of a Na^+ gradient for proton translocation. Finally, kinetic evidence from antiporters in renal epithelial cells (8) has demonstrated a cytoplasmic proton effector site that alters the affinity of the proton transport site and thus provides a direct method of pH regulation.

These arguments do not rule out a role in proton translocation for the anion transporter. However, the regulation of intracellular pH would require that the affinity towards phosphate on the cytoplasmic side of the membrane be regulated by a pH sensitive mechanism. The

specific binding of hemoglobin to the cytoplasmic domain of the anion exchanger could provide such a regulatory mechanism, since hemoglobin is sensitive to pH changes. Since net proton movement as a result of monohydrogen phosphate translocation by the anion exchanger does not require metabolic energy, the observed dependence of the pH regulation on metabolic energy suggests that the primary mediator in pH regulation is more likely to be a Na^+/H^+ antiporter than the anion exchanger.

Effect of Deoxygenation

Deoxygenation of red blood cells produces an alkaline shift in the intracellular pH. The shift is sample dependent and the magnitude of the shift varies over the pH range 6.80 to 8.50. The alkaline shift is the end result of several competing cellular events. Central to these events is the acid/base behavior of hemoglobin upon deoxygenation. Primarily, as hemoglobin releases O_2, protons are added to the hemoglobin molecule (the Bohr effect), decreasing the negative charge at a given pH. The absorption of CO_2 results in an increase in bicarbonate concentration, which promotes carbamylation and a net increase in negative charge. The net effect of these changes is an increase in the pI of hemoglobin from 6.85 to 7.10. Such a change in pI affects the Donnan equilibrium and causes a translation of the pH_i vs. pH_e curve along that curve by an amount equal to the

difference in pI. In the pH range that is physiologically significant, the pH dependence of the Donnan equilibrium is linear with a slope of 0.67, thus the change in pI of 0.25 should result in a constant vertical offset of 0.16 pH units.

The actual alkaline shift caused by deoxygenation is not constant over the pH range 6.5 to 8.5. Below pH_e 7.20, the alkaline shift is 0.20 and at pH_e above 7.55 the observed shift is 0.30. Most significantly, between pH_e 7.20 and 7.55, the observed shift is 0.06. These shifts indicate that the cell is able to mitigate the intracellular pH change caused by the change in pI of hemoglobin upon deoxygenation. If the change in intracellular pH reflected a constant difference over the entire extracellular pH range, the change in Donnan ratio would be a sufficient explanation. However, the alkalinization is not constant and indeed is greatly depressed within the pH region where active buffering has been demonstrated. Furthermore, the slopes at the extracellular pH extremes of the curves are nearly equal (within experimental error) in both oxy- and deoxygenated cells. This similarity is expected if the alkaline shift of deoxygenated red blood cells (at the pH extremes) is a result of a shift in Donnan ratio caused by an increase in pI of hemoglobin.

The small alkaline shift that is observed in the physiologically significant pH range 7.20 to 7.55, compared with the larger shift that is observed outside this range, demonstrates that active proton fluxes are sufficient to lessen the effect of the decreased Donnan ratio within the physiologically important pH range. The observed alkaline shift in intracellular pH as a function of extracellular pH in deoxygenated red blood cells is consistent with a shift in Donnan ratio, mitigated in the physiologically important pH range 7.20 to 7.55 by active translocation of protons. That the observed curve and the curve predicted from the Donnan equilibrium have the same slope outside of this range is indicative of saturation of the active proton translocating mechanism.

AA vs. SS Erythrocytes

The results show that oxygenated SS erythrocytes actively regulate intracellular pH with the same effectiveness as AA erythrocytes. The alkaline pH shift of 0.07 observed in SS erythrocytes compared to SS erythrocytes is consistent with the increased pI of SS hemoglobin caused by the substitution Glu $_{-6}$--> Val. The pI of oxygenated SS hemoglobin is similar to the pI of deoxygenated normal hemoglobin, and direct comparison of the pH dependence of intracellular pH in deoxygenated normal red blood cells and oxygenated SS red blood cells confirms the similarity of

their intracellular pH behavior. As previously argued for deoxygenated erythrocytes, the increased pI of SS hemoglobin also results in a lower than expected (0.06) pH_i increase as a direct result of active proton translocation in SS erythrocytes.

Recent studies have implicated a pH sensitive K^+ transport mechanism in CC and SS blood cells in the regulation of cell volume (20, 21). The Na^+/H^+ exchanger is of primary importance in the volume regulation of canine red blood cells (14). These findings suggest that SS erythrocyte cell volume may be decreased following a decrease in intracellular pH even when hemoglobin is fully ligated (20). Thus, the ability of oxygenated SS erythrocytes to regulate intracellular pH within a relatively narrow range is a distinct survival advantage, as the formation of tactoid rods is pH and concentration dependent.

The effects of deoxygenation on intracellular pH regulation in SS erythrocytes are more complicated than those observed in normal red blood cells. At an extracellular pH 7.40, deoxygenation of SS red blood cells gives a monotonic increase in intracellular pH similar to the increase observed in normal AA erythrocytes. However, at an extracellular pH of 7.10, partial deoxygenation initially results in alkalinization of the cytosol. Continued deoxygenation produces a rapid decrease in

intracellular pH. The intracellular pH approaches the extracellular pH and remains constant with further deoxygenation. Additionally, the loss of active pH regulation is not reversible. Reoxygenation does not restore the initial pH gradient, nor is the loss of pH regulation a result of ATP depletion. Normal concentrations of ATP are observed during the entire course of the experiment. Sickling and hemolysis also accompany the irreversible loss of intracellular pH regulation. These results clearly show the profound effect intracellular pH has upon the initiation of tactoid rod formation and show that sickling may occur in cells with significant concentrations of oxyhemoglobin.

Irreversible loss of active pH regulation and the concurrent sickling are catastrophic events. Since increasing pH directly inhibits tactoid rod formation by decreasing the gelation rate and indirectly inhibits it by decreasing MHC (16), the increase in intracellular pH that initially accompanies deoxygenation delays the onset of tactoid rod formation. However, as the concentration of deoxyhemoglobin increases further, the threshold for initiation of tactoid rod formation is reached. The resulting sickling leads to irreversible damage of the cytoskeletal framework and loss of membrane integrity. Until initiation of tactoid rod formation, the cell regulates intracellular pH in a manner that delays the onset of sickling. Once sickling is initiated, intracellular

pH regulation is lost and the rate of tactoid rod formation increases with the now more rapid decrease in intracellular pH. This leads to catastrophic irreversible sickling. Interestingly, active buffering actually minimizes the intracellular pH rise that is expected upon deoxygenation, limiting the effectiveness of alkalinization in reducing the rate of sickling.

Possibilities for Treatment

The observation of pH homeostasis in RBC has interesting applications toward possible in vivo treatments of sickle cell disease. The conditions of low plasma pH, and low oxygen concentration that exist in venous capillaries has been shown to contribute to irreversible sickling (41). Since intracellular pH is actively regulated within the range 7.20 to 7.45, the use of agents that inhibit sickling of solutions of hemoglobin by increasing the pH may not prevent sickling of intracellular hemoglobin when added to plasma (42). Thus, the observation that administration of base to sickle cell patients in crisis has little or no therapeutic value is consistent with the observation of active intracellular pH homeostasis in red blood cells. Since a decrease in intracellular pH is a significant factor in tactoid rod formation, and plasma pH in the capillaries is known to decrease to 7.15 or lower (41), inhibition of the active pH regulation mechanism in

conjunction with administration of base should ameliorate the intracellular pH decrease that accelerates tactoid rod formation. Amiloride is a potent inhibitor of the Na^+/H^+ exchanger (43) and has been used clinically as a potassium sparing diuretic. Administration of amiloride with base might therefore prove effective in lessening the occurrence of irreversible sickling *in vivo*.

REFERENCES

1. Moore, R.D. (1979) **Biochem. Biophys. Res. Comm. 91**, 900-904.
2. Johnson, J.D., Epel, D., Paul, M. (1976) **Nature (London) 262**, 661-664.
3. Satre, M., Martin, J. (1985) **Biochem. Biophys. Res. Comm. 132**, 140-146.
4. Waddell, W.J., Bates, R.G. (1969) **Physiol. Rev. 49**, 285-329.
5. Roos, A., Boron W.F. (1981) **Physiol. Rev. 61**, 297-434.
6. Mitchell, P., Moyle, S. (1969) **Eur. J. Biochem. 7**, 471-484.
7. Pouyssegur, J., Franchi, A., L'Allemain, G. Paris, S. (1985) **FEBS Lett. 190**, 115-119.
8. Kinsella, J., Sacktor, B. (1985) **Proc. Natl. Acad. Sci. USA 82**, 3606-3610.
9. Kashiwagura, T., Deutsch, C.J., Taylor, J. Erecinska, M., Wilson, D.F. (1984) **J. Biol. Chem. 259**, 237-243.
10. Aronson, P.S., Nee, J., Suhm, M.A. (1982) **Nature 299**, 161-163.
11. Chaillet, Richard J., Amsler, K. Boron, W.F. (1986) **Proc. Natl. Acad. Sci. USA 83**, 522-526.
12. Astrup, P., Rorth, M.(eds.), (1971) **Oxygen Affinity of Hemoglobin and Red Cell Acid Base Status.** Academic Press, New York.

13. Parker, J.C., Castronova, V. (1984) **J. Gen. Physiol. 84**, 379-401.

14. Parker, J.C. (1983) **J. Am. Physiol. Soc.** C324-C330.

15. Van Slyke, D.D., Wu, H., McLean, F.C. (1923) **J. Biol. Chem. 56**, 765-849.

16. Hofrichter, J., Ross, P.D., Eaton, W.A. (1974) **Proc. Natl. Acad. Sci. USA 71**, 4864-4868.

17. Bookchin, R.M., Balazs, T., Landau, L.C. (1976) **J. Lab. Clin. Med. 87**, 597-616.

18. Bunn, H.F., Forget, B.G., Raney, H.M., Smith, L.H.(eds.) (1977) **Sickle Cell Anemia and Related Disorders: Hemoglobinopathies, Vol XII**, p 130.

19. Hahn, E.V., Gillespie, E.B. (1927) **Arch. Intern. Med. 39**, 233-254.

20. Brugnara, C., Bunn, H.F., Tosteson, D.C. (1986) **Science 232**, 388-390.

21. Brugnara, CC., Kopin, A., Bunn, H.F.,Tosteson, D.C. (1985) **J. Clin. Invest. 75**, 1608-1617.

22. Manfred, B., Spread, C.Y., Richard,Reithmeier, A. F., Sykes, B. (1985) **J. Biol. Chem. 260**, 11643-11650.

23. Warth, J.A., Desorges, F., Stolberg, S. (1977) **Brit. J. of Haemotology 37**, 373-377.

24. Waddell, W.J., Butler, T.C. (1959) **J. Clin. Invest. 38**, 720.

25. Irvine, R.O.H., Saunders, S.J., Milne, M.D., Crawford, M.A. (1960) **Clin. Sci. 20**, 1.

26. Moon, R.B., Richards, J.H. (1973) **J. Biol. Chem. 248**, 7276-7278.

27. Huestis, W. A., Raftery, M.A. (1972) **Biochem. Biophys. Res. Comm. 49**, 428-433.

28. Deutsch, C., Taylor, J.S., Wilson, D. F. (1982) **Proc. Natl. Acad. Sci. USA 79**, 7944-7948.

29. Labotka, R.J., Kleps, R.A. (1983) **Biochemistry 22**, 6089-6095.

30. Labotka, R.J. (1984) **Biochemistry, 23**, 5549-5555.

31. Harris, E.S., Maizels, M. (1961) **J. Physiol. 118**, 40-53.

32. Fitzsimons, E.J., Sendroy, Jr. J. (1961) **J. Biol. Chem. 236**, 1595-1601.

33. Funder, J., Wieth, J.O. (1966) **Acta. Physiol. Scand. 68**, 234-245.

34. Bramberg, P.A., Theodore, J., Robin E.D., Jensen, W.M. (1965) **J. Lab. Clin. Med. 66**, 464-475.

35. Sanslone, W.R., Muntwyler, E. (1964) **Proc. Soc. Exptl. Biol. Med. 116**, 582-585.

36. Dalmark, M. (1975) **J. Physiol. 250**, 65-84.

37. Salling, N., Siggaard-Andersen, O. (1971) **Scand. J. Clin. Lab. Invest. 28**, 1.

38. Duhm, J. (1971) **Pflugers Arch. 326**, 341-356.

39. Aronsong, P.S. (1985) **Ann. Rev. Physiol. 47**, 545-560.

40. Premachandria, B.R. (1986) **Biochemistry 25**, 3455-3462.

41. Barreras, L., Diggs, L.W. (1964) **Am. J. Med. Sci.** **247**, 710.

42. Kong, H., Ho, P., Alleyne, G.A.O. (1969) **Brit. Med. J.** **3**, 271-273.

43. Mahnensmith, R.L., Aronson, P.S. (1985) **J. Biol. Chem.** **260**, 12586-12592.

FIGURE 1

^{31}P NMR Spectra of MEP in Whole Blood

80.9 MHz proton decoupled ^{31}P NMR spectra of 10 mM MEP in normal whole blood. The sample was drawn by venous puncture and anticoagulated with EDTA. The blood sample was oxygenated and pre-equilibrated with 10 mM MEP for 90 minutes at 37°C prior to NMR signal acquisition. The final hematocrit of the sample was 36. 2400 transients were accumulated with a 45° pulse, an acquisition time of 0.2 seconds and a spectral width of 30 ppm. The FID was transformed, using an exponential broadening of 5 Hz.

A) Spectra recorded at pH_e = 7.36.

B) Spectra of lysed cells from A).

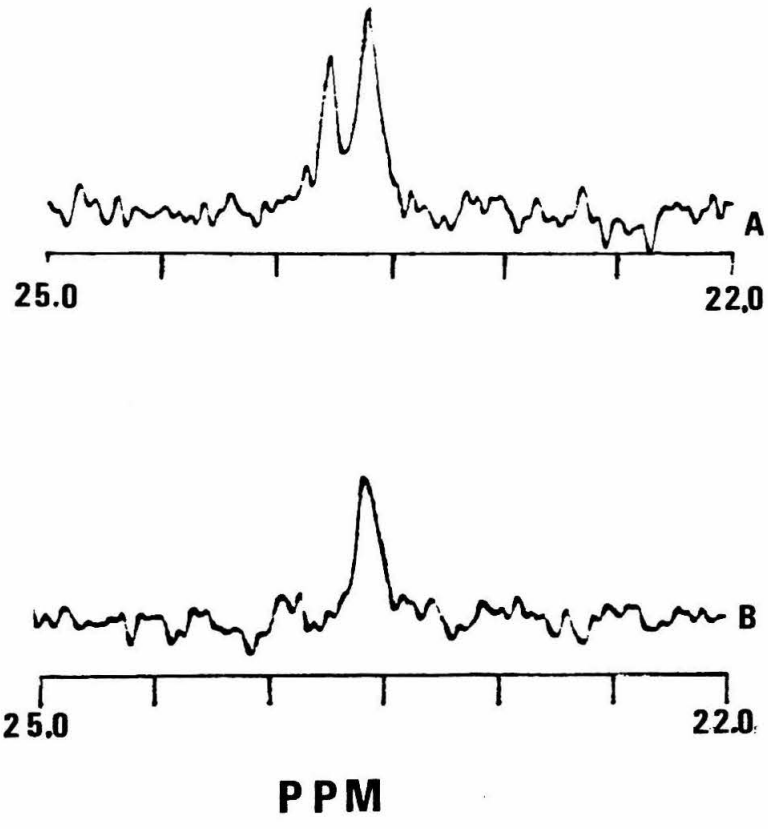
A
25.0
22.0
B
25.0
22.0
PPM

FIGURE 2

^{31}P NMR Titration Curve of MEP

The pH dependence of the ^{31}P chemical shift of MEP was measured by diluting a stock solution (1.0 M) of MEP in the indicated buffer to the indicated final concentration. All spectra were recorded using a 60° pulse, a 0.2 second acquisition time, a 30 ppm spectral width, no relaxation delay, and accumulating 2400 transients. The FID was transformed using an exponential broadening of 5 Hz.

A) ● 10 mM MEP in HBS (150 mM NaCl, 50 mM HEPES).

B) ■ 100 mM MEP in HBS.

C) ▲ 100 mM MEP in HBLS (50 mM NaCl, 50 mM HEPES).

D) ○ 100 mM MEP in plasma.

E) □ 100 mM MEP in cell lysate.

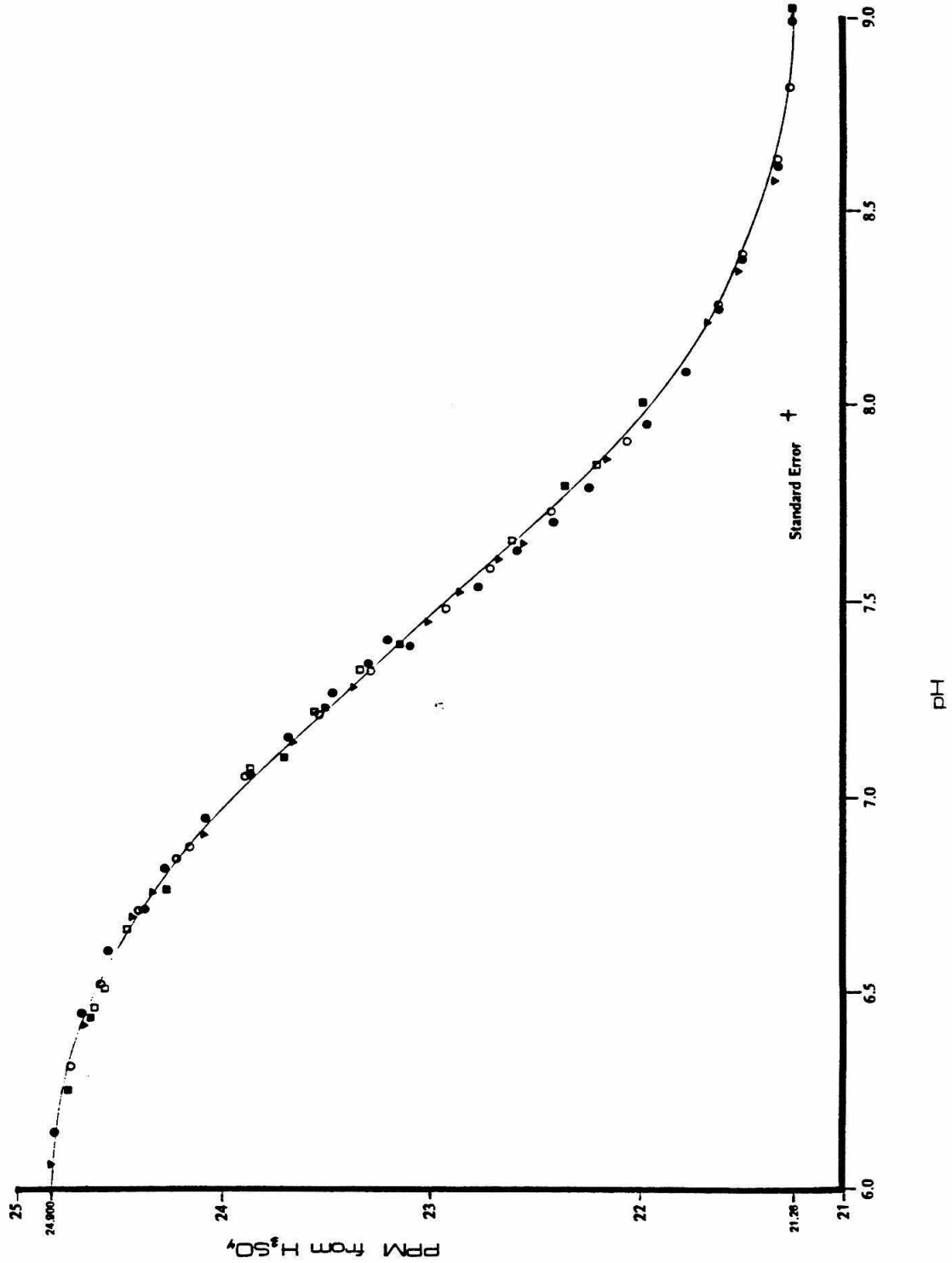
PPM from H_2SO_4
25
24.900
24
23
22
21.20
21
6.0
6.5
7.0
7.5
8.0
8.5
9.0
pH
Standard Error +

FIGURE 3

Rate of MEP uptake by Red Blood Cells

Anticoagulant was added to freshly drawn, oxygenated red blood cells suspended in plasma (hematocrit 50) at pH 7.42. MEP was added to a final concentration of 10 mM and spectra recorded at 30 minute intervals. ^{31}P spectra were recorded by accumulating 1200 transients using a 90° pulse, no relaxation delay and an accumulation time of 1.0 seconds. All spectra were proton noise decoupled during acquisition. The FID was transformed using an exponential broadening of 10 Hz.

A) ▲ 5.0 mg/ml Heparin.

B) △ 1.0 mg/ml Heparin.

C) ● 5.0 mg/ml Citrate.

D) □ 1.0 mg/ml Citrate.

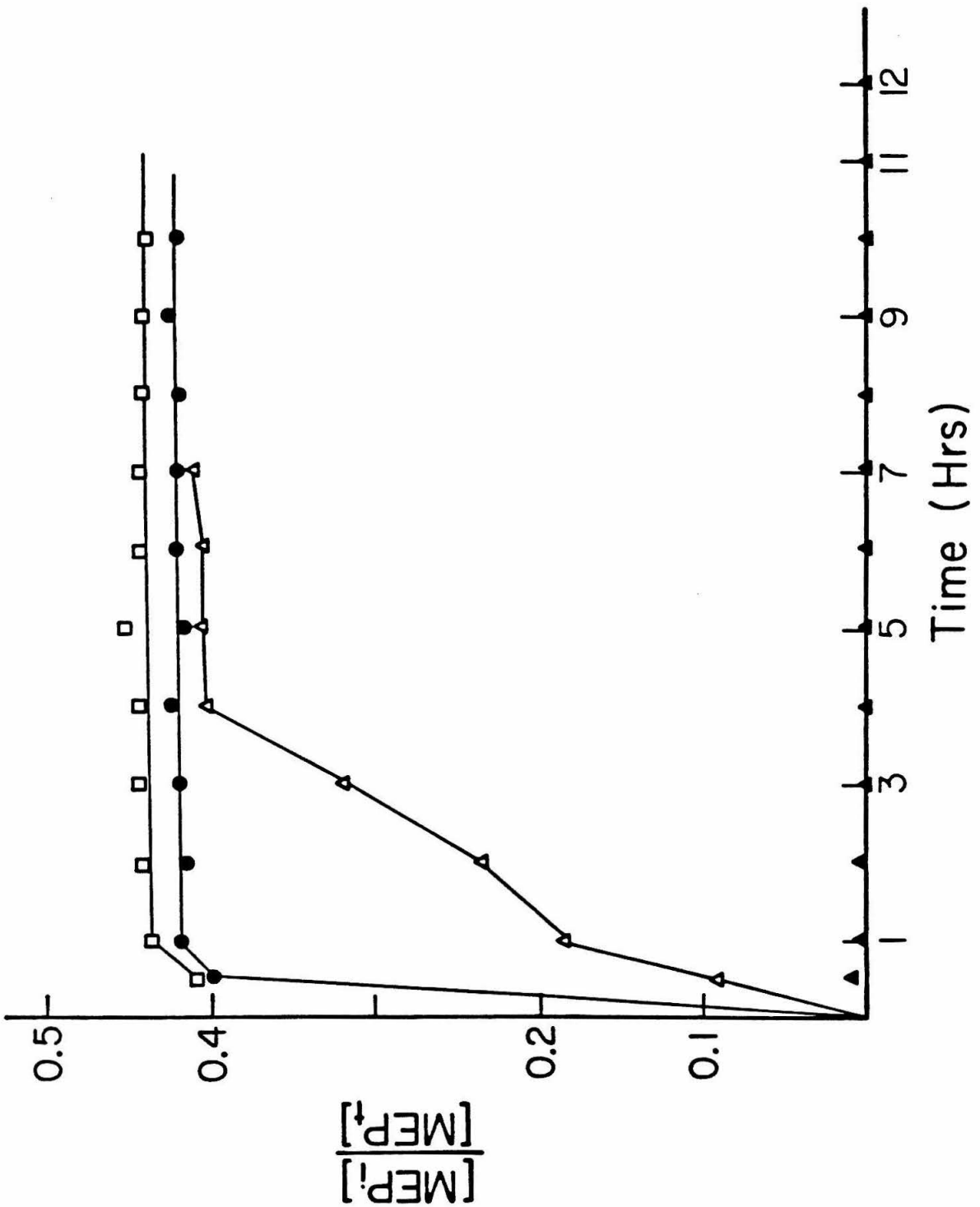
0.5
0.4
0.2
0.1
[MEP_i] / [MEP_f]
1
3
5
7
9
11
12
Time (Hrs)

FIGURE 4

pH_i vs pH_e in AA Erythrocytes

Oxygenated red blood cells, anticoagulated with EDTA, from normal adult volunteers were incubated at 37°C with 10 mM MEP. The cells were then washed in plasma at the indicated extracellular pH and suspended (hematocrit 50) in plasma containing 5 mg/ml heparin to prevent diffusion of MEP. Spectra were recorded by accumulating 2400 transients using a 45° pulse, 0.2 second acquisition time, 25 ppm spectral width, no relaxation delay and proton noise decoupling. The FID was transformed, using an exponential broadening of 10 Hz.

A) ●Average values from 5 individuals.

B) ✕Sample from individual with lowest intracellular pH.

C) □Sample from individual with highest intracellular pH.

D) ■Second sample from individual in C), 2 weeks later.

E) - -pH_i expected from the Donnan equilibrium.

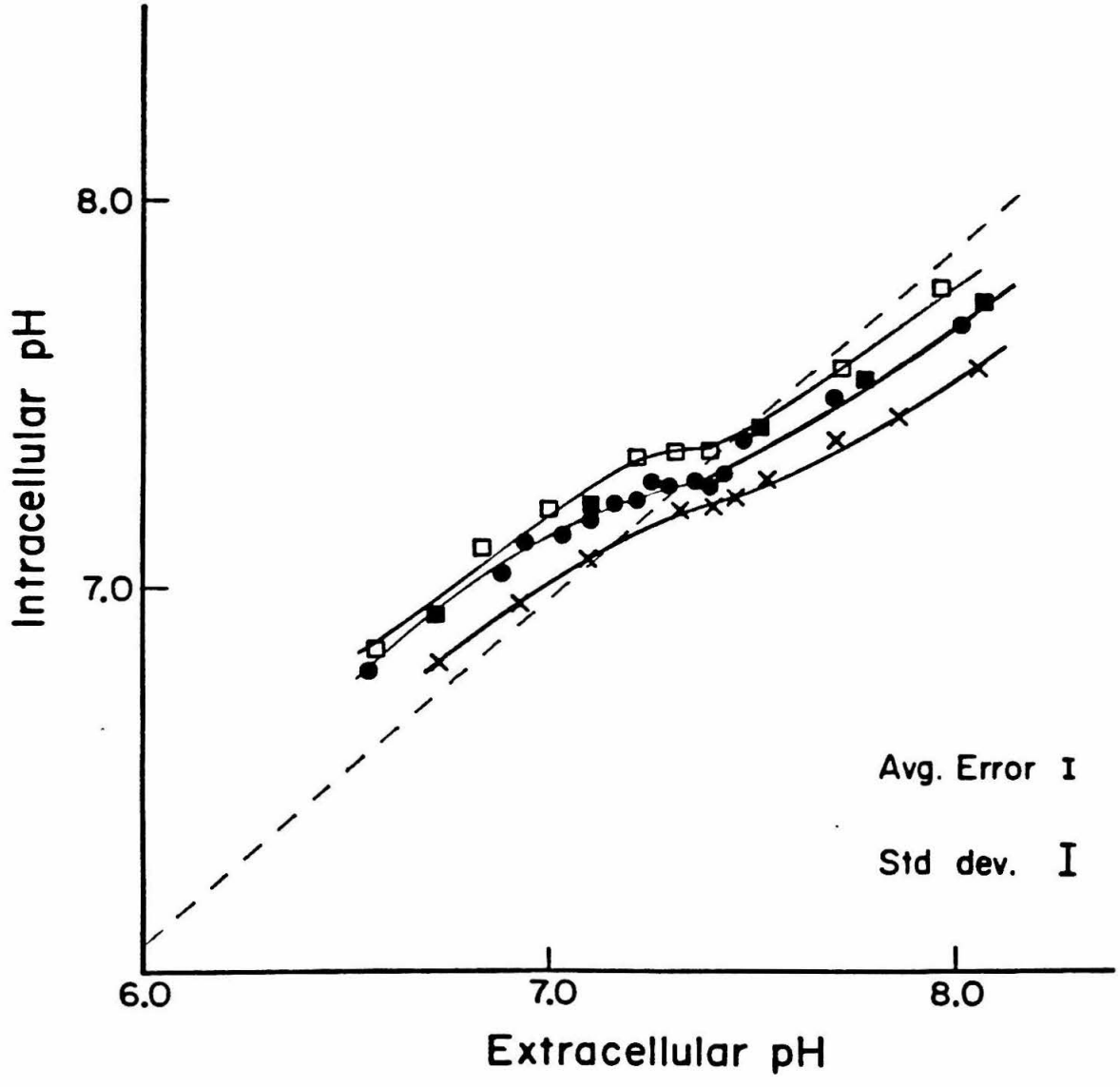
8.0
7.0
Intracellular pH
6.0
7.0
8.0
Extracellular pH
Avg. Error I
Std dev. I

FIGURE 5

Metabolic Dependence of pH_i vs pH_e in AA Erythrocytes

A) △ Red blood cells, from whole blood anticoagulated with EDTA, from a single normal volunteer were metabolically depleted by storage at 4°C until the ^{31}P ATP resonance was reduced to background noise levels. The ATP depleted sample was oxygenated, incubated with 10 mM MEP at 37°C for 90 minutes and extracellular pH adjusted by washing with plasma at the appropriate pH. Cells were then suspended (hematocrit 50) in plasma containing 5 mg/ml heparin to prevent diffusion of MEP. Spectra were recorded by accumulating 2400 transients using a 45° pulse, 0.2 second acquisition time, 25 ppm spectral width, no relaxation delay and proton noise decoupling. The FID was transformed using an exponential broadening of 5 Hz.

B) ● Red blood cells used in A) were suspended in plasma (pH 7.42, 5 mg/ml glucose) and the build-up of ATP monitored by ^{31}P NMR. When ATP levels had reached 85% of the initial levels, pH_i vs pH_e was measured as in A).

C) □ Cells from B) were deoxygenated and pH_i vs pH_e measured as in A).

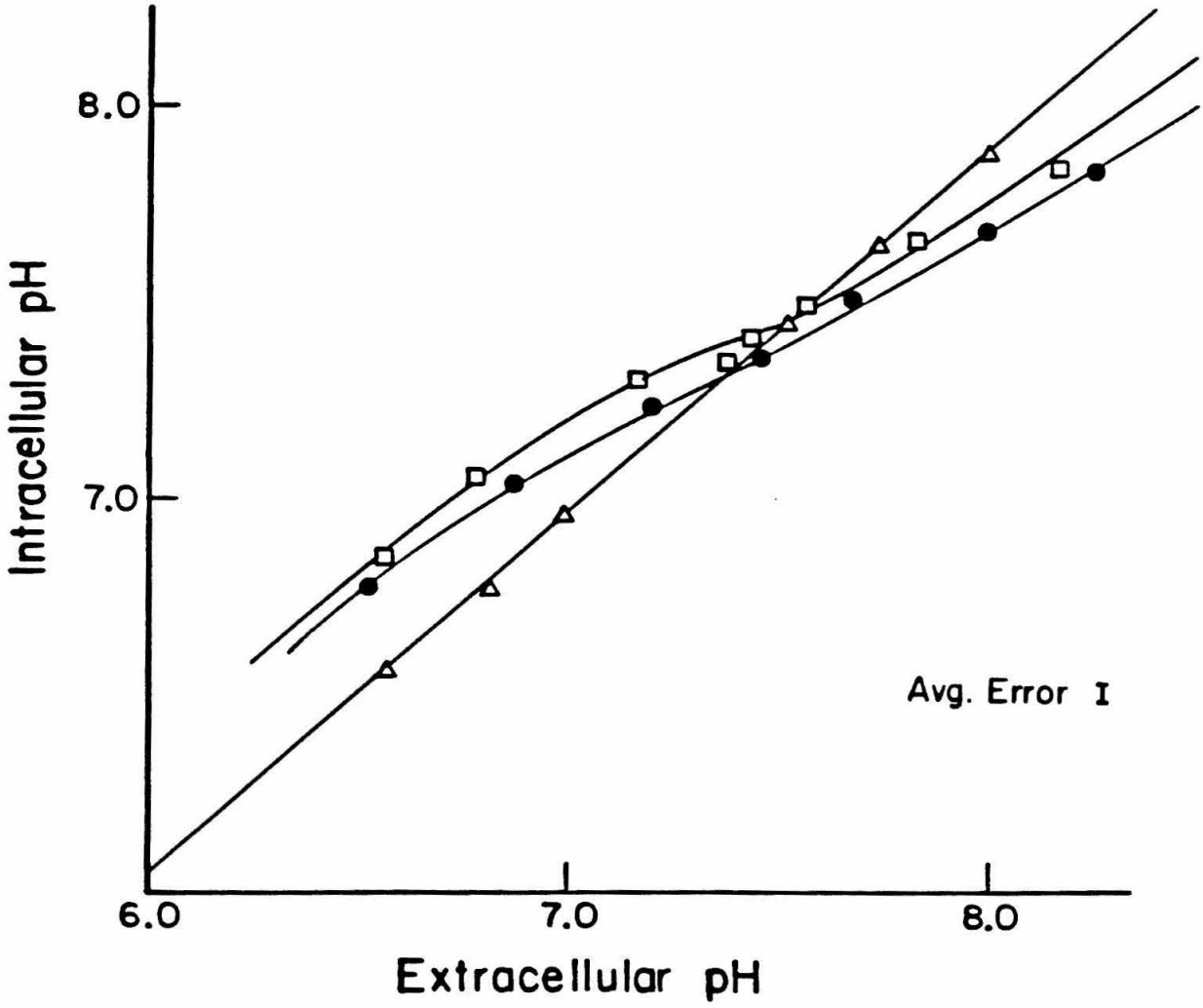
8.0
7.0
Intracellular pH
Avg. Error I
6.0
7.0
8.0
Extracellular pH

FIGURE 6

pH_i vs pH_e in SS Erythrocytes

A) ○ SS red blood cells were collected from 5 volunteers not in crisis. Each sample was anticoagulated with EDTA, oxygenated, incubated with 10 mM MEP at 37°C for 90 minutes, followed by adjusting the extracellular pH by washing with plasma at the appropriate pH. Cells were then suspended (hematocrit 50) in plasma containing 5 mg/ml heparin to prevent diffusion of MEP. Spectra were recorded by accumulating 2400 transients using a 45° pulse, 0.2 second acquisition time, 25 ppm spectral width, no relaxation delay and proton noise decoupling. The FID was transformed, using an exponential broadening of 10 Hz. The pH_i vs pH_e values for each sample were averaged and the standard deviation calculated.

B) △ Cells from A) were deoxygenated and the pH_i vs pH_e curve determined as in A).

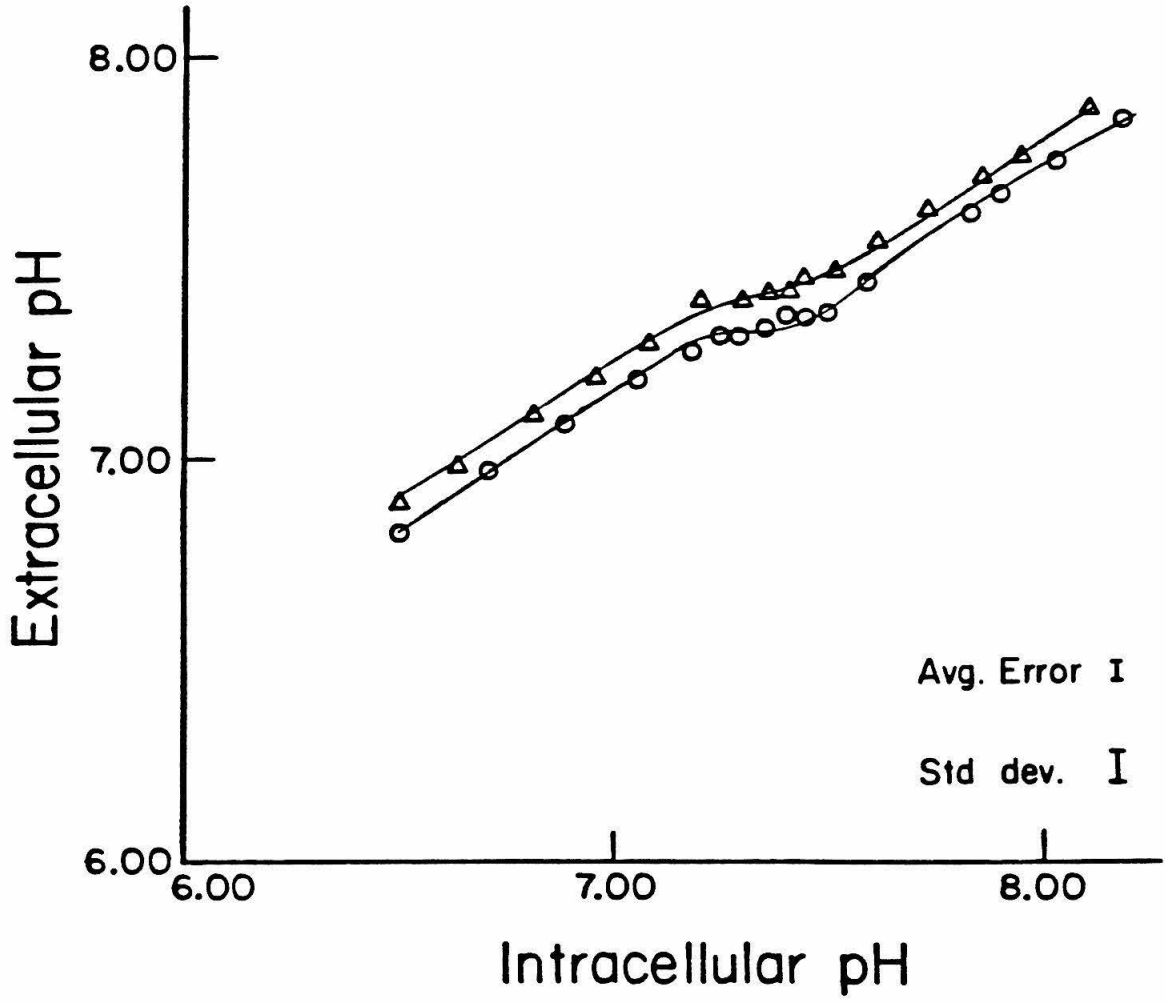
8.00
7.00
6.00
Extracellular pH
6.00
7.00
8.00
Intracellular pH
Avg. Error I
Std dev. I

FIGURE 7

Effect of the Ligation State of Hemoglobin on pH_i Regulation in AA and SS Erythrocytes

Red blood cells from normal donors (▲ ■ ●) or SS donors ( ) were anticoagulated with EDTA and incubated with 10 mM MEP at 37°C for 90 minutes. The cells were washed in plasma at pH 7.36 (○ ●▲) or 7.04 (■ □) and suspended in plasma containing 5 mg/ml heparin at a hematocrit of 50. The samples were fully oxygenated and pH_i measured from spectra recorded by accumulating 2400 transients, using a 45° pulse, 0.2 second acquisition time, 25 ppm spectral width, no relaxation delay and proton noise decoupling. The FID was transformed, using an exponential broadening of 5 Hz. The samples were partially deoxygenated, the degree of ligation measured spectrophotometrically and pH_i measured from ^{31}P spectra recorded as above.

A) ○ SS red blood cells, pH_e = 7.36, +5 mg/ml glucose.
B) □ SS red blood cells, pH_e = 7.04, +5 mg/ml glucose.
C) ● Normal red blood cells, pH_e = 7.36, +5 mg/ml glucose.
D) ■ Normal red blood cells, pH_e = 7.04, +5 mg/ml glucose.
E) ▲ Normal red blood cells, pH_e = 7.36, metabolically depleted.

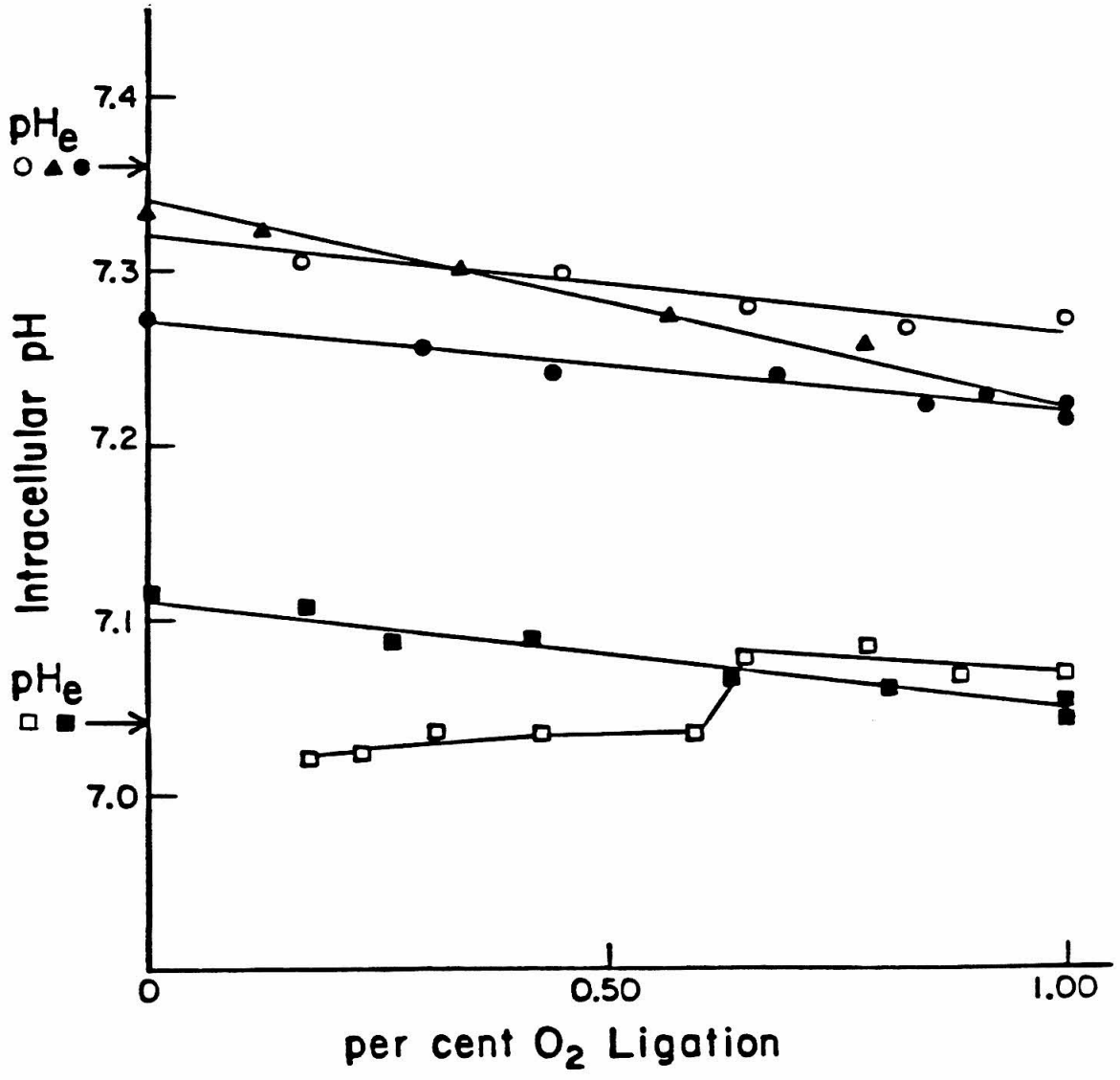
7.4
pHe
7.3
7.2
Intracellular pH
7.1
pHe
7.0
0
0.50
1.00
per cent O2 Ligation

Chapter 2

Measurements of Cell Volume by Nuclear Magnetic Resonance

INTRODUCTION

A detailed knowledge of how cell volume changes in response to intracellular processes or extracellular conditions is essential to an understanding of cell behavior. Cell volume, or equivalently, water content, is of special interest in studies of cellular transport, ion flux (1), and rates of glycolysis (2). In particular, cellular volume and mean hemoglobin concentration (MHC) are important determinants in sickle cell anemia (3, 4).

Gelation of sickle cell hemoglobin (SS Hb) is highly dependent upon the concentration of deoxy SS Hb (5). As MHC increases, the rate of gelation of hemoglobin S increases geometrically. A recent report described a pH-dependent mechanism for regulating cellular cation and water concentrations in SS and CC red blood cells. Brugnara et al. (6) observed that decreasing extracellular pH results in a decrease in cellular water concentration. This decrease in cell volume would lead to an increase in intracellular SS Hb concentration and a concomitant increase in the rate of gelation and sickling. These events would be exacerbated by the breakdown of pH homeostasis of red blood cells at low pH (7), which might explain the anomalously high rate of sickling observed in some cases.

These observations, along with our observations of pH regulation in both normal and sickle cell erythrocytes

prompted us to develop an accurate, non-invasive method of rapidly determining the cell volume.

This was necessary because traditional methods of determining cell volume have various limitations. Measurements of cell volume by lyophilization or oven drying are straightforward, but destructive. Measurements by light scattering are non-invasive and non-destructive, but are not very accurate. ^{31}P Nuclear Magnetic Resonance (NMR) measurements (8) are non-invasive and also monitor metabolic changes, but add an exogenous compound, and provide only a relative measure of cell volume.

The ability to monitor cell volume and the effect of agents (valinomycin, nystatin, amiloride, etc.) known to affect ion transport on the cell volume has considerable experimental value. For example, the use of NMR to determine cell volume values directly and non-destructively would provide a method to evaluate the effect of various agents on cell volume in viable cells and would find wide applicability to the study of antisickling agents.

Kinetic Measurements by NMR in Intact Cells

NMR has proven extremely useful in the study of dynamic processes (9). This is especially true in whole cell systems where the equilibrium nature and non-invasive aspect of NMR measurements allow direct application of the results to <u>in vivo</u> conditions.

The application of NMR to whole cell systems has provided a wealth of information on the metabolic state of cells (10), the transport of metabolites (11), the flux of ions (12), the maintenance of intracellular pH (13), and intracellular chemical equilibria. Proton NMR has been used to study transmembrane transport (14), rates of intracellular reactions (15), and the dynamics of membrane interactions (16). ^{31}P NMR has found wide application in determinations of intracellular pH (17), metabolism of organo-phosphates (18) and phosphate ion flux (19).

NMR can provide information on the dynamical parameters, rate constants (k_i), populations (p_i), relaxation times (T_{1i}), and the chemical shift $_i$ for each site of a system undergoing chemical exchange (20). Lineshape analysis (for fast exchange) or magnetization transfer measurements (for slow exchange) provide direct measurements of the dynamic parameters of the system when easily distinguishable resonances exist.

The majority of cases of membrane transport do not result in an observable change in chemical shift, thus limiting the applicability of standard dynamic NMR methods. Similar requirements for distinct chemical shift differences between product and reactant have limited the usefulness of NMR in studies of intracellular metabolism.

Under special conditions it is possible to extract dynamic information by utilizing differences between

intracellular and extracellular spin-lattice relaxation rates (21). Ion fluxes and intracellular metabolite concentrations have been measured by utilizing differences in intracellular and extracellular spin lattice (T_1) or spin-spin (T_2) relaxation rates (22). In favorable cases, sufficient intrinsic relaxation differences exist. Alternatively, T_1 or T_2 differences may be created by the addition of relaxation agents (23).

NMR Measurements of Fractional Populations

Both the rate of transfer from site A to site B (k_a) and the fractional population of the sites (i.e., the equilibrium constant) are of interest. Even though fewer NMR measurements of the fractional population are reported (better methods are generally available), the information needed to determine the population is readily available from the general description of exchange phenomena. One of the most visible examples of the use of population measurements in conventional dynamic NMR is the use of ^{31}P NMR to measure intracellular pH (24).

Just as spin lattice relaxation measurements are used to measure microscopic reaction rates (k_i) where lineshape analysis or magnetization transfer experiments are ineffective, spin lattice relaxation measurements should make determinations of fractional populations possible even in the absence of observable chemical shift differences.

For example, intracellular water spin-lattice relaxation rates were determined, and used to calculate the rate of water exchange across the red cell membrane (25,26). These measurements relied upon the removal of the extracellular contribution to the total NMR water signal by complete relaxation of the extracellular water signal. Addition of the paramagnetic relaxation reagent Mn^{2+}, which cannot cross the membrane, increases the extracellular relaxation rate (27). Thus, the short-lived extracellular proton signal does not contribute to the total observed NMR signal. Furthermore, the relaxation behavior of the signal depends only upon intracellular events. By studying the relaxation behavior of such a signal, the lifetime of the intracellular water can be measured and the rate of water exchange across the membrane calculated.

When the extracellular signal is not altered by the addition of relaxation reagents, there is still a measurable difference between the intracellular and extracellular relaxation rates caused by intracellular paramagnetic iron and magnetic field gradients arising from the particulate nature of the cell suspension (28). This difference should be sufficient to allow the determination of the ratio between intracellular and extracellular water signals by measuring the total integrated signal intensity as a function of recovery time after an inverting pulse.

The time course of the NMR signal intensity is described by the sum of mixed exponentials. The exponential time constants are related to the spin lattice relaxation times of each site and the average exchange lifetime. The leading coefficients are functions of intracellular water fraction (p_a) and extracellular water fraction (p_b). Since the intracellular and extracellular water relaxation rates can be determined independently, and the average exchange lifetime is known, the rate of relaxation of the system can be fit to the experimental curve by varying p_a and p_b, subject to the constraint $p_a + p_b = 1$. The values p_a, p_b and the hematocrit can then be used to calculate the MHC.

This chapter describes the application of ^1H and ^{17}O water spin lattice relaxation measurements to the determination of cell volume in intact, viable cells. The difference between intracellular proton T_1 relaxation and extracellular T_1 relaxation rates provides the means for determining non-invasively the total intracellular water concentration and thence, the MHC.

MATERIALS and METHODS

Chemicals and Buffers

All chemicals were obtained from standard sources. Citrate, bicarbonate and HEPES buffer solutions were prepared by adding the appropriate buffering compound to a final concentration of 50 mM in a physiological saline solution (total osmolarity 300 mOsm, 110 mM NaCl, 0.15 mM KCl) and adjusting the pH to 7.40. Blood plasma was isolated from normal whole blood provided by the Red Cross Blood Bank. Erythrocytes and white blood cells were removed by centrifugation, the pH adjusted to 7.40 by slow addition of concentrated NaOH, and the plasma stored at 4°C until just prior to use.

Red Cell Blood Samples

Normal whole blood (10 - 15 ml) was obtained from adult volunteers by venous puncture into vacutainers containing either heparin, citrate, or EDTA as anticoagulant. SS Blood collected at the USC Sickle Cell Center was drawn from patients not in crisis and not currently receiving drug treatment. The SS samples (15 - 20 ml) were obtained by venous puncture into vacutainers containing either heparin or citrate. All samples were stored on ice at 4°C and used as soon as possible.

Preparation of Blood Samples for NMR studies

All blood samples were fully oxygenated by passing a steady stream of humidified gas (95% O_2, 5% CO_2, by volume) at room temperature over the sample with gentle agitation until completely oxygenated as measured by U.V. absorbance. Cell suspensions for NMR measurements were prepared by washing either normal or sickle cell red blood cells three times in plasma at pH 7.40. The cells were then suspended in plasma at a final hematocrit of 30 to 50. Packed red blood cells were prepared by washing in plasma (3X, pH 7.40) followed by centrifugation in centricon ultrafiltration tubes to remove residual interstitial water. Red blood cell lysate was obtained by sonication of tightly packed cells. The sample was maintained at 4°C during sonication to reduce changes caused by heating of the sample. Samples containing shift or relaxation agents were prepared by washing in plasma without relaxation reagents, followed by suspension of the cells in plasma containing the appropriate concentration of relaxation reagent.

NMR Spectra

^{1}H and ^{17}O NMR spectra were recorded on a Varian XL-200 spectrometer operating in the Fourier transform mode at 200.00 (^{1}H) or 27.00 (for ^{17}O) MHz, using quadrature detection. Typically, each proton spectrum of a relaxation

series was obtained by accumulating 4 scans of 8K data points, using a standard non-correcting inversion recovery pulse sequence [180° - t - 90°], and a 2.00 second signal acquisition. Data acquisition was followed by a 10.00 second delay to allow complete relaxation of the NMR signal and to minimize cellular damage due to localized temperature increases. Because of the lower sensitivity and faster intrinsic relaxation time of ^{17}O, spectra were recorded by accumulating 1024 or 2048 scans, using a 0.05 second acquisition time and 4K data points. For most relaxation measurements, 12 delay times, t, were used. The delay time ranged from 0.01 x T_1 to 3 x T_1, to ensure sufficient data range to justify multiple exponential analysis. The shorter acquisition time used for ^{17}O compensated for the increase in the number of scans, such that the total experiment time for both ^{1}H and ^{17}O relaxation experiments was approximately 15 minutes.

Samples were capped by a Teflon plug to minimize gas exchange, and to prevent vortexing of the sample. To reduce field inhomogeneity caused by red blood cells in suspension, the sample was spun at 15 to 20 Hz. Spinning the sample also reduced the sedimentation of the red blood cells during FID acquisition. The probe temperature was maintained at 37° $\pm$ 2°C whenever the sample was in the instrument. The FID was zero-filled to 16K data points and weighted with a Gaussian convolution difference function

and 1 Hz (^{1}H) or 10 Hz (^{17}O) line broadening, to improve signal to noise prior to Fourier transformation.

Determination of Cellular Dry Weight

Red blood cells from NMR samples were collected by centrifugation in centricon centrifuge filtration cells. The pellets were weighed to determine total wet weight of the cells, and then dried at 80°C for 2 days or lyophilized overnight to remove cellular water. The difference between wet and dry weight, and initial sample volume were used to calculate the fractional water content of the original sample.

Analysis of NMR Results

Inversion recovery measurements were fit to single or double exponential relaxation equations as appropriate. Single exponential decay constants were determined by non-linear least-squares regression, using the Varian Assoc. prepackaged routines. Calculations of the dynamic parameters (p_i, k_i, T_{1i}) of cell suspensions were made by non-linear exponential least-squares regression using the full mixed exponential decay equation. In most calculations, the average water exchange lifetime (τ) was fixed at the previously reported (29) value 0.01 sec, while the other dynamic parameters were allowed to vary to achieve the best fit to the data. As is often the case in

multiple exponential regression analysis, it was frequently necessary to restrict or fix the value of T_{1i} in order to obtain physically meaningful population values. When it was necessary to restrict the range of the spin-lattice relaxation times, they were fixed at the values independently measured for packed cells, or plasma.

Theory

We are interested in the relaxation behavior of a two-compartment system undergoing chemical exchange.

$$A \underset{k_b}{\overset{k_a}{\rightleftharpoons}} B$$

The Bloch equations for two-site exchange including spin lattice (T_1) relaxation as formulated by Leigh are (30):

$$\frac{dM_{za}(t)}{dt} = M_{zb}(t)k_b - M_{za}(t)k_{1a} + M_{za}(\infty)/T_{1a} \qquad (1a)$$

$$\frac{dM_{zb}(t)}{dt} = M_{za}(t)k_a - M_{zb}(t)k_{1b} + M_{zb}(\infty)/T_{1b}, \qquad (1b)$$

where

$$k_{1i} = k_i + 1/T_{1i} \qquad i = A \text{ or } B, \qquad (2)$$

and k_a is the rate constant for conversion of A to B. $M_{zi}(t)$ is the magnetization of site i at time t, and $M_{zi}(\ )$ is the magnetization of site i at equilibrium.

The general solution to these coupled differential equations is given by (31):

$$M_{za}(t) = M_{za}(\infty) + C_1\exp(-\lambda_1 t) + C_2\exp(-\lambda_2 t) \qquad (3a)$$

$$M_{zb}(t) = M_{zb}(\infty) + C_1D_1\exp(-\lambda_1 t) + C_2D_2\exp(-\lambda_2 t), \qquad (3a)$$

where C_1 and C_2 are constants of integration, λ_i are effective time constants, D_i are mixing coefficients, and p_i are fractional populations:

$$\lambda_1 = 1/2(1/T_{1a} + 1/T_{1b} + k_b/p_a) + [1/4(k_{1a} - k_{1b})^2 + k_b^2 p_b/p_a]^{(1/2)} \qquad (4a)$$

$$\lambda_2 = 1/2(1/T_{1a} + 1/T_{1b} + k_b/p_a) - [1/4(k_{1a} - k_{1b})^2 + k_b^2 p_b/p_a]^{(1/2)} \quad (4b)$$

$$D_1 = [(k_{1a} - \lambda_1)/k_b] \quad (5a)$$

$$D_2 = [(k_{1a} - \boldsymbol{\lambda}_2)/k_b] \quad (5a)$$

$$(p_a + p_b = 1). \quad (6)$$

If Equation 3a is added to Equation 3b, the total magnetization as a function of time, $M_{zt}(t)$, is given by:

$$M_{zt}(t) = M_{zt}(\infty) + C_1(1 + D_1)\exp(-\boldsymbol{\lambda}_1 t) + C_2(1 + D_2)\exp(-\boldsymbol{\lambda}_2 t), \quad (7)$$

where

$$M_{zt}(t) = M_{za}(t) + M_{zb}(t) \quad (8a)$$

$$M_{zt}(\infty) = M_{za}(\infty) + M_{zb}(\infty), \quad (8b)$$

For an inversion recovery (Π - t - $\Pi/2$) pulse sequence, assuming complete inversion and normalizing the total magnetization ($M_{zt}(\infty) = 1$), we have:

$$M_{za}(\infty) = p_a \quad (9a)$$

$$M_{zb}(\infty) = p_b \quad (9b)$$

$$\text{and} \quad M_{zi}(0) = -M_{zi}(\infty); \quad (10)$$

with these boundary conditions, the integration constants become:

$$C_1 = 2(p_a D_1 - p_b)/(D_2 - D_1) \quad (11a)$$

$$C_2 = -2p_a - [(2p_a D_1 - p_b)/(D_2 - D_1)]. \quad (11b)$$

Equations 1 to 7 are written in terms of rate constants k_i; for our purpose it is informative to express

the time constants λ_i in terms of the mean lifetime for exchange tau. This is most easily accomplished by noting that at equilibrium

$$p_a k_a = p_b k_b, \tag{12}$$

and defining

$$tau_i = 1/k_i \tag{13}$$

from Equation 11 and 12,

$$p_a tau_b = p_b tau_a \tag{14}$$

$$tau_a/p_a = tau_b/p_b \equiv tau, \tag{15}$$

using these equalities, we can rewrite λ_i in terms of the mean lifetime for exchange, tau:

$$\lambda_1 = 1/2[1/T1a + 1/T1b + 1/papbtau] - 1/2[(1/T1a + 1/T1b + 1/papbtau)^2 - (4/pbtau)(1/T1a - 1/T1b)]^{(1/2)} \tag{16a}$$

$$\lambda_2 = 1/2[1/T1a + 1/T1b + 1/papbtau] - 1/2[(1/T1a + 1/T1b + 1/papbtau)^2 - (4/pbtau)(1/T1a - 1/T1b)]^{(1/2)}. \tag{16b}$$

Equation 3 demonstrates that chemical exchange between two sites results in double exponential relaxation behavior at each site. Equation 7 shows that in the absence of chemical shift differences of the resonances of the two sites, the relaxation behavior of the single observed resonance is the superposition of the individual relaxation curves. Thus non-linear regression analysis of relaxation

data for the single resonance will provide values for T_{1a}, T_{1b}, P_a, P_b, and tau.

Inspection of Equation 16 shows that in the special case where the exchange lifetime is short compared to the relaxation time (tau << T1i), the first time constant $_1$ becomes negligible compared to $_2$, and the observed relaxation is adequately described by a single exponential with a population-weighted time constant. In the case of cell suspensions or tissue samples, the exchange lifetime for water is short compared to the proton relaxation times (25). Therefore, we expect the ^1H relaxation behavior of the single observable water resonance to be governed by a single time constant given by the population-weighted average of the individual relaxation rates. However, the relaxation time of ^{17}O is short compared to the transmembrane exchange time of water. Inspection of Equations 16 and 7 shows that under these conditions, the observed relaxation will be a superposition of the independent relaxation responses of the individual sites. Thus, comparison of dynamic parameters calculated from ^1H and ^{17}O relaxation measurements should provide direct verification of the accuracy of the methods.

RESULTS and DISCUSSION

Single Component Relaxation Measurements

Figures 1 and 2 show the results of ^{1}H and ^{17}O T_1 relaxation measurements in plasma, packed red blood cells and cellular lysate. The water proton T_1 relaxation time ranges from 0.69 $\pm$ 0.15 seconds in oxygenated packed red blood cells to 2.20 $\pm$ 0.20 seconds in plasma. Independent analysis of normal and sickle cell samples yielded an intracellular T_1 of 0.64 $\pm$ 0.11 seconds in normal erythrocytes and 0.75 $\pm$ 0.14 seconds for sickle cell samples. The plasma proton T_1 is 3.2 times the intracellular proton T_1.

Measurements of ^{17}O water relaxation times gave values of 3.85 $\pm$ 0.30 X 10^{-3} seconds in plasma and 1.75 $\pm$ 0.30 X 10^{-3} seconds for cytoplasmic water. The water ^{17}O relaxation times in plasma, packed cells, and cell lysate are all approximately 10^{3} times faster than the corresponding proton T_1's. The plasma ^{17}O T_1 is 2.2 times the intracellular ^{17}O T1, compared to 3.2 times for ^{1}H. Thus, the difference in T_1 between intracellular water and plasma water is similar for both ^{17}O and ^{1}H, indicating that similar mechanisms shorten both proton and oxygen T_1 within the cell.

Simulation of Multi-Component Relaxation

Figure 3 shows the proton relaxation curves calculated from Equation 7, using the average T_1 values for plasma and intracellular water measured above, and a 0.01 second exchange lifetime for water across the cell membrane (29). Varying the fractional population of water in the intracellular compartment from 0 (plasma) to 1.00 (packed cells) produces a series of curves that demonstrate the results of relaxation in two compartments. Inspection of the curves indicates that the relaxation is adequately described by a single exponential decay. This is also evident from Equation 7, when $T_{1i} >> tau$. Under these conditions the time constants $_{1,2}$ reduce to

$$\lambda_1 \approx 0 \qquad (17a)$$

$$\lambda_2 \approx (p_a/T_{1a} + p_b/T_{1b}) \qquad (17b)$$

and the bulk contribution to relaxation then derives from the sum $(p_a/T_{1a} + p_b/T_{1b})$ in a single exponential decay.

The calculated relaxation curves expected for T_1 values measured for ^{17}O water resonances are shown in Figure 4. Comparison of Figures 3 and 4 clearly shows the effect that the ratio tau/T_1 has on the complete relaxation behavior of an exchanging system. The ^{17}O relaxation curves are clearly biphasic, demonstrating distinct two-compartment relaxation. In the case of distinct chemical shift differences for each site, the relaxation of each site would be a single exponential decay with a simple time

constant. However, in the absence of distinct chemical shifts, the observed relaxation is a superposition of the individual relaxations.

Effect of the ratio tau/T_1 on Relaxation Behavior

In order to evaluate the effect of changes in tau on the ability to obtain reliable measurements of fractional populations from relaxation measurements, simulated relaxation curves were calculated from Equation 7. Figure 5 shows the calculated relaxation curves for fixed values of T_{1a} (intracellular), T_{1b} (extracellular), and p_a (intracellular fractional population), and varying the exchange lifetime between 10.00 seconds (5 times T_1, essentially no exchange) and 0.01 (the actual exchange lifetime measured in normal red blood cells). Analysis of the curves demonstrates that at very long lifetimes, the relaxation is a linear combination of two exponential decays with time constants T_{1a} and T_{1b}. When the exchange lifetime is the same magnitude as the relaxation time, the exchange dominates the relaxation mechanism. As the lifetime decreases, such that $T_1 >> \text{tau}$, the observed relaxation time constant becomes a population-weighted average of the individual relaxation times.

Reproducibility and Reliability of the Fitting Algorithm

As a preliminary test of the reliability of the fitting algorithm, data points calculated from Equation 7 were used as input to the regression program. Fitting to the exact calculated data points results in values of T_{1a}, T_{1b}, tau, and p_a that agree exactly with the values used to generate the data. To test the effect of experimental error on the fitting algorithm, a randomly generated error (standard deviation $\pm$ 10%) was added to the individual data points. When all parameters were allowed to vary, the agreement of the final fitted parameters and the known parameters depends upon the initial estimate of the parameters. If the initial estimates are close (within a factor of three) to the real value, the fitted values agree with the known value within $\pm$ 12%. The agreement between the values from curve fitting and the known parameters increases as additional parameters are fixed at the known value. If all parameters except the fractional population of the sites are fixed, the agreement between the known population and the fitted value is $\pm$ 4%.

Double exponential non-linear regression analysis is known to be particularly sensitive to the precision of the initial estimates of the parameters (32). In the present system, ^1H and ^{17}O T_1 relaxation rates for intracellular and extracellular water are different only by a factor of 3, and the exchange lifetime is much different than T_1.

Thus, the observed relaxation is closely approximated by either a single exponential (^1H) or a sum of similar exponentials (^{17}O). Under these conditions, there are several physically real solutions to the complete equation, and we are outside the range of greatest sensitivity, where tau = T_1. So whenever possible, T_{1a}, T_{1b} and tau were fixed at their independently measured values and p_a was allowed to vary to obtain the best fit to the observed data.

Population Measurements Using Shift Reagents

In order to create a chemical shift difference between intracellular and extracellular water ^1H resonances, the contact shift reagent europium (33) was added to the cell suspension. Europium is a membrane impermeable paramagnetic shift reagent that also provides an efficient contact relaxation mechanism. The spectra obtained from inversion-recovery measurements of normal red blood cells in plasma (hematocrit 30) containing 1 X 10^{-3} M europium are shown in Figure 6. The broad signal is the result of rapid relaxation of extracellular water protons by europium, while the sharp, slowly relaxing resonance represents intracellular water protons. While the two resonances may be readily identified, the spectral separation caused by the shift reagent is insufficient to allow accurate integration of the relative intensities of the individual signals. The total signal intensity, plotted

as $\ln(M_o - M_z)$ vs time is shown in Figure 7. These data points were fit to Equation 7, using the independently measured T_{1a} and tau values and allowing the extracellular T_1 (T_{1b}) and fractional population (p_a) to vary. The calculated extracellular T_1 was 1 X 10^{-2} sec., while the fractional population of intracellular water was 0.18.

Population Measurements Using Relaxation Reagents

In order to further test the method, the membrane-impermeable relaxation agent Mn^{2+} (27) was added to suspensions of normal red blood cells. Figure 8 shows typical spectra from inversion-recovery measurements of Mn^{2+} doped samples. Under these conditions, separate peaks can be discerned for intracellular and extracellular water even in the absence of chemical shift separation. The integrated intensity vs. time is plotted in Figure 9 for three different Mn^{2+} concentrations. Biphasic behavior is visible in all three curves, and exponential peeling (33) gives approximate values of intracellular water fraction (p_a) of 0.3. Fitting of the data to the complete relaxation Equation using tau = 0.01, T_{1a} = 0.69 sec. and allowing p_a and T_{1b} to vary results in $p_a = 0.34 \pm 0.02$ and T_{1b} between 3 X 10^{-2} and 1 X 10^{-4}, depending on Mn^{2+} concentration. The consistent value of the intracellular water fraction over a wide range of extracellular relaxation times indicates the power and accuracy of the exponential fitting procedure.

Measurements of Cell Water Content in Normal and Sickle Cell Erythrocytes

Figure 10 plots integrated intensity vs. time for three different samples of normal red blood cells. The data points were fit to the full relaxation equation, allowing only the population of each site to vary and using the previously measured values of T_{1a}, T_{1b} and tau. From these relaxation curves, the intracellular water fraction varied from 0.352 $\pm$ 0.008 to 0.386 $\pm$ 0.007. Similar fitting of ^{17}O relaxation data (not shown) resulted in intracellular water fractions between 0.327 $\pm$ 0.010 and 0.391 $\pm$ 0.012. The close comparison of the intracellular water concentration derived from ^{1}H and ^{17}O relaxation data is further evidence of the reliability of the method, since the relaxation times of the two nuclei bracket the transmembrane water exchange lifetime and thus rely on very different aspects of the full relaxation Equation to determine the fractional population parameter. Shown in Figure 11 are the relaxation data for two samples of SS red blood cells. Similar fitting yields intracellular water fractions of 0.40 $\pm$ 0.02 and 0.42 $\pm$ 0.02.

The mean hemoglobin concentration of the samples may be easily calculated from the intracellular water fraction determined from relaxation data (p_a), the measured hematocrit (HC, 0.50 in these cases), the assumption that

hemoglobin provides 95% of the dry weight of the cell and the relationship:

$$MHC = 95 \times (1 - p_a/HC). \quad (18)$$

The calculated MHC of normal red blood cells ranged from a low of 25% to a high of 29%, in agreement with published values (35). Similar calculations for the SS red blood cells resulted in MHC values of 18% and 21%.

While it is possible to calculate absolute MHC values, the fractional population determined directly from the relaxation data provides an accurate indication of cell volume without relying on any assumptions about the cell content. Furthermore, any changes in cell volume may be stated in terms of the directly measurable parameter, p_a, making direct comparisons of different samples more meaningful.

Comparison to the ^{31}P NMR Method

A recent study (8) reported the use of dimethylmethylphosphonate (DMMP) as a probe of intracellular volume in red blood cells. The chemical shift of DMMP is dependent on the cell volume and thus serves as a reporter of intracellular volume. The method described here has three distinct advantages compared to the use of DMMP. First, no exogenous compound is added to the system, reducing the opportunity of non-physiologic effects or interactions. Second, the volume measured by relaxation times is

absolute, while the ^{31}P DMMP chemical shift gives a relative measurement that must be calibrated against a known standard under carefully controlled conditions. Third, since the chemical shift dependence of DMMP is presumably due to changes in the ratio of the concentrations of DMMP bound to Hb and free DMMP and thus to changes in hemoglobin concentration, the technique is useful only in red blood cells. While cell volume measurements based on T_1 differences are generally applicable to many cell types.

CONCLUSION

Under conditions present in whole cell suspensions or in tissue samples, the average lifetime for exchange of water across the cell membrane is 2 orders of magnitude less than either intracellular or extracellular ^{1}H spin-lattice relaxation times. Because of the relatively large difference, the contribution of membrane exchange to the total relaxation is minimized. This results in simplification of the relaxation calculations. Furthermore, the extracellular T_1 is longer than the intracellular T_1, providing a mechanism for determining the relative populations of the sites even in the absence of observable chemical shift differences.

The absolute volume and relative volume changes of whole cells in suspension may be accurately measured by either proton (^{1}H) or oxygen (^{17}O) NMR. The technique is fast, simple, non-invasive, and non-destructive. Multiple determinations may be made on single samples, reducing the probability of substantial sample variation. The technique is generally applicable to cells in suspension and should prove equally applicable to cells in whole tissue.

REFERENCES

1. Parker, J.C. (1983) **J. Am. Physiol. Soc. C**, 324-330.
2. Glaser, R., Heinrich, R., Brumen, M. and Svetina, S. (1983) **Biochem. Biophys. Acta. 42**, 577-582.
3. Bookchin, R.M., Balazs, T. and Landau, L.C. (1976) **J. Lab. Clin. Med. 87**, 597-616.
4. Glader, B.E. and Nathan, D.G. (1978) **Blood 51**, 983-989.
5. Hofrichter, J., Ross, P.D. and Eaton, W.A. (1974) **Proc. Natl. Acad. Sci. USA 71**, 4864-4868.
6. Brugnara, C., Bunn, H.F. and Tosteson, D.C. (1968) **Science 232**, 388-390.
7. Antypas, Jr., W.G. and Richards, J.H. (1987) **Blood**, submitted.
8. Kirk, K. and Kuchel, P.W. (1985) **J. Magn. Reson. 62**, 568-572.
9. Binsch, G. (1975) **Dynamic Nuclear Magnetic Resonance Spectroscopy, Academic Press,** N.Y., [Lloyd M. Jackson. ed.]
10. Radda, G.K. and Seeley, J.P. (1979) **Ann. Rev. Physiol. 41**, 749-769.
11. King, G.F. and Kuchel, P.W. (1984) **Biochem. J. 220**, 553-560.
12. Brauer, M., Spread, C.Y., Reithmeier, R.A.F. and Sykes, B. (1985) **J. Biol. Chem. 260**, 11643-11650.

13. Kashiwagura, T., Deutsch, C.J.,Taylor, J. Erecinska, M. and Wilson, D.F. (1984) **J. Biol. Chem. 259**, 237-243.

14. Guy, R.D., Razi, M.T. and Rabenstein, D.L. (1986) **J. Magn. Reson. 66**, 434-444.

15. King, G.F., York, M.J., Chapman, B.E. and Kuchel, P.W. (1983) **Biochem. Biophys. Res. Comm. 110**, 305-312.

16. Kostelnik, R.J. and Castellano, S.M. (1973) **J. Magn. Reson. 9**, 291-295.

17. Labotka, R.J. (1984) **Biochemistry 23**, 5549-5555.

18. Navon, G., Navon, R. Shulman, R.G. and Yamana, T. (1978) **Proc. Natl. Acad. Sci. USA 75**, 891-895.

19. Schnell, K.F., Besl, E. and van der Mosel, R. (1981) **J. Mem. Biol. 61**, 173-192.

20. Binsch, G. (1969) **Top. Steriochem. 3**, 97-192.

21. Eisenstadt, M. (1980) **J. Magn. Reson. 38**, 507-527.

22. Jones, A.J. and Kuchel, P.W. (1980) **Clin. Chem. Acta 104**, 77-.

23. Degani, H. (1978) **Biochem. Biophys. Acta 508**, 364-369.

24. Moon, R.B. and Richards, J.H. (1973) **J. Biol. Chem. 248**, 7276-7278.

25. Conlon, T. and Outhred, R. (1972) **Biochem. Biophys. Acta 288**, 354-361.

26. Shporer, M. and Civan, M.M. (1975) **Biochem. Biophys. Acta 385**, 81-87.

27. Pirkle, J.L., Ashley, D.L. and Goldstein, J.H. (1979) **Biophys. J. 25**, 389-406.

28. Brindle, K.M., Brown, F.F., Campbell, I.D., Grathwohl, C. and Kuchel, P.W. (1979) **Biochem. J. 180**, 37-44.

29. Niera,F.L., Sha'afi, R. I. and Solomon, A.K. (1970) **J. Gen. Physiol. London 55**, 451-466.

30. Leigh, Jr., J.S. (1971) **J. Mag. Reson. 4**, 308-311.

31. Forsen, S. and Hoffman, R.A. (1963) **J. Chem. Phys. 39**, 2892-2901.

32. Osborne, M. (1976) **J. Aust. Math. Soc. B 55**, 343-.

33. Fabry, M.E. and Eisenstadt, M. (1975) **Biophys. J. 15**, 1101-1110.

FIGURE 1

1H Relaxation Time of H_2O

The ^1H T_1 of water was measured by Inversion Recovery. Spectral width was 3.0 ppm, acquisition time was 2.00 seconds, recovery delay was 60.00 seconds and 14 variable delay times (0.001 to 90 seconds) were used. Four transients were recorded for each spectrum and the FID transformed without exponential weighting. Peak intensities vs. time were plotted and T_1 calculated using Varian Assoc. standard fitting procedures.

A) Plasma H_2O from normal donors.

B) Plasma H_2O from sickle cell donors.

C) Packed red blood cells from normal donors.

D) Cellular lysate from normal donors.

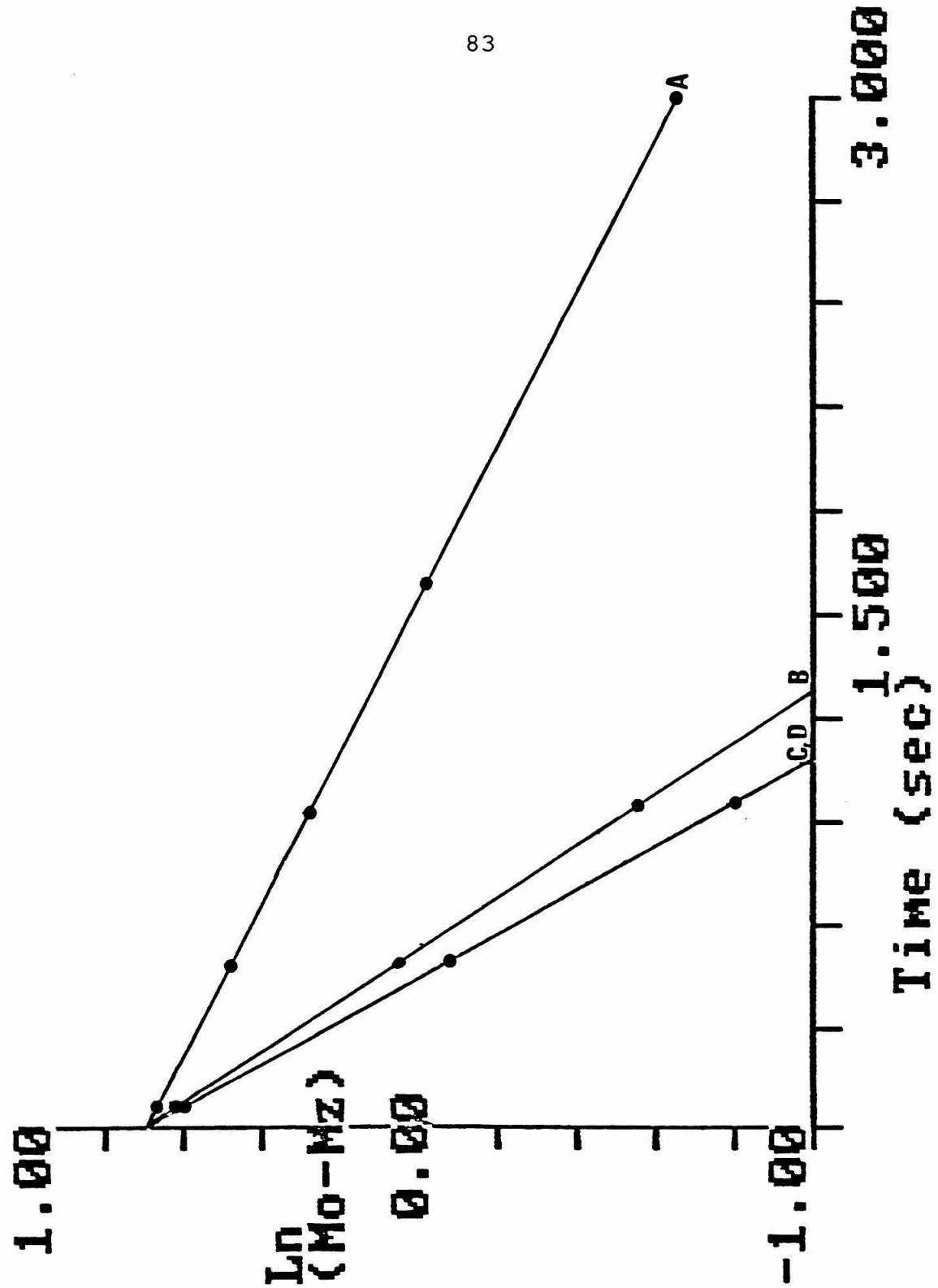
1.00
0.00
-1.00
Ln (Mo-Mz)
1.500
3.000
Time (sec)
A
B
C,D

FIGURE 2

^{17}O Relaxation Time of H_2O

Spectra were accumulated using a 440 ppm spectral width, a 0.5 second acquisition time, a 0.40 second recovery delay, 240 transients and 16 variable delay times (0.00001 to 0.40 seconds). The FID's were transformed without exponential weighting, the peak intensity plotted as a function of time and T_1 calculated using the Varian Assoc. standard procedures. Note the time scale compared with Figure 1.

A) Plasma H_2O from normal donors.

B) Packed red blood cells from normal donors.

C) Cellular lysate from normal donors.

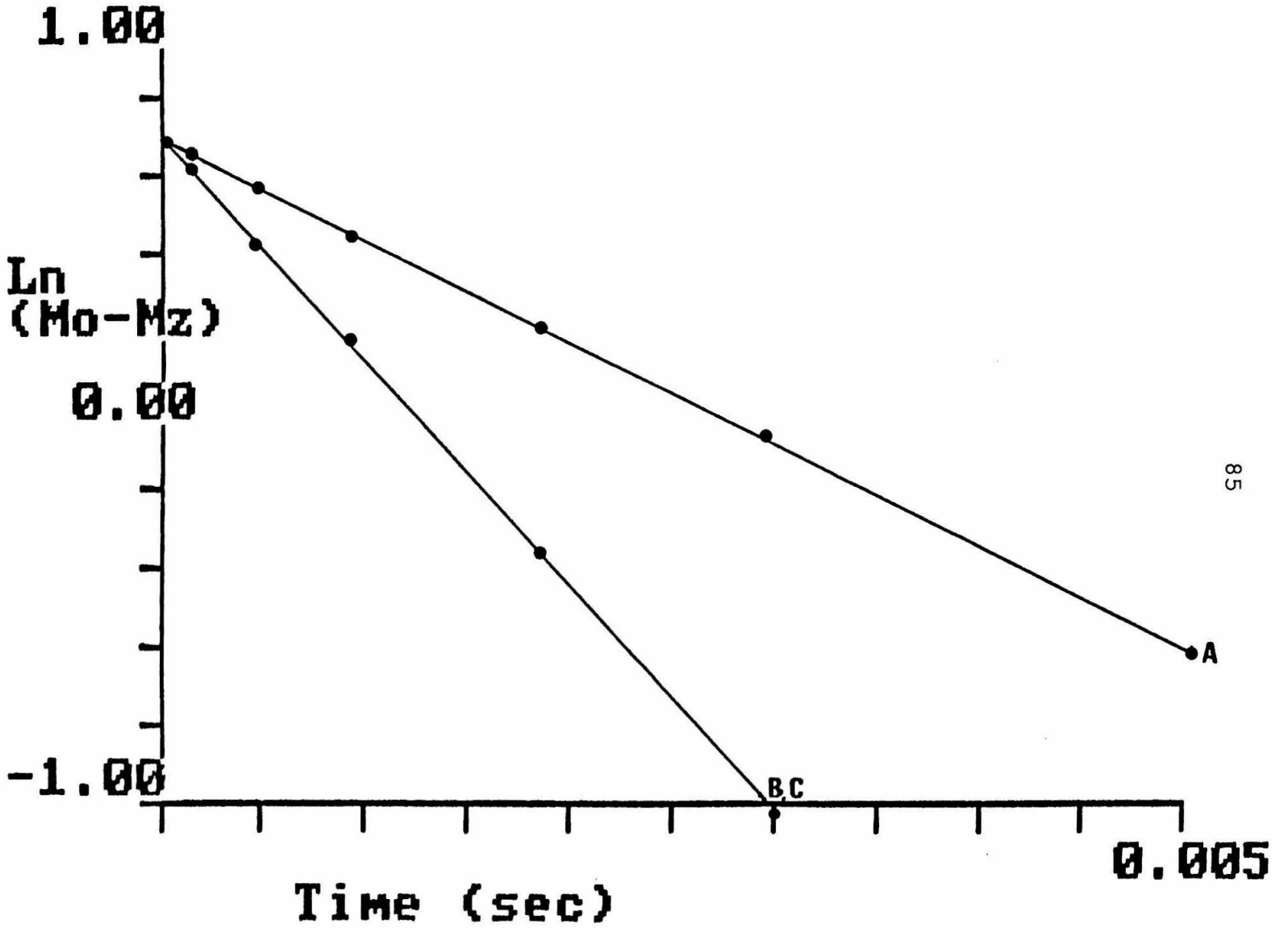
1.00
Ln
(Mo-Mz)
0.00
-1.00
A
B,C
0.005
Time (sec)

FIGURE 3

Simulated Relaxation Curve for ^1H Relaxation in Whole Blood

Effect of Changes in Intracellular H_2O Concentration

Relaxation curves were calculated from the full relaxation Equation (Equation 7), using:

T_{1a} = 0.69 seconds

T_{1b} = 2.20 seconds

Tau = 0.01 seconds.

A) p_a = 0.00

B) p_a = 0.20

C) p_a = 0.40

D) p_a = 0.60

E) p_a = 0.80

F) p_a = 1.00

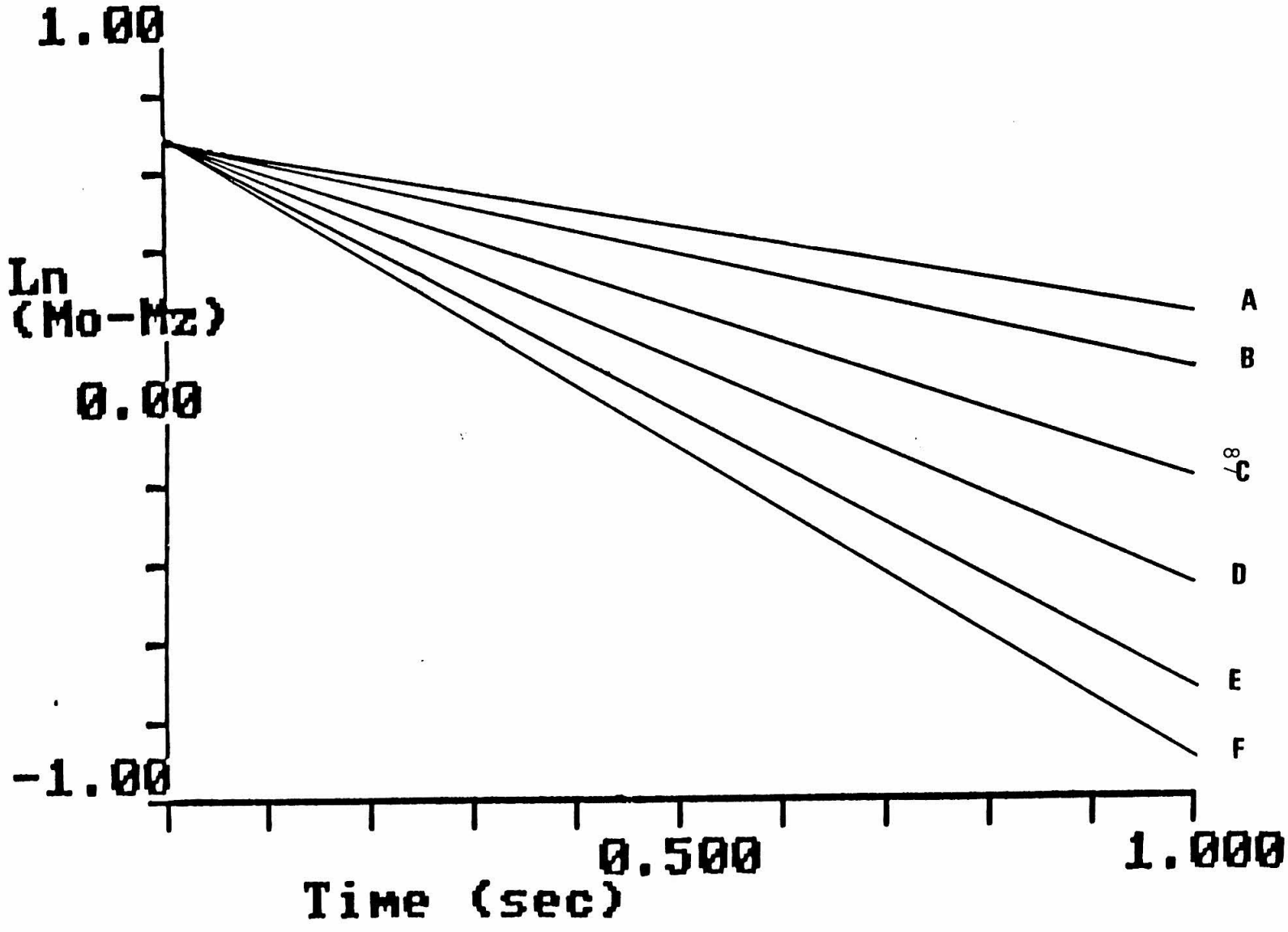
1.00
Ln
(Mo-Mz)
0.00
-1.00
0.500
1.000
Time (sec)
A
B
C
D
E
F

FIGURE 4

Simulated Relaxation Curve for ^{17}O Relaxation in Whole Blood

Effect of Changes in Intracellular H_2O Concentration

Relaxation curves were calculated from the full relaxation Equation (Equation 7), using:

T_{1a} = 0.0018 seconds

T_{1b} = 0.0039 seconds

Tau = 0.01 seconds.

A) p_a = 0.20

B) p_a = 0.40

C) p_a = 0.60

D) p_a = 0.80

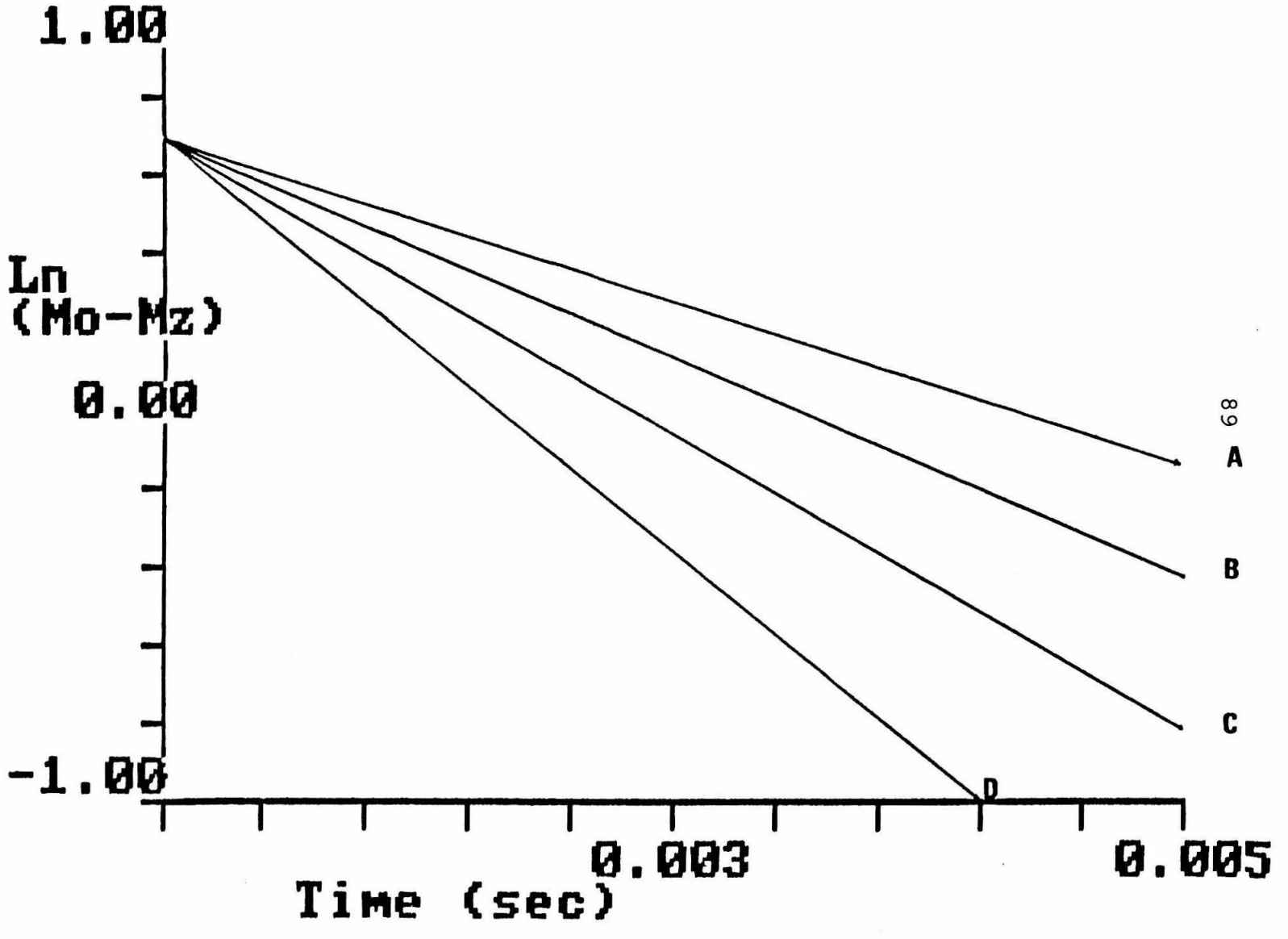
1.00
Ln
(Mo-Mz)
0.00
-1.00
A
B
C
D
0.003
0.005
Time (sec)

FIGURE 5

Simulated Relaxation Curve for ^{1}H Relaxation in Whole Blood

Effect of Changes in Transmembrane Exchange Rates

Relaxation curves were calculated from the full relaxation Equation (Equation 7), using:

T_{1a} = 0.69 seconds

T_{1b} = 2.20 seconds

p_a = 0.5.

A) Tau = 10.00

B) Tau = 1.00

C) Tau = 0.1

D) Tau = 0.01

E) Tau = 0.001

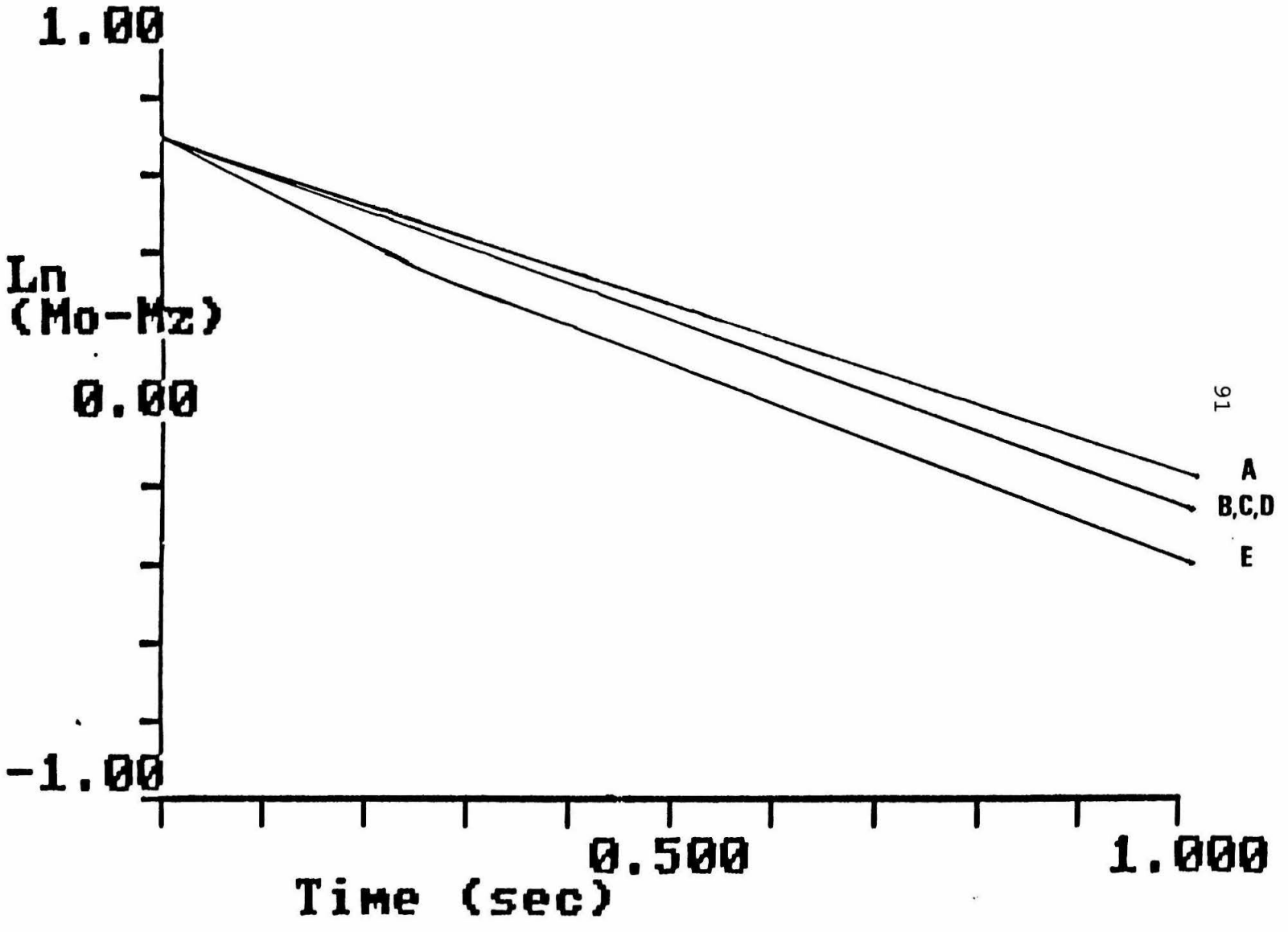
1.00
Ln
(Mo-Mz)
0.00
-1.00
0.500
1.000
Time (sec)
A
B,C,D
E

FIGURE 6

^{1}H Spectra of Whole Blood Doped with Europium

Normal whole blood was collected from volunteers by venous puncture with EDTA as anticoagulant. Europium was added from a 0.5 M stock to a final concentration of 0.01 M. Spectra were recorded using a 10.0 ppm spectral width, a 3.00 second acquisition time, a 30.00 second recovery delay and 10 variable recovery delays (0.0005 to 2.3 seconds). Four transients were accumulated, and the FID transformed using 10 Hz line broadening and a Gaussian convolution difference to reduce baseline roll. The plots are 10.0 ppm and linewidth at half-height is 850 Hz.

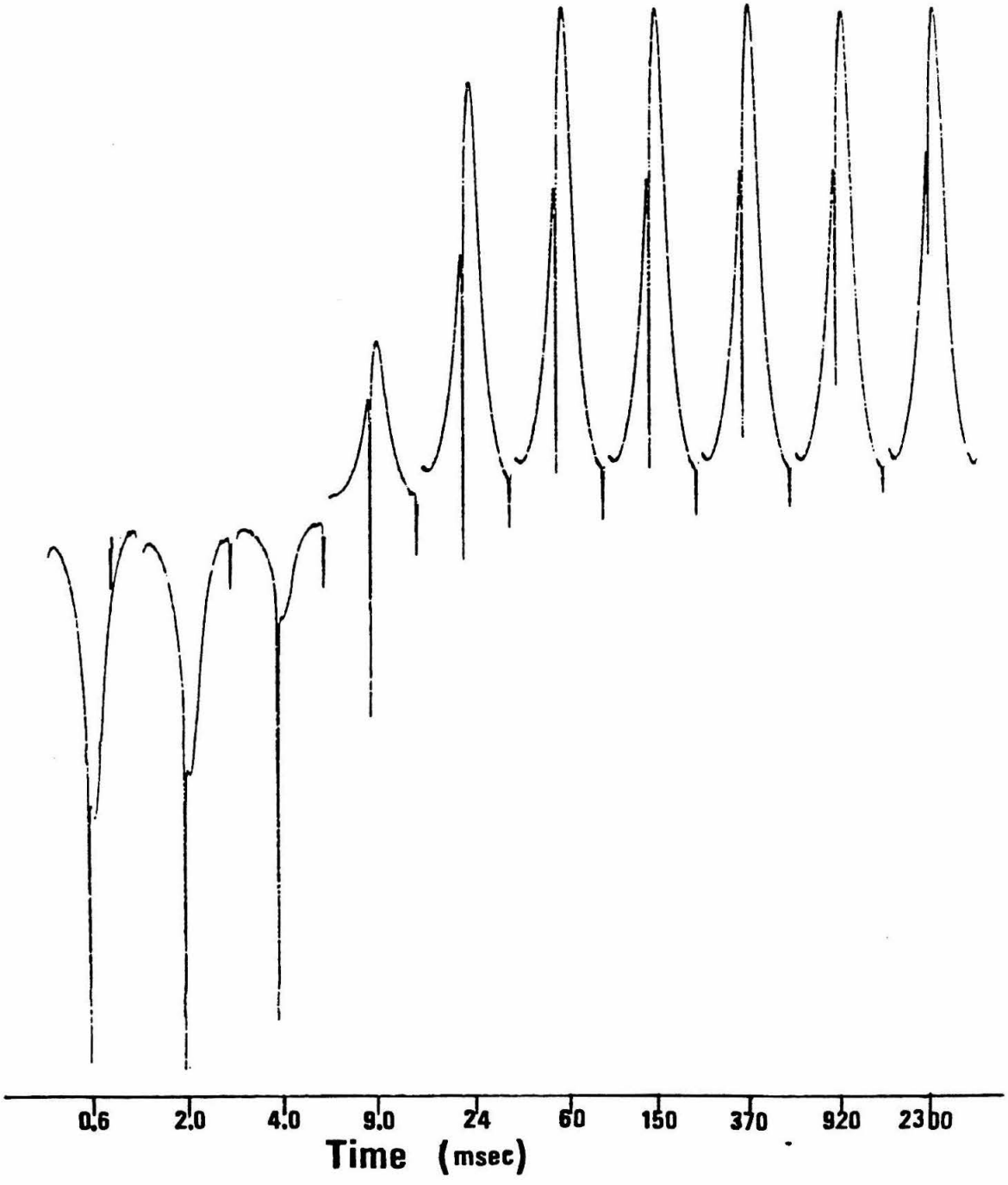
0.6
2.0
4.0
9.0
24
60
150
370
920
2300
Time (msec)

FIGURE 7

Double Exponential Fit to the Relaxation Data of Figure 6

The integrated intensities from the spectra in Figure 6 were used as input to the double exponential fitting program. T_{1a} was fixed at 0.69 seconds and Tau was fixed at 0.01 seconds. The initial estimate of T_{1b} was 0.001 and p_a started at 0.5. The calculated T_{1b} is 0.01 and p_a is 0.18. The average error of the NMR measurements was propagated through the calculations and is enclosed within the symbols.

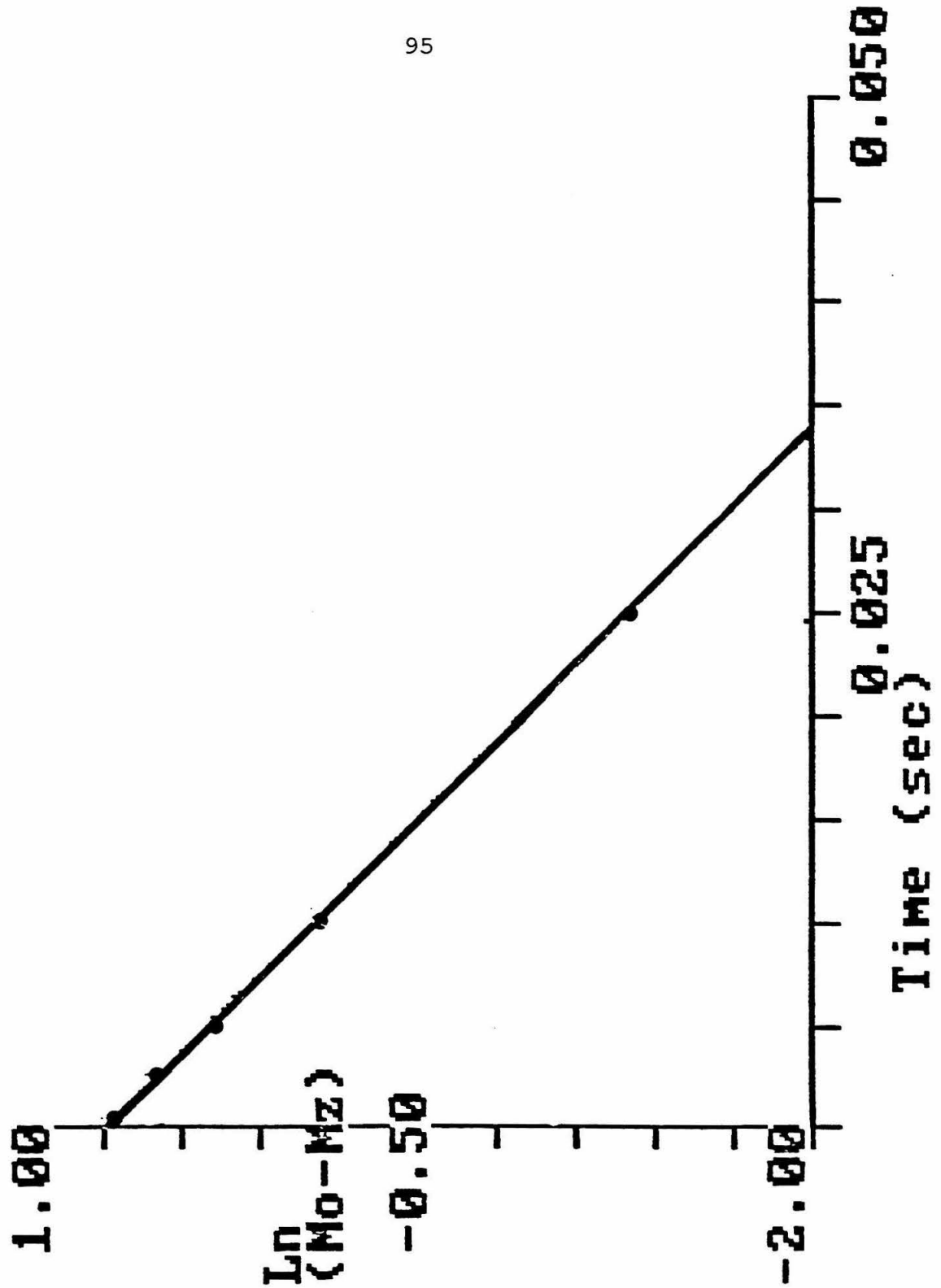
1.00
-0.50
-2.00
Ln (Mo-Mz)
0.025
0.050
Time (sec)

FIGURE 8

^{1}H Spectra of Whole Blood Doped with Manganous

The inversion recovery spectra of whole blood doped with 0.02 M Mn^{2+} were recorded with a 13.0 ppm spectral width, a 3.0 second acquisition time, a 10.00 second recovery delay and the use of 16 variable recovery delays (0.00001 to 15.0 seconds). Four transients were accumulated, the FID was weighted with 50 Hz line broadening and a Gaussian convolution difference to reduce baseline roll. Each spectral plot is 13.0 ppm wide and the linewidth at half-height is 910 Hz.

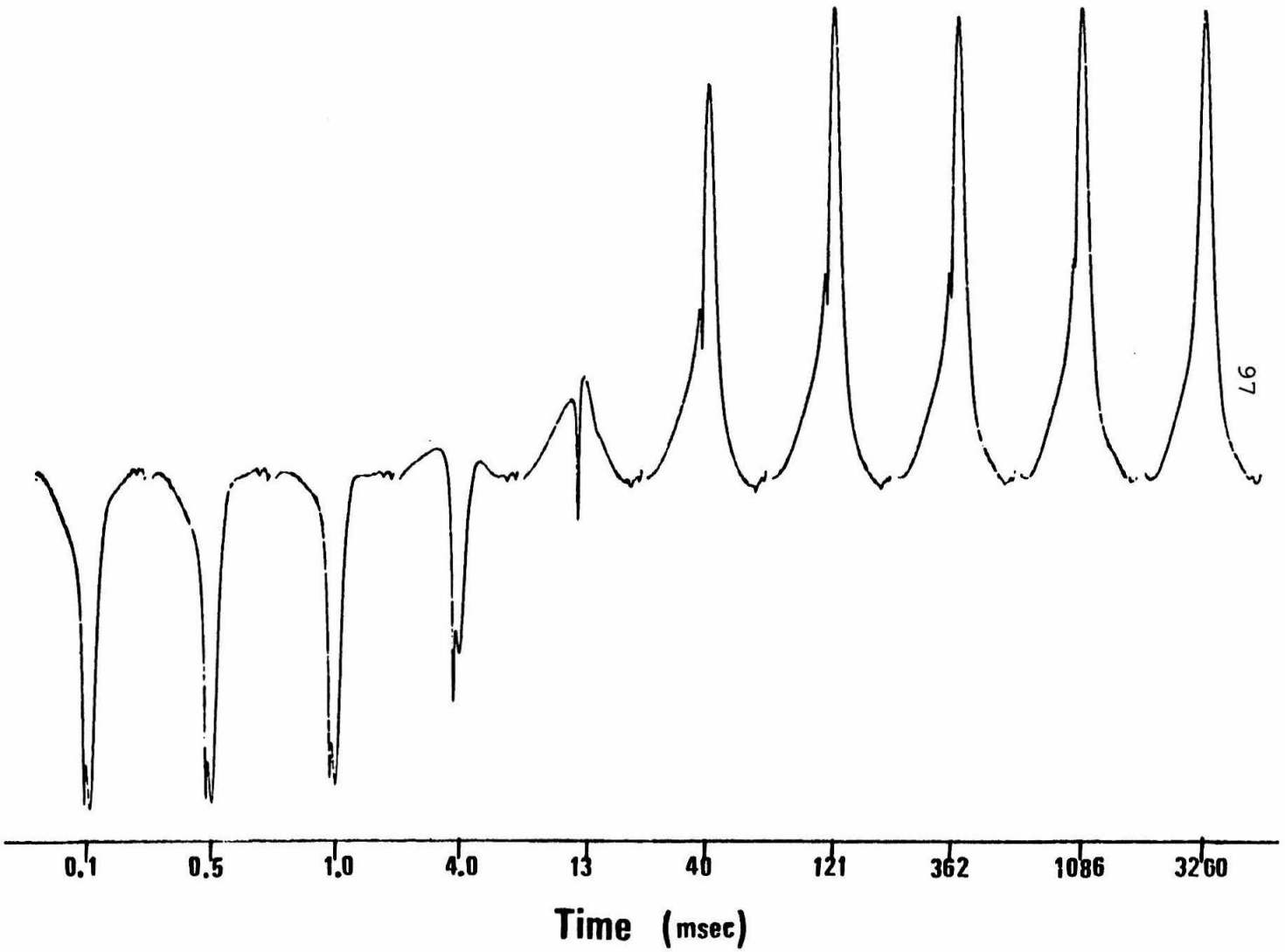
97
0.1
0.5
1.0
4.0
13
40
121
362
1086
3260
Time (msec)

FIGURE 9

Double Exponential Fit to the Relaxation Data of Figure 8

The integrated intensity from the spectra in Figure 8, and two other experiments (at 0.05 M Mn^{2+} and at 0.1 M Mn^{2+}) were used as input to the double exponential fitting program. T_{1a} was fixed at 0.69 seconds and Tau was fixed at 0.01 seconds. The initial estimate of T_{1b} was 0.01 seconds (0.001, 0.0005 seconds) and p_a started at 0.5. The average error of the NMR measurements was propagated through the calculations and is enclosed within the symbols.

A) 0.02 M Mn^{2+}, $p_a = 0.32$, $T_{1b} = 0.03$ seconds

B) 0.05 M Mn^{2+}, $p_a = 0.35$, $T_{1b} = 0.005$ seconds

C) 0.1 M Mn^{2+}, $p_a = 0.34$, $T_{1b} = 0.0001$ seconds

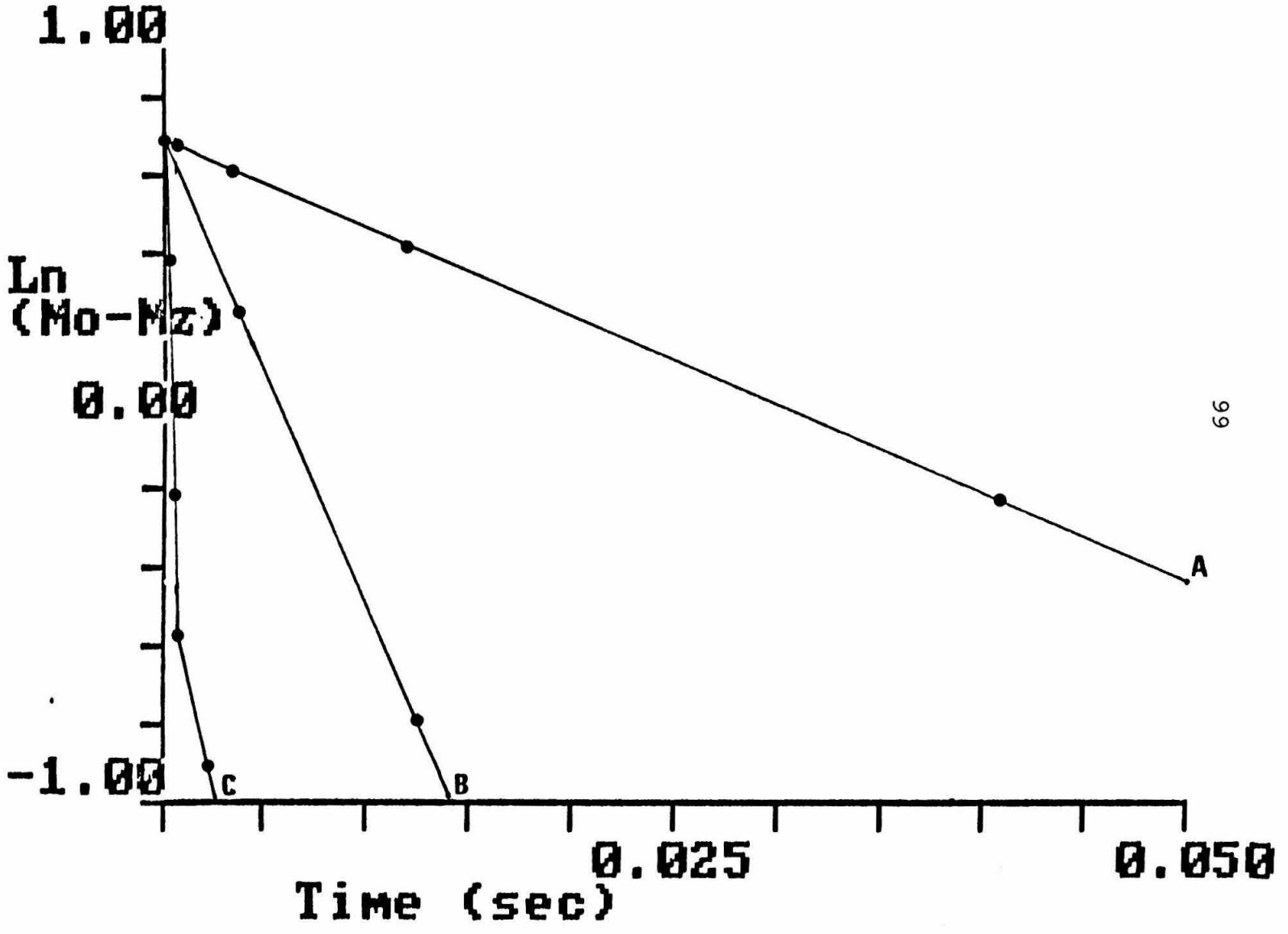
1.00
Ln
(Mo-Mz)
0.00
-1.00
A
B
C
0.025
0.050
Time (sec)

FIGURE 10

Measurements of Intracellular Water Fraction in AA Erythrocytes

Samples of normal whole blood were collected from three adult volunteers by venous puncture into vacutainers containing EDTA as anticoagulant. Spectra were recorded with a spectral width of 3.0 ppm, acquisition time was 2.00 seconds, recovery delay was 60.00 seconds and 14 variable delay times (0.001 to 90 seconds) were used. Four transients were recorded for each spectrum and the FID transformed without exponential weighting. The integrated intensity from the spectra were used as input to the double exponential fitting program. T_{1a} was fixed at 0.69 seconds, T_{1b} was fixed at 2.20 seconds, and Tau was fixed at 0.01 seconds. The initial estimate of p_a was 0.5. The average error of the NMR measurements was propagated through the calculations and is enclosed within the symbols.

A) $p_a = 0.34$

B) $p_a = 0.36$

C) $p_a = 0.38$

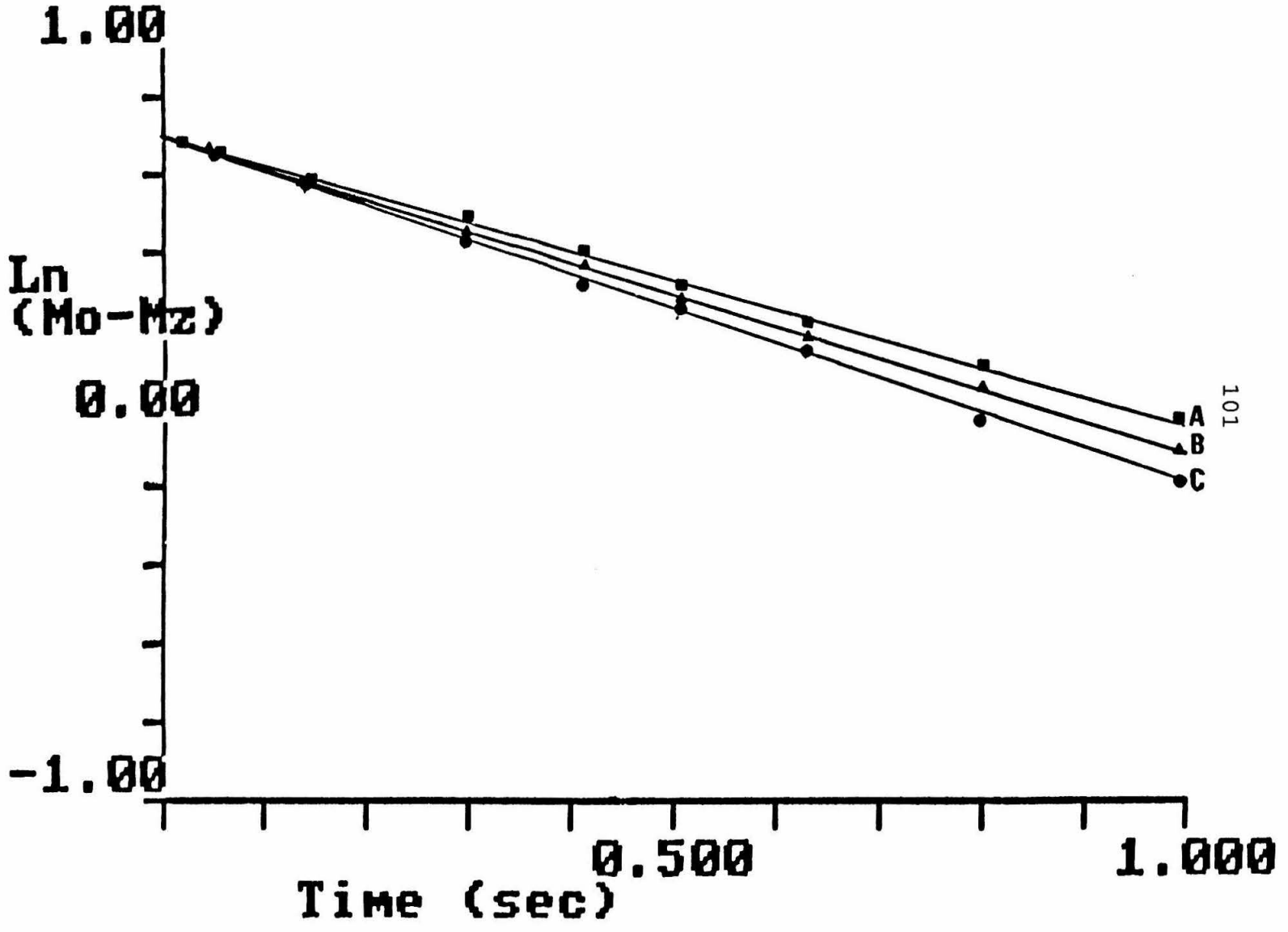
1.00
Ln
(Mo-Mz)
0.00
-1.00
0.500
1.000
Time (sec)
A
B
C

FIGURE 11

Measurements of Intracellular Water Fraction in SS Erythrocytes

Samples of SS whole blood were collected from three adult volunteers, not in crisis, by venous puncture into vacutainers containing heparin as anticoagulant. Spectra were recorded with a spectral width of 3.0 ppm, acquisition time was 2.00 seconds, recovery delay was 60.00 seconds and 14 variable delay times (0.001 to 90 seconds) were used. Four transients were recorded for each spectrum and the FID transformed without exponential weighting. The integrated intensity from the spectra were used as input to the double exponential fitting program. T_{1a} was fixed at 0.75 seconds, T_{1b} was fixed at 2.20 seconds, and Tau was fixed at 0.01 seconds. The initial estimate of p_a was 0.5. The average error of the NMR measurements was propagated through the calculations and is enclosed within the symbols.

A) $p_a = 0.39$

B) $p_a = 0.40$

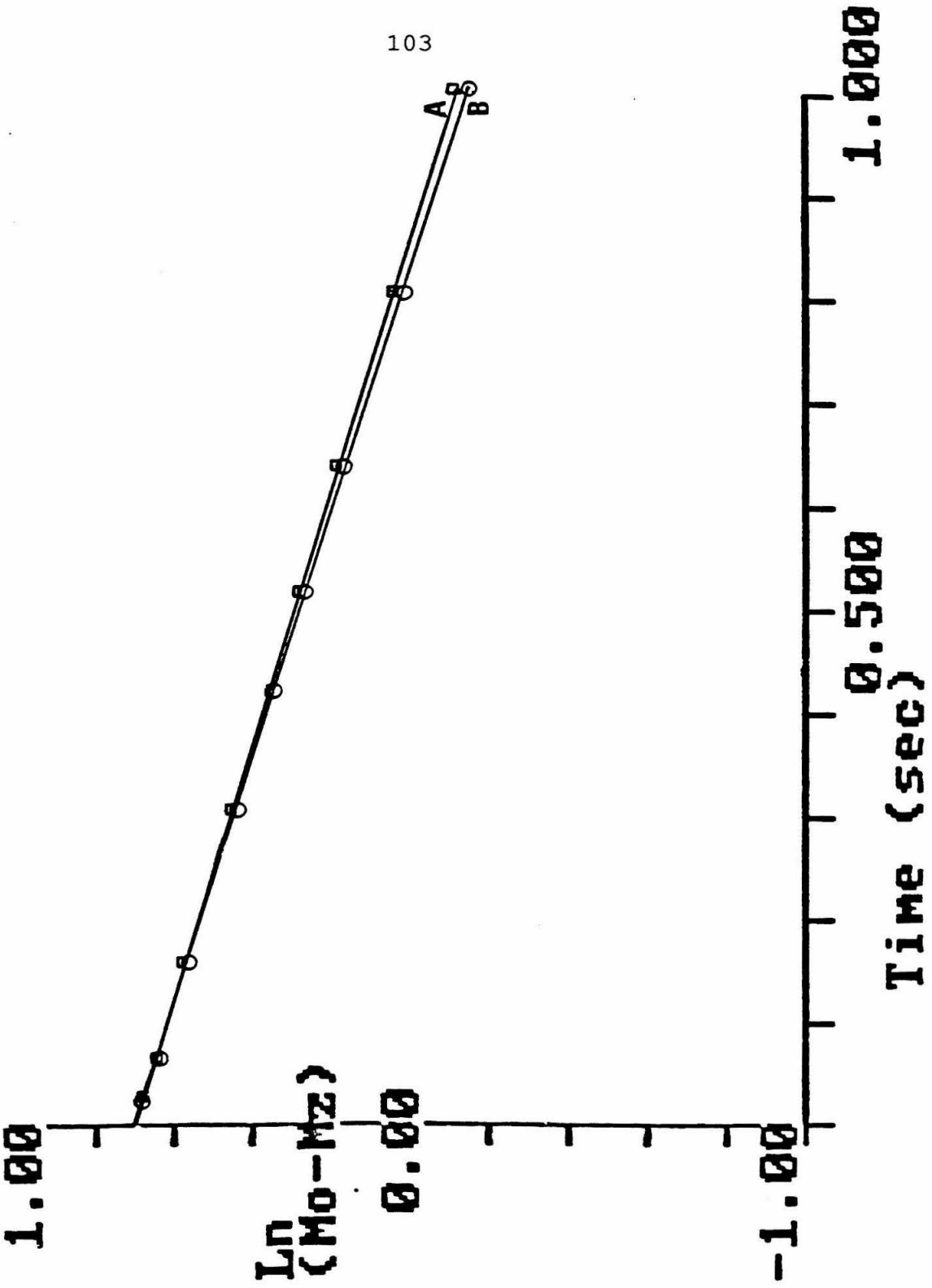
A
B
1.00
0.00
-1.00
Ln
(Mo-Mz)
0.500
1.000
Time (sec)

Chapter 3

^{31}P NMR Studies of the Binding Site of anti-Phosphorylcholine Antibodies

INTRODUCTION

Antibodies are proteins whose primary function is the recognition of substances foreign to the host organism. An antigen can be identified as foreign if antibodies that are able to bind preferentially to specific molecular determinants of the antigen are present in the host. Once bound by antibodies, the foreign antigen can be removed by various effector functions.

Antibody Structure

Large glyco-proteins built on a common framework, each antibody unit consists of two light chains (25,000 daltons) and two heavy chains (50,000-70,000 daltons). The chains are arranged in a "dual Y" with the amino terminus of the heavy and light chains positioned at the same end of the molecule, resulting in a symmetrical molecule containing two binding sites (1, 2). The light and heavy chains are held together primarily by non-covalent interactions, but interchain disulfide bonds also help maintain the structural integrity of the antibody molecule (3). The light chain, heavy chain dimer (L_2H_2) is the basic antibody monomeric unit. Higher polymers of the L_2H_2 unit are formed as a result of disulfide bonds between the monomer and an accessory protein termed the "J" chain (4).

An analysis of the amino acid sequence of several antibodies has shown that there are regions of sequence

homology within each chain (2). The homology regions contain approximately 110 amino acid residues; there are two homology regions in the light chain and four or five homology regions in the heavy chain. The amino terminus homology unit of both the heavy and light chains is highly variable and forms the molecular basis of the specificity of the antibody. The sequence of the remainder of the heavy and light chains is constant and conserved within each antibody class (5, 6). The large degree of sequence conservation between homology units led Hill et al. (7) and Singer and Doolittle (8) to propose that the homology units are the result of repetitive gene duplication of a single ancestral gene.

The 3-dimensional structure of the antibody molecule also reveals regions of structural homology. X-ray structures of immunoglobulins (9) show that the homology units contain a highly conserved structure which Padlan (10) has called the "immunoglobulin fold." The main feature of this structure is a 4+3-stranded, anti-parallel beta-pleated sheet maintained by an absolutely conserved disulfide bond (11). Corresponding homology units from light and heavy chains form a compact globular domain. The integrity of the domain is maintained in part by interchain disulfide bonds, but primarily by non-covalent interactions. X-ray studies indicate that the antibody

molecule consists of a series of these globular domains connected by stretches of extended chain structure (12).

Antibody Binding Site

The antigen binding site is located in the variable domain, which consists of the N-terminal homology regions of the light and heavy chains. The amino acid sequence of the variable domains shows distinct regions that typically are even more variable than the rest of the variable domain (13). From three to 10 amino acid residues in length, these areas have been called the hypervariable regions.

X-ray crystallographic studies of F_{ab}' fragments of a mouse IgA and a human IgG show that the antigen binding site is a cleft (14), groove (15), or pocket (16) located at the end of the F_{ab}' fragment. Residues from the hypervariable regions of the heavy and light chains line the binding site, making it strongly dependent on the nature, sequence and number of amino acid residues in the individual hypervariable loops. This feature is the major factor in the different binding specificities exhibited by antibodies (10).

Repeating antigens of increasing length provided the first understanding of the size of the binding site of various antibodies. These studies indicated that the combining site will accommodate five linked carbohydrate residues (17) or a tetrapeptide (18). Electron spin

resonance studies of anti-DNP antibodies bound to haptens with spin labels of various lengths showed that the binding site is 10-12 Å deep (19). The electron microscopic study of the same system resulted in a value of 12-13 Å for the binding site depth (20). Thus, the specificity of antibody-antigen interactions is based upon recognition of a very small portion of the complete antigen by an equally small portion of the antibody molecule.

Nuclear magnetic resonance (NMR) also provides information about the specificity of binding interactions. Dwek et al. (21), used differences between the proton NMR spectra of bound and unbound anti-DNP antibody (M315) to propose a structure for the binding site. This structure was refined by Dwek, based upon the preliminary crystallographic data and model building studies of Padlan et al. (22). Further refinement of the binding site interactions was accomplished by using ^{19}F NMR and a fluorine labelled hapten to monitor the binding environment of the α-DNP antibodies (23, 24).

Specificity of Antibody-Antigen Interaction

Much work has been devoted to the elucidation of the nature of the antigen-antibody interaction. Early work by Nissonoff and Pressman (25) demonstrated the extreme specificity of the immune response. Antibodies are very sensitive to alterations in the structure of the haptens;

changes of as little as 1 Å in the conformation of the hapten can lead to a total loss of binding. All types of molecular interactions: coulombic attractions, hydrogen bonds, hydrophobic interactions, charge transfer complexes, and van der Waals contacts contribute to the binding specificity of an antibody (26). Specifically, the complementary ionic interaction of charged haptens with charged residues in the binding site is well established (27, 28, 29).

Chemical modification of the antibody binding site was used to identify the important residues and regions in the binding reaction. The use of haptens containing a reactive group (affinity labelling) showed that the hypervariable loops form the binding site (30, 31). Furthermore, Singer et al. (31), demonstrated that in most systems the majority of the contacts arise from heavy chain residues. Amino acid analysis of affinity labelled immunoglobulin has shown that only a limited number of amino acids are actually involved in the formation of the binding site. These studies also demonstrated large variations in labelling patterns of different proteins with affinity for the same hapten, indicating the wide response repertoire (32, 33).

Binding Kinetics

The kinetics of the binding interaction has been extensively studied and, in most cases, the association constant is of the order 10^8 M^{-1} sec^{-1} (34, 35). This is close to the theoretical limiting value of 10^9 M^{-1} sec^{-1} (36) and indicates that the activation barrier for association is very low. The difference in affinity of a given antibody and a series of haptens is generally due to differences in the rate of dissociation of the antibody-hapten complex (37, 38, 39). This argues that differences in affinity are due to differences in the activation energy of dissociation of the complex. Kooistra and Richards (23), using an NMR method called perturbation mixing, determined the association and dissociation rates for binding of DNP and DNP analogues to -DNP antibodies. The effects of amino acid substitutions on the kinetics of hapten-antibody interactions have also been studied by ^{31}P and ^{13}C NMR in a series of phosphorylcholine (PC) binding myeloma proteins (40).

Myeloma Proteins

The discovery of a malignant state of the plasma cell (plasmacytoma) increased our ability to study the antigen-antibody interaction at the molecular level (41). The myeloma proteins secreted by plasmacytomas permitted the study of homogeneous antibody preparations that

advanced our understanding of the mechanics of antibody action. About six percent of isolated myeloma proteins show a known antigenic specificity. Most of these proteins bind to 2,3-dinitrophenyl derivatives, polysaccharides or PC (41). It is generally believed that myeloma proteins represent a clonal expansion of the normal antibody repertoire of the animal (41). Direct evidence for this assumption in the case of PC binding myeloma proteins stems from the observation that immunization of mice with the hapten-carrier conjugate results in a response that is idiotypically identical to the most common myeloma idiotype (42, 43).

PC Binding Myeloma Proteins

The 11 known PC binding plasmacytomas (44, 45) were first observed to bind the pneumococcal type c polysaccharide (46). It was later shown that the antigenic specificity arose from the phosphorylcholine group (47).

Of the 11 myeloma proteins shown to bind PC, only five are idiotypically distinct: T-15, M603, W3207, M167 and M511. The rest have identical heavy chain sequences and are idiotypically identical to T-15. The five distinct proteins show high affinities for phosphorylcholine that are within an order of magnitude of each other (32, 48, 49). However, they vary greatly in their affinity for different PC analogues (47, 50), and have different affinity labelling

profiles (32, 48). Thus, these proteins provide an ideal model system in which to study the specific molecular interactions that contribute to antibody specificity.

Crystal Structure of a PC Binding Antibody

The three-dimensional structure of M603 F_{ab}' fragments was determined to 3.1 Å resolution (16), and provides the structural basis for the comparison of the molecular changes in the binding site of the other PC binding antibodies. The binding site of M603, a 12 x 15 x 20 wedge-shaped cavity, is lined exclusively by residues from the hypervariable regions of the heavy and light chains. The choline moiety intrudes into the cavity, in close van der Waals contacts with hydrophobic amino acid side chains, while the phosphate group is bound near the exterior of the cavity. In addition, M603 binds PC asymmetrically such that heavy chain residues provide most of the binding contacts (51). In fact, only a single light chain residue (96L) appears to contact the PC molecule (16). The importance of complementary ionic interactions in the binding of PC has been shown by chemical modification experiments (52) and by NMR studies (50), and is evident in the x-ray structure. The quaternary nitrogen of PC is stabilized by the acidic side chains of Glu_{35H} and Glu_{59H}; the negative phosphate group is stabilized by the ionic influence of Arg_{52H} and Lys_{54H}. The phosphate group is stabilized by hydrogen bonds

from Tyr_{33H} and Arg_{52H}, and the choline residue makes extensive van der Waals contact with residues from the first and third hypervariable regions of the light chain and Tyr_{33H} and Trp_{104aH}. The binding pocket allows the binding of the PC determinant when it occurs (as a phosphate diester) as part of a larger antigenic structure (50). Conversely, significant structural changes in the choline moiety cannot be tolerated because of the close complementary fit of the antibody to this portion of the hapten. The extent of the interaction of the hapten with the hypervariable loops is shown in Figure 14. The important contact residues are shown in Figure 15.

Examination of the Subsites of PC Binding Antibodies

The X-ray structure identifies three distinct interaction subsites (38). These sites are a positive, hydrogen bond donating subsite which interacts with the phosphate group; a hydrophobic subsite that would interact with the central methylene groups of PC; and a negatively charged subsite which interacts with the quaternary nitrogen. Specific interactions consistent with these subsite interactions are indicated in the three-dimensional structure of the binding site of M603 (16, 51). The specific interactions between the phosphate-binding subsite and the phosphate group of PC were extensively studied by ^{31}P NMR (50, 39), and the results were used to construct a

detailed description of these interactions. The results were also used in conjunction with amino acid sequence analysis of the other PC binding antibodies to show the effect of amino acid substitutions and other modifications on the specific interactions in the phosphate-binding subsites.

The choline subsite was probed, using ^{13}C NMR (40). However, the trimethyl ammonium group rotates freely, so that the ^{13}C nucleus sees an averaged picture of the binding site. Thus, information on the charge distribution and charge density is masked, and little information about the similarities and differences of the choline subsites of the PC binding proteins was obtained.

^{31}P NMR as a Probe of the Choline Subsite

The chemical shift of the ^{31}P nucleus is dominated by the paramagnetic term (53). The paramagnetic contribution to the shielding constant contains terms that are dependent upon the magnetic moment of the orbital electrons and is therefore dependent on the symmetry of the electron orbitals of the ^{31}P nucleus. Because of the large change in this symmetry upon ionization of the phosphate group, ^{31}P NMR has been used to monitor the ionization state of phosphate esters (54). The pH dependence of the phosphate resonance of PC when bound to several PC binding myeloma proteins has been used to provide information about the

specific molecular interactions between the phosphate group and the phosphate subsite (39, 40). The potential usefulness of PPC in examinations of the choline subsite arises from the sensitivity of the phosphorous chemical shift to changes in charge distribution, which might occur in the choline subsite. This chapter reports the use of a phosphorous-containing analog of choline as an NMR probe of the choline-binding site of these proteins.

MATERIALS and METHODS

Chemicals and Buffers

Buffer solutions were prepared by adding the appropriate buffer to a final concentration of 100 mM in distilled water. All saline-buffered solutions were 140 mM NaCl, and 50 mM in the appropriate buffer.

Phosphorylcholine Affinity Column

p-Diazonium phenylphosphorylcholine was prepared by the methods of Chesebro and Metzger (48) and Bird (55) as modified by Goetze (50). Choline iodide was prepared by adding methyl iodide to a 10-fold excess of dimethylaminoethanol in ether. The reaction mixture was stirred at room temperature for 16 hours. The white precipitate was washed with ether, dried in an Abderhalden and stored over potassium pentoxide. The yield was quantitative.

Stoichiometric amounts of choline iodide, p-nitrophenylphosphorodichloridate (Aldrich) and quinoline were dissolved in acetonitrile, which had been distilled and dried over barium oxide. The reaction mixture was kept in the dark at 0-4°C with stirring for six hours. At the end of this time, pyridine (0.6 volumes) and water (0.1 volumes) were added and the reaction mixture was allowed to rise to room temperature with continued stirring. Solvent was removed by evaporation, the product dissolved in water

and purified from starting material and reaction by-products by ion-exchange chromatography on Amberlite MB-3. The product, p-nitrophenylphosphorylcholine, was isolated from the eluate by lyophilization. The overall yield was 61%.

p-Diazoniumphenylphosphorylcholine was prepared from 1.2 mmol p-nitrophenylphosphorylcholine by reduction with $^1H_2$ and 5% palladium/charcoal in methanol. The catalyst was removed by filtration and the solvent removed by evaporation. The unstable amine was quickly dissolved in cold 1N HC1 and diazotized with $NaNO_2$. A small excess of $NaNO_2$ was used and, after completion of the diazotization reaction, destroyed by addition of urea. The p-diazonium phenylphosphorylcholine was used immediately.

The coupling procedure is a modification of the method described by March et al. (56). 100 ml (packed volume) of carefully washed Sepharose 4B, was suspended in 200 ml 2M Na_2CO_3. To this slurry, 10 ml of acetonitrile:CNBr (1:2, v:w) was added and the reaction mixture stirred vigorously for 20 minutes. At the end of the reaction, the activated gel was washed quickly with 500 ml of ice-cold bicarbonate buffer (pH 9.5) followed by chilled water and finally with bicarbonate-buffered saline (pH = 8.0). The activated gel was then stirred with 1 g glycyltyrosine for 24 hours at 4°C. Unreacted ligand was removed by extensively washing with chilled borate-buffered saline. At this point, 0.6 m

mole p-diazonium phenylphosphorylcholine was added to the derivatized sepharose in borate-buffered saline. The reaction mixture was stirred at room temperature for 12 hours, during which time an intense orange color developed. The gel was washed with chilled, borate-buffered saline until no orange color was evident in the wash. The gel was poured in a 2.5 cm x 20 cm column and stored in 1N acetic acid at 4°C to prevent base-catalyzed hydrolysis. The gel was equilibrated prior to use with the appropriate buffer.

Isolation of Phosphorylcholine Binding Antibodies

Ascites from mice containing the tumors McPC 603, TEPC 15 and MOPC 167 was collected by peritoneal lavage and stored frozen after centrifugation to remove cellular material. Ascites was thawed and brought to 45% ammonium sulfate by the careful addition of saturated ammonium sulfate solution. The solution was then stirred for 12-16 hours at 4°C. Precipitated protein was collected by centrifugation at 6.0 Kg for 20 minutes and redissolved in 2M Tris pH 8.6. The solution was reduced with 0.01 M dithiothreitol for one hour at room temperature. The pH was lowered to 8.0 by the addition of an equal volume of 2M Tris, pH 7.3, and alkylated with 0.01-0.03 M iodoacetamide for one hour at 4°C.

The protein solution was then applied to the PC-Sepharose affinity column, equilibrated with borate

buffered saline (BBS, 50 mM NaBorate, 140 mM NaCl, 0.02% NaN_3) or with HEPES-buffered saline (HBS, 50 mM HEPES, 140 mM NaCl, 0.02% NaN_3) pH 7.4. The column was washed with the appropriate buffer until the absorbance at 280 nm had reached background levels. The PC binding protein was immunospecifically eluted with 10 mM PC in BBS or with 1.0 M choline in HBS. The protein solution was then dialyzed extensively to remove bound hapten and then concentrated by ultrafiltration in an Amicon diaflow apparatus with a PM-10 membrane.

F_{ab}' fragments of T-15 and M603 were prepared by limited pepsin digestion (50, 57). To purified protein (10 mg/ml in 0.05 M sodium acetate, pH 4.7) 1% pepsin (2x recrystalized Sigma, 4100 units/mg) was added. The solution was allowed to sit at 37°C for six hours, during which time large amounts of precipitated protein appeared. The precipitate redissolved upon raising the pH to 7.4. The entire digestion mixture was applied to the PC-Sepharose affinity column equilibrated with HBS, and protein which retained binding activity was eluted with 3 mM PC or 1.0 M choline. The protein solution was dialyzed extensively against HBS and concentrated by ultrafiltration.

Synthesis of 2-(trimethylphosphonio)-ethyl Phosphate

2-(Trimethylphosphonio)-ethyl phosphate (phosphoryl-phosphocholine, PPC) was synthesized by an adaptation of

the method of Edwards and Hands (58). 2-Hydroxyethyltrimethylphosphonium chloride was prepared by the method of Renshaw and Bishop (59). Distilled 2-chloroethanol (10.5 ml) and 17.0 ml ethanol were placed in a pyrex bomb. The solution was degassed by repeated freeze-thaw cycles under vacuum. To the degassed solution, trimethylphosphene (10.0 g Orgmet Chemical Co.) was added under one atmosphere nitrogen. The reaction flask was sealed and heated to 100°C in an oil bath for seven hours. The reaction mixture was then cooled to room temperature and allowed to stand for 16 hours. At the end of this reaction time the reaction mixture was diluted with ethanol. Phosphocholine chloride was precipitated by the addition of ethyl ether. The phosphocholine chloride was immediately dissolved in 2 l. dried acetone containing 1956 g NaI. The reaction mixture was refluxed for 14 hours. The precipitate that appeared during this time was filtered and the solvent removed under reduced pressure. The white solid was redissolved in a minimum amount of ethanol and phosphocholine iodide was precipitated by the addition of ethyl ether (25.0 g, 76% yield).

Phosphocholine iodide (35.70 mmol) was dissolved in 36 ml dry pyridine and 36 ml acetonitrile. The reaction mixture was cooled to 4°C and kept in the dark. Methylphosphorodichloridate (36.0 mmol, Aldrich) was slowly added with vigorous stirring. The reaction mixture was

allowed to rise to room temperature and then stirred for 12 hours. The reaction mixture was cooled to 4°C, 10.5 ml H_2O was added and stirring continued for one hour. The syrup left upon removal of solvent was dissolved in 1 l H_2O and passed through a mixed bed column of Amberlite IR-120 (^1H) and IRA-400 (formate) ion-exchange resin. The column was then thoroughly washed with water. The eluate from the column was lyophilized, leaving PPC as a white powder (2.2 g, 30% yield).

Binding Assays

Equilibrium dialysis was performed in 2 ml compartments in lucite cells, using reduced and alkylated IgA monomers or F_{ab}' fragments at concentrations of 6.0-15.0 x 10^{-6} M. Protein concentration was determined from the absorbance at 280 nm using ϵ = 1.36. This value was reported by A. Goetze (50) and was confirmed for M603 by absorbance measurements of weighed, lyophilized protein samples. A molecular weight of 150,000 for the IgA monomer and 55,000 for the F_{ab}' fragment was assumed in the calculations.

Phosphoryl (methyl ^{14}C) choline was obtained from New England Nuclear. A 0.5 mM stock solution of labelled PC was prepared and appropriate aliquots were added to the non-protein chamber, adjusting the final volume to 2.0 ml by the addition of buffer. The cells were then agitated for

18-24 hours at a constant temperature. One ml aliquots from both the protein and non-protein chamber were dissolved in 210 ml Aquasol scintillation cocktail (New England Nuclear). Samples were counted on a Beckman scintillation counter and contained 100-12,0-00 cpm. Counting time ranged from five to 20 minutes and the average counting error was 1.0%

The data were plotted as R/[H] vs R where:

$[H]$ = unbound hapten concentration

$R = \frac{[AbH]}{[Ab]_t}$

$[AbH]$ = antibody bound hapten concentration

$[Ab]_t$ = total antibody concentration.

A least-squares fit was used to obtain the best straight line through the data points.

The binding affinities for the hapten PPC were determined indirectly by inhibition of phosphoryl (methyl-^{14}C) choline binding. 2 ml of a 5-15 x 10^{-6} M protein solution was placed on one side of a series of equilibrium chambers. The opposing chambers contained a stoichiometric concentration of labelled PC and increasing concentrations of PPC. A control chamber contained equal concentrations of labelled and unlabelled PC. After equilibration and counting, an inhibition curve of protein-bound cpm vs PPC concentration was drawn and the concentration that resulted in the same protein-bound cpm as the control was found. The relative affinity of antibody

for PPC is equal to the ratio of unlabelled PC in the control chamber to the PPC concentration, which gave 50% inhibition. The absolute affinity was then calculated by using the known affinity for PC.

Preparation of Samples for NMR Experiments

Protein samples that had been extensively dialyzed against HBS or BBS and concentrated by ultrafiltration were used in the NMR experiments. NMR samples were made 1-2 mM (IgA monomers) or 2-4 mM (F_{ab}' fragments) by adding the required amount of buffer to the concentrated stock solution. Hapten was added as small aliquots of a concentrated (200 mM) solution in buffer, pH 7.0, to achieve the desired hapten concentration.

The samples used in NMR titration experiments were prepared in a similar manner. Titrations were begun at high pH by preparing the protein sample in buffer of the appropriate pH. Samples were titrated to low pH by the addition of 1 N HC1. With careful addition of HCl, it was possible to prevent protein precipitation above pH 3.0. The pH of each sample was measured immediately after each experiment.

NMR Experiments

NMR spectra were obtained on a Varian XL-100-15 spectrometer interfaced with a Varian 620i computer and

operated in the Fourier transform mode. Phosphorus spectra were obtained at 40.5 MHz and were proton-noise decoupled. The probe temperature was maintained at 25.0 $\pm$ 0.5°C. An external deuterium lock was provided by a 5 mm capillary insert containing D_2O. Data were accumulated with a pulse width of 55 μsec (flip angle of 40°), which was chosen to prevent saturation of the signal with the 0.3-0.4 sec accumulation time. The spectral width was set at 2500 Hz, and the filter chosen to optimize the signal. Spectra were usually recorded with 75,000 to 100,000 transients, and the resulting FID was exponentially weighted to increase the signal-to-noise ratio.

Gel Electrophoresis

The discontinuous gel electrophoresis system of Laemmli (60) was used to monitor the purity of material from the affinity isolation procedure.

Amino Acid Numbering

The amino acid numbering system for the heavy chain is that used by Rudikoff and Potter (61) for M603. The light chain amino acid numbering system is that of Barstad et al. (62).

RESULTS

Affinity Purification of T-15, M603 and M167

Reduced and alkylated ascites protein was applied to the PC-Sepharose affinity column and PC binding antibody immunospecifically eluted with 3 mM PC in BBS. Figure 1 shows a typical UV absorption profile of the eluate from the affinity column. Washing the column with 1 N acetic acid resulted in little or no protein being eluted from the column. SDS disc gel electrophoresis of the immunospecifically eluted protein showed a single band with an apparent molecular weight of 150 Kd. This material, when reduced and run on SDS gel electrophoresis showed two bands at apparent molecular weights of 24 Kd and 55 Kd corresponding to light chain and heavy chain, respectively.

Reapplying the breakthrough peak to the affinity column resulted in a small amount of protein immunospecifically binding to the column. This binding generally amounted to 2-5% of the protein that was specifically bound from the first pass through the affinity column. This occurred regardless of the total amount of protein that was applied to the column, indicating that the column was not being overloaded, but that the column did not remove all protein with PC specificity from a given sample.

To remove the PC that was used to elute the antibody from the affinity column, the protein sample was

extensively dialyzed against BBS or HBS. The extent of dialysis was followed by ^{31}P NMR, and it was found that 10-12 buffer changes (30:1 buffer:sample) over a six-day period were required to reduce the PC concentration to the point where 87% of the antibody was free. In an effort to speed up the purification, dialysis was carried out at high pH (8.0-8.5) and low pH (4.5-6.5). High pH did not appreciably increase the rate at which PC could be removed by dialysis, and low pH resulted in faster removal of PC, but also had a tendency to precipitate the protein.

Elution of the specifically bound antibodies was also accomplished with 1.0 M choline in HBS. The elution profile of material isolated with choline is shown in Figure 2. Elution with 3 mM PC following elution with choline did not result in the isolation of additional PC binding protein. Dialysis of material eluted with choline against four changes of buffer, pH 6.0, for 24 hours was sufficient to remove most hapten (97%).

Hapten Binding Studies

Scatchard plots of PC binding to reduced and alkylated T-15, M167 and M603 IgA monomers are shown in Figures 3-5. The equilibrium dialysis data were fit using a linear least-squares analysis. The resulting curves are linear with correlation coefficients from 0.98 to 0.99. The curves extrapolate close to the expected two binding sites per IgA

monomer. The association constants determined in this work are summarized in Table 1.

A typical inhibition curve used to determine the association constants of T-15, M603 and M167 for PPC is shown in Figure 6. From this curve, it is seen that 50% inhibition of PC binding is obtained with an equimolar concentration of PPC. This is typical of all three proteins that were studied, and the other inhibition curves are identical. The PPC association constants are given in Table 1.

The pH dependence of the association constant of M603 for PC and PPC is shown in Figure 7. As can be seen from the graph, the affinities for PC and PPC show identical behavior over the pH range studied. The affinity of M603 for PPC reaches a maximum at pH 7.0 and does not decrease appreciably as the pH is raised to 8.5. However, as the pH is lowered from pH 7.0, a significant drop in the affinity constant is observed. This decrease amounts to a 25-fold decrease in affinity between pH 4.0 and 7.0. Furthermore, the decrease in log K_a (with pH) is not linear, with the slope increasing as the pH is lowered. The NMR titration cures for PC and PPC are shown in Figure 8. The phosphate groups of both PC and PPC show a 3.7 ppm upfield shift upon monoprotonation. While the total shifts of PC and PPC are identical, PPC shows a slight upfield shift compared to PC in both the dianionic and monanionic states of about 0.15

ppm. The pK_a of PPC is shifted to higher pH, from 5.3 $\pm$ 0.1 for PC to 5.7 $\pm$ 0.1 for PPC. The phosphonium resonance of PPC is pH-independent over the range 3-9, and shows a downfield shift of 25.7 ppm from 85% H_2PO_4. A proton noise decoupled spectrum of PPC is shown in Figure 9. The transverse relaxation times of PPC bound to T-15 were determined using a progressive saturation pulse sequence. The spectra used in determining the T_1 values of the phosphate and phosphonium phosphorous nuclei are shown in Figure 10. The T_1 values obtained from these data, using a three-parameter exponential fit, are 3.0 $\pm$ 0.1 seconds for the phosphonium resonance and 2.5 $\pm$ 0.2 seconds for the phosphate resonance. This compares to 12.0 $\pm$ 2.0 seconds for the phosphonium resonance and 7.4 $\pm$ 2.0 seconds for the phosphate resonance in free PPC. As these values were obtained using a progressive saturation pulse sequence, they are therefore subject to large systematic error due to small deviations from the 90° pulse, pulse inhomogeneity or phase errors and long longitudinal relaxation times which do not allow complete dephasing of the signal between acquisition sequences. Because of the possibility of systematic error, these T_1 values were used as a rough guide for determining the optimum flip angle and acquisition times for data acquisition, and were not used for other purposes.

The pH dependence of the observed chemical shifts for PPC bound to T-15 (Figure 11), M167 (Figure 12), and M603 (Figure 13) is shown in the following figures. The phosphate resonances of PPC bound to all three proteins have the same chemical shift as PC bound to the proteins. For T-15 and M603, binding of PPC results in a 1.3 ppm upfield shift relative to free PC at pH greater than 7.5. At pH 3.0, the difference between the free chemical shift and the bound chemical shift is 0.6 ppm upfield for T-15 and 0.37 ppm upfield for M603. At intermediate pH values, the titration curves are identical within experimental error and show a pK_a value of 4.7 $\pm$ 0.2, compared to the pK_a of 5.3 $\pm$ 0.1 for PC and 5.7 $\pm$ 0.1 for PPC. The phosphate resonance of PPC bound to M167 shows a downfield shift of 0.40 $\pm$ 0.05 ppm compared to free hapten. At low pH (5.0) there is a small (0.15 ppm) downfield shift when compared to the free hapten. The PPC phosphate resonance titrates between these two extremes with a pK_a of 6.0 $\pm$ 0.1.

The phosphonium resonance of PPC, when bound to T-15 or M167, shows a small (0.1 ppm) upfield shift, which is pH independent over the range 3.0 to 8.0. The phosphonium resonance exhibits a 2.7 ppm upfield shift when bound to M603 at pH 6.5 or above. Below pH 6.0, the observed chemical shift is both concentration- and pH-dependent.

The experiments cited above were carried out with antibody excess. To determine whether conditions of slow exchange were met over the range studied, spectra were recorded with hapten excess at the pH extremes. For T-15 and M167, this showed two separate resonances for the phosphate signal over the pH range 3.5 to 8.5. This indicates that conditions of slow exchange existed and that the observed chemical shifts were indeed bound chemical shifts. For M603, the situation is different. At a onefold excess of hapten over antibody, two phosphonium resonances are observed above pH 6.0. These have the chemical shift of free and bound PPC. At pH less than 6.0, the peaks coalesce and give a single resonance, indicating moderate to fast exchange. With a onefold excess of hapten, the phosphate resonance is in fast exchange at pH less than 7.0. Thus, the observed chemical shifts do not represent the bound chemical shifts, but rather a weighted average of the bound and free chemical shifts. The bound chemical shift may be calculated, using the known pH dependence of the affinity constant and the hapten and antibody concentration.

DISCUSSION

Antibody Isolation and Purification

SDS gel electrophoresis indicates that the protein (either IgA monomers or F_{ab}' fragments) eluted from the PC affinity column is pure and does not require a further purification step. NMR results showing 13% of the antibody still bound to PC after extensive dialysis demonstrate the high affinity of these proteins for PC. In an effort to decrease the time required to remove the hapten used as an eluant, haptens with lower affinities for these proteins were sought. Choline exhibits affinities that are 5 (M167) to 870 (M603) fold less than the corresponding PC affinities (39). Thus, 1.0 M choline was used as an eluant. Since a subsequent wash of the affinity column with 3 mM PC did not result in the elution of additional material, and material eluted with choline was electrophoretically identical to material eluted with PC, it appears that choline can be used effectively as an eluant in the isolation procedure. Furthermore, because of the lowered affinity of the proteins toward choline, removal of the hapten by dialysis is much more rapid. Therefore, elution by choline is a practical alternative to elution with PC followed by extensive dialysis.

Binding Constants

The affinity constants for PC binding to T-15, M603 and M167 reported in Table 1 are in good agreement with previously reported values (32, 41, 49, 50, 62). The affinity constants of T-15, M603 and M167 for the PC analogue PPC are 97% to 105% of the respective PC affinities. These experimentally identical values are one indication that these proteins bind PPC with a similar if not identical mechanism as PC.

The pH dependence of the affinity constant of M603 for PPC measured at 25°C mimics the pH dependence of the K_a for binding to PC measured at 0°C (Figure 7) (50). The K_a (vs pH) values obtained at 25°C are uniformly 0.3 times the values reported at 4°C, indicating that the temperature dependence of the affinity constants are not pH dependent. The similarity of the pH dependence of the binding constants of these proteins for PPC and PC is a further indication that the proteins see these two haptens in a similar, if not identical, manner.

The affinity constants reported here were obtained using reduced and alkylated IgA monomers under conditions used in the NMR experiments. Two exceptions were necessary; the protein concentrations were two orders of magnitude higher in the NMR experiments; also in most NMR experiments, F_{ab}' fragments were used in place of IgA monomers. Sher et al. (45) have shown that the affinity

constants are independent of antibody concentration, and Goetze (50) reported similar binding results for IgA monomers and F_{ab}' fragments. Accordingly, one can assume that the binding constants in the NMR experiments were equivalent to those obtained by equilibrium dialysis.

Interactions of PPC at the Phosphate Subsite of T-15 and M603

At pH greater that 7.5, the phosphate ^{31}P resonance of PPC bound to T-15 and M603 exhibits an upfield shift of 1.3 ppm compared to the free hapten. The chemical shift of bound PPC is equal to the observed shift of PC bound to these proteins (50). The fact that these two haptens show identical phosphate shifts when bound to T-15 and M603 indicate that the specific interactions between the phosphate subsites of T-15 and M603 and the phosphate groups of these two haptens are essentially identical. The observed ^{31}P shift of the phosphate group of PC when bound to M603 has been attributed to the formation of specific hydrogen bonds from Tyr_{33H} and Arg_{52H} of the antibody to the phosphate oxygens of bound hapten (39). The results of this work indicate that these specific interactions are maintained when PPC is bound by T-15 and M603.

The pK_a of PPC is lowered from 5.8 in solution to 4.8 when bound to T-15 or M603. This is equal to the pK_a of PC

when bound to these proteins, and examination of the titration curve of these two haptens bound to T-15 (Figure 11) and M603 (Figure 13) show that the titration curves are identical. The lowering of the pK_a of PC upon binding has been attributed to the electropositive ionic influence of the phosphate-binding subsites of these two proteins (50).

Interactions of PPC at the Phosphate Subsite of M167

The pH dependence of the phosphate ^{31}P resonance of PPC bound to M167 is shown in Figure 12. The phosphate group of PPC apparently experiences the same environment as the phosphate group of PC when bound to M167 as indicated by the identical titration curves. The pK_a of the phosphate group is raised to 6.0 and the phosphate resonance shows a downfield shift at pH about 7.5. It has been suggested that these differences are due to amino acid substitutions in the phosphate subsite (Asp_{56H}--> His, Thr_{58aH}--> Arg, Trp_{104aH}--> Gly; see Figure 16) that alter the structure of the subsite such that the hydrogen bonding and electrostatic interactions characteristic of T-15 and M603 are not possible in M167. These results support the conclusion that PPC and PC share the same binding interactions at the phosphate binding subsite even in widely different antibodies.

Interactions at the Choline Subsite

The phosphonium resonance of PPC bound to T-15 and M167 shows an upfield shift of 0.1 ppm compared to the free hapten (Figures 11 and 12). This shift is pH independent over the range 3.0 - 9.0 as is the resonance of the free hapten. The bound shift of the phosphonium phosphorous of PPC bound to M603 is shown in Figure 17, where the effects of fast exchange and the lowered affinity constant at pH less than 5.5 have been subtracted. It is evident that above pH 6.0, binding of PPC results in an upfield shift of 2.7 ppm, and that this bound shift titrates at pH less than 5.5 with a pK_a of 3.6. These results indicate that T-15 and M167 have similar choline subsites and that M603 has a choline subsite that is significantly different. ^{13}C NMR studies of the methyl group of the PC hapten (40) bound to T-15, M603 and M167 provide indirect support of this observation. Binding of PC to T-15 and M167 results in an upfield shift of 1.2 - 1.4 ppm, while binding to M603 resulted in a smaller upfield shift of 0.7 ppm. None of these ^{13}C shifts were pH-dependent.

The Choline Subsite of T-15 and M167

The small upfield shift observed upon binding of PPC to M167 and T-15 suggests that the bound environment of the phosphonium moiety is not significantly different from the environment that it experiences in solution. The contact

residues of the choline subsite of T-15 and M167 are contributed by the heavy chain (Figure 15), specifically Asp_{99H}, Glu_{35H} and Glu_{59H}. The presence of three acidic residues in close proximity to the positive phosphonium group creates a symmetric anionic environment that stabilizes the positive charge of the phosphonium group and probably mimics the magnetic environment of the hapten in solution.

In addition to the contact residues, the first and third hypervariable regions of the heavy chain are in close proximity to the choline subsite. The first hypervariable regions of T-15 and M167 are identical and exhibit a 60% polar nature. The third hypervariable region of M167 contains four amino acid substitutions and two insertions (Figure 16). However, the overall polar nature of the third hypervariable segment is maintained in both proteins.

Residues 30e-35 of the light chain are in close proximity to the choline subsite (Figure 14) and might contribute to the microenvironment experienced by the phosphonium moiety. Figure 18 shows that M167 contains a deletion and two amino acid substitutions in this region, compared to T-15. These changes alter the nature of this region from 67% nonpolar in M167. However, because of the similarity of the observed chemical shift of the bound phosphonium resonance to T-15 and M167, it is unlikely that

the light chain provides major contributions to the environment of the choline subsite.

For these reasons, it seems likely that the major contributions to the environment of the choline subsite stem from the heavy chain, particularly the amino acids of the first hypervariable region. Furthermore, the fact that the phosphonium resonance does not titrate over the pH range 3.0 to 9.0 indicates that the observed upfield shift is probably not due to diamagnetic shielding of the phosphonium group by the anionic residues Asp_{99H}, Glu_{59H} and Glu_{35H} (Figure 18). Instead, it seems likely that the small (0.1 ppm) upfield shift is due to paramagnetic deshielding, a difference in conformation of the bound hapten compared to the conformation of the hapten in solution, the polar nature of the choline subsite, or a combination of all three. Such mechanisms have been used to explain the larger ^{13}C methyl group shifts (39).

Alternatively, the carboxylate residues could titrate with pK_a's less than 3.0, examples of which have been reported in the literature (63). Regardless of the precise assignment of the origin of the bound shift, the important observation is that the environment of phosphonium group of PPC bound to T-15 and M167 is very similar to the environment of the free hapten, and that this environment is not pH-dependent.

The Choline Subsite of M603

Compared to T-15 and M167, M603 exhibits a different choline subsite. This is demonstrated by the upfield shift of 2.7 ppm of the phosphonium group when bound by M603. In addition to the large chemical shift, the bound chemical shift is tritratable with a pK_a of 3.6. Comparison of the slope of this titration curve with that of calculated titration curves of one, two and three ionizations indicates that more than one but less than three residues are titrating over this range. The structural changes that lead to this behavior may be deduced by comparing the binding sites of M603 and T-15. Of the interactions described above for T-15 and M167, the most significant change is the amino acid substitution, Asp_{99H}--> Asn. This single amino acid substitution decreases the local anionic environment and destroys its symmetry. The change in symmetry of the anionic environment of the choline subsite perturbs the symmetry of the phosphonium group, resulting in paramagnetic deshielding of the phosphorous nucleus and an upfield shift relative to the free hapten. As the acidic residues Glu_{59H} and Glu_{35H} titrate, the resulting decrease in the charge density would cause less perturbation of the phosphonium group and would result in a downfield shift as is observed.

A report published after the completion of this work (64) suggested that PPC bound to M603 exhibited a smaller

upfield shift than we observed. The authors observed that the phosphonium resonance titrates below pH 5.0, and that only one residue (Asp_{97L}) titrated. At first glance these observations seem to contradict the results presented here. However, Gettins conducted his experiments under conditions of hapten excess, and did not consider that PPC is in fast exchange under these conditions, claiming that slow exchange conditions were met over the entire pH range. Both hapten excess and fast exchange can decrease the apparent chemical shift and mask the titration of the phosphonium resonance. Even as a twofold excess of hapten reduces the observed chemical shift (Figure 7), larger hapten excess reduces the observed shift even more.

It has been suggested (65) that Asp_{97L} can participate in the formation of the symmetric anionic environment of the choline subsite. However, the ^{31}P NMR results presented here indicate that the choline environment of M603 is not symmetric, and that residues from the light chain do not participate in the formation of the choline subsite.

The asymmetry of the anionic environment created by the substitution Asp_{99H}--> Asn would cause the hapten to be bound asymmetrically in the binding cleft to maximize the ionic interactions between the hapten and the remaining negative charges of the choline subsite. This is indeed seen in the x-ray crystallographic model (16). The asymmetric binding causes the hapten to be closer to Tyr_{33H}

than would be expected if the hapten were bound toward the center of the binding cavity. This proximity might result in an upfield shift caused by diamagnetic shielding due to the ring current of Tyr_{33H}.

The results presented here support the view that the major contributions to the choline subsite of PC-binding proteins are from the heavy chain (62). This is evident from the relatively small, if any, effect that amino acid substitutions in the first hypervariable region of the light chain have on the microenvironment of the choline subsite (compare T-15 and M167). However, the choline subsite is extremely sensitive to a single amino acid substitution in the second hypervariable region of the heavy chain (compare T-15 and M603). This demonstrates the importance of this region in the formation of this subsite.

REFERENCES

1. Lennox, E.S. and Cohn, M. (1967) **Ann. Rev. Biochem. 36**, 365.
2. Edelman, G.M. and Gall, W.E. (1969) **Ann. Rev. Biochem. 38**, 415.
3. Edelman, G.M. and Poulik, M.D. (1961) **J. Exp. Med. 113**, 861.
4. Frangione, B. and Milsten, C. (1969) **Nature (London) 224**, 597.
5. Smith, G.P., Hood, L.E. and Fitch, W.H. (1971) **Ann. Rev. Biochem. 40**, 969.
6. Dreyer, W.S. and Bennet, J.C. (1965) **Proc. Natl. Acad. Sci. USA 54**, 864.
7. Hill, R.L., Delayney, R., Fellows, R.E. and Lebowitz, H. (1966) **Proc. Natl. Acad. Sci. USA 56**, 1762.
8. Singer, S.J. and Doolittle, R.F. (1966) **Science 153**, 13.
9. Poljak, R.J., Amzel, L.M., Avery, H.P., Chen, B.L., Phizackerley, R.P. and Saul, F. (1973) **Proc. Natl. Acad. Sci. USA 70**, 3305.
10. Padlan, E.A. (1977) **Quart. Rev. Biophys. 10**, 35.
11. Davies, D.R., Padlan, E.A. Segal, D.M. (1975), **Ann. Rev. Biochem. 44**, 639.
12. Huber, R., Deisenhofer, J., Colman, P.M., Matsushima, M. and Palm, W. (1976) **Nature 264**, 415.
13. Wu, T.T. and Kabat, E.A. (1970) **J. Exp. Med. 132**, 211.

14. Amzel, L.M., Poljak, R.J., Saul, F., Varga, J.M. and Richards, F.F., (1974) **Proc. Natl. Acad. Sci. USA 71**, 1427.

15. Poljak, R.J., Amzel, L.M., Avery, H.P., Chen, B.L., Phizackerley, R.P. and Saul, F. (1974) **Proc. Natl. Acad. Sci. USA 71**, 3440.

16. Segal, D.M., Padlan, E.A., Cohen, G.H., Rudikoff, S., Potter, M. and Davies, D.R. (1974) **Proc. Natl. Acad. Sci. USA 71**, 4298.

17. Kabat, E.A. (1960) **J. Immunol. 84**, 82.

18. Schecter, I. (1970) **Nature (London) 228**, 639.

19. Hsia, J.C. and Piette, L.N. (1969) **Arch. Biochem. Biophys 129**, 296.

20. Valentine, R.C. and Green, N.M. (1967) **J. Mol. Biol. 27**, 615.

21. Dwek, R.A. (1977) Contempory Topics in Molecular Immunology, Vol 6, R.R. Porter and G.L. Ada, eds., Plenum Press, New York and London, pg 1.

22. Padlan E.A., Davies, D.R., Pecht, I., Givol, D. and Wright, C.F. (1976) **Cold Spring Harbor Symp. Quant. Biol. 41**, 627.

23. Kooistra, D.A. and Richards, J.H. (1978) **Biochemistry 17**, 345.

24. Hardy, R.R. and Richards, J.H. (1978) **Biochemistry 17**, 3866.

25. Nissonoff, A. and Pressman, D. (1957) **J. Am. Chem. Soc. 79**, 1616.

26. Karaush, F. (1962) **Adv. Immunol. 2**, 1.

27. Grossberg, A.L. and Pressman, D. (1968) **Biochemistry 7**, 272.

28. Freedman, M.H., Grossberg, A.L. and Pressman, D. (1968) **Biochemistry 7**, 1941.

29. Pressman, D. and Siegel, M. (1953) **J. Am. Chem. Soc. 75**, 686.

30. Wofsy, L., Metzger, H. and Singer, S.J. (1966) **Science 153**, 13.

31. Singer, S.J., Slobin, L.I., Thorpe, N.O. and Fenton, J.W. (1967) **Cold Spring Harbor Symp. Quant. Biol. 32**, 99.

32. Metzger, H.J., Chesebro, B., Hadler, N.M., Lee, J. and Otchin, N. (1971) **Prog. Immunol. 1**, 253.

33. Chesebro, B., Hadler, N. and Metzger, H. (1973), "Specific Receptors of Antibodies, Antigens and Cells", **3rd Intl. Convoc. Immunol.**, Buffalo, New York, 1972, p. 205 (Karger, Basel, 1973)

34. Froese, A. and Sehon, A.H. (1975) **Contemp. Topics Mol. Immunol. 4**, 23.

35. Pecht, I. and Lancet, D. (1976) Chemical Relaxation in Molecular Biology, R. Rigter and I. Pecht, eds., Springer-Verlag, Heidelberg.

36. Froese, A. and Sehon, A.H. (1965) Immunochemistry 2, 135.

37. Smith. T.W. and Skubitz, K.M. (1975) Biochemistry 14, 1496.

38. Haselkorn, D., Friedman, S., Givol, D. and Pecht, I. (1974) Biochemistry 13, 2210.

39. Goetze, A.W. and Richards J.H. (1977) Biochemistry 16, 228.

40. Goetze, A.W. and Richards J.H. (1978) Bichemistry 17, 497.

41. Potter, M. (1972) Physiol. Rev. 52, 684.

42. Clafin, J.L. and Davie, J.M. (1974) J. Immunol. 113, 1678.

43. Cosenza, H. and Kohler, H. (1972) Science 276, 1027.

44. Potter, M. and Lieberman, R. (1970) J. Exp. Med. 132, 737.

45. Sher, A., Lord, E. and Cohn, M. (1971) J. Immunol. 107, 1226.

46. Glaudemans, C.P.J., Manjula, B.N., Bennett, L.G. and Bishop, C.T. (1977) Immunochemistry 14, 675.

47. Leon, M.A. and Young, N.M. (1971) Biochemistry 19, 1424.

48. Chesebro, B. and Metzger, H. (1972) Biochemistry 11, 766.

49. Pollet, R. and Edelhoch, H.J. (1973) J. Biol. Chem. 248, 544.

50. Goetze, A.W. (1978) Ph.D. Dissertation, California Institute of Technology, California.

51. Padlan, E.A., Davis, D.R., Rudikoff, S. and Potter, M. (1976) **Immunochemistry 13**, 945.

52. Grossberg, A.L., Krausz, L.M., Rendina, L. and Pressman, D. (1974) **J. Immunol. 113**, 1807.

53. Emsly, J.W., Feeney, J. and Sutcliffe, L.H. (1966) "High Resolution Nuclear Magnetic Resonance Spectroscopy," Vol. 2, Pergamon Press, London, pg. 1054.

54. Cohn, M. and Hughes, T.R. (1960) **J. Biol. Chem. 235**, 3250.

55. Bird, P.R. (1967) **J. Chem. Soc., C**, 447.

56. March. S.C., Parikh, I. and Cuatrecasas, P. (1974) **Anal. Biochem. 60**, 149.

57. Inbar, D., Rotman, M. and Givol, D. (1971) **J. Biol. Chem. 246**, 6272.

58. Edwards, R.G. and Hands, A.R. (1976) **Biochim. Biophys. Acta 431**, 303.

59. Renshaw and Bishop

60. Laemmli, U.K. (1970) **Nature (London) 277**, 680.

61. Rudikoff, S. and Potter, M. (1974) **Biochemistry 13**, 4033.

62. Barstad, P., Rudikoff, S., Potter, M., Cohn, M., Konigsberg, W. and Hood, L. (1974) **Science 183**, 962.

63. Hartsuck, J.A. and Tang, J. (1972) **J. Biol. Chem. 247**, 2575.

64. Gettins P., Potter, M., Leatherbarrow, R.J., Dwek, R.A. (1982) **Biochemistry 21**, 4927.

65. Satow, Y., Cohen, G.H., Padlan, E.A. and Davies, D.R. (1986) **J. Mol. Biol. 190**, 593.

FIGURE 1

Affinity Isolation of T-15

The affinity column UV (A_{280}) profile of ascites fluid from mice containing the tumor T-15. Peak A is protein that is not specifically bound by the affinity column. Peak B was immunospecifically eluted with 0.003 M PC.

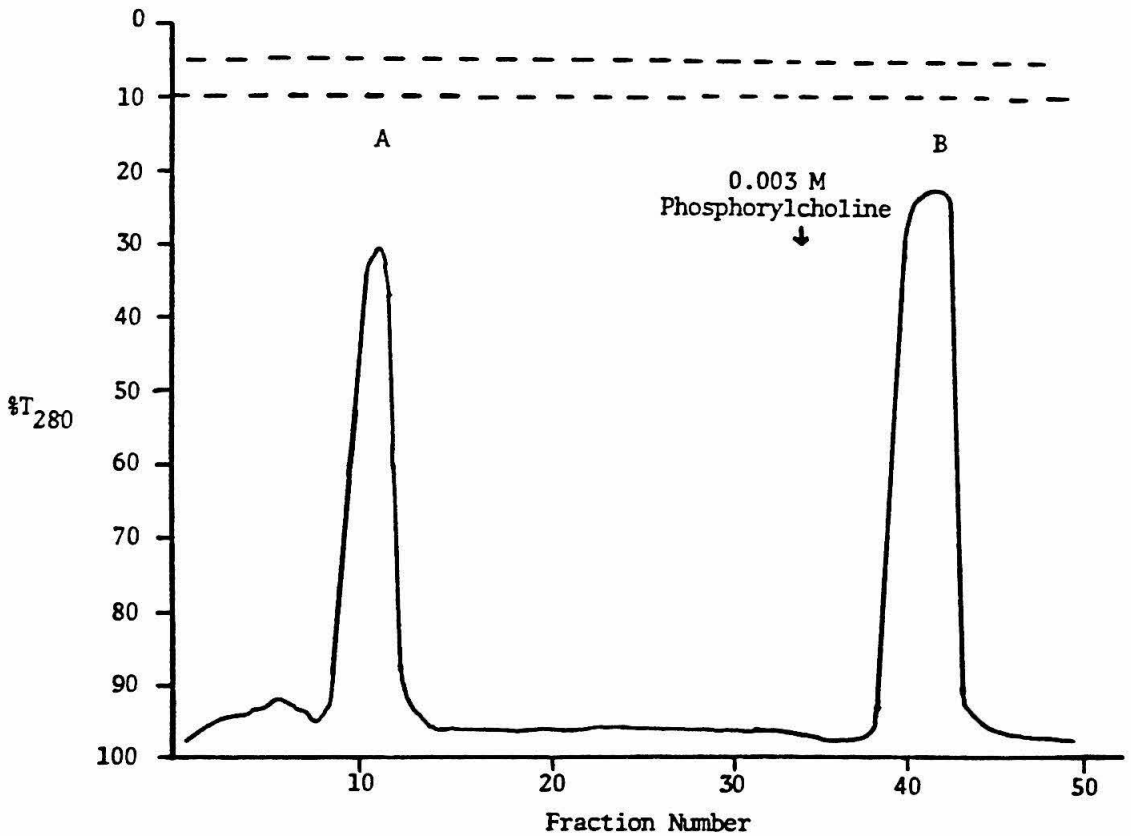
0
10
20
30
40
50
60
70
80
90
100
%T280
A
B
0.003 M
Phosphorylcholine
10
20
30
40
50
Fraction Number

FIGURE 2

Affinity Isolation of M603

The affinity column UV (A_{280}) profile of ascites fluid from mice containing the tumor M603. Peak A is protein that is not specifically bound by the affinity column. Peak B is protein immunospecifically eluted with 1.0 M choline. Peak C was eluted with 0.003 M PC.

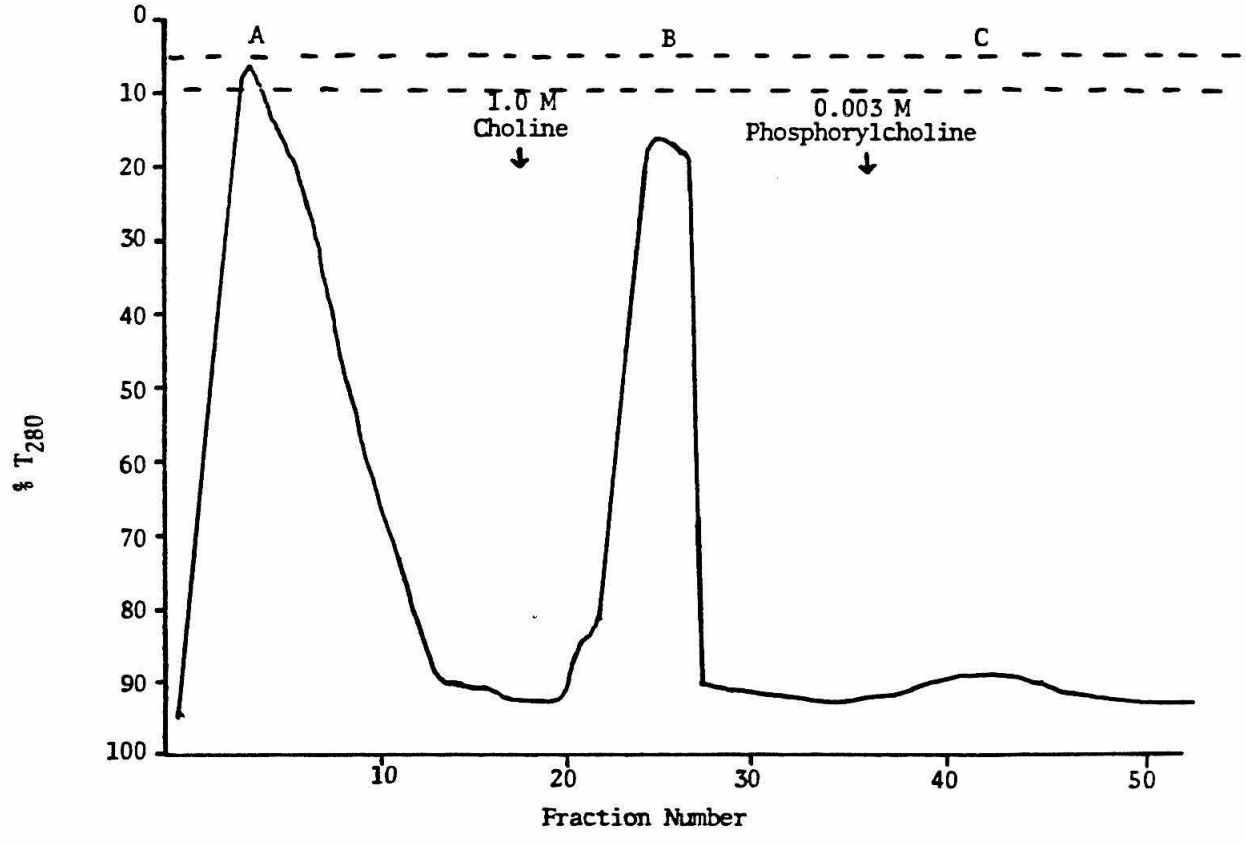
A
B
C
1.0 M
Choline
0.003 M
Phosphorylcholine
% T_{280}
0
10
20
30
40
50
60
70
80
90
100
10
20
30
40
50
Fraction Number

FIGURE 3

Scatchard plot of the equilibrium dialysis data for binding of PC to T-15 at 25°C, pH 7.4

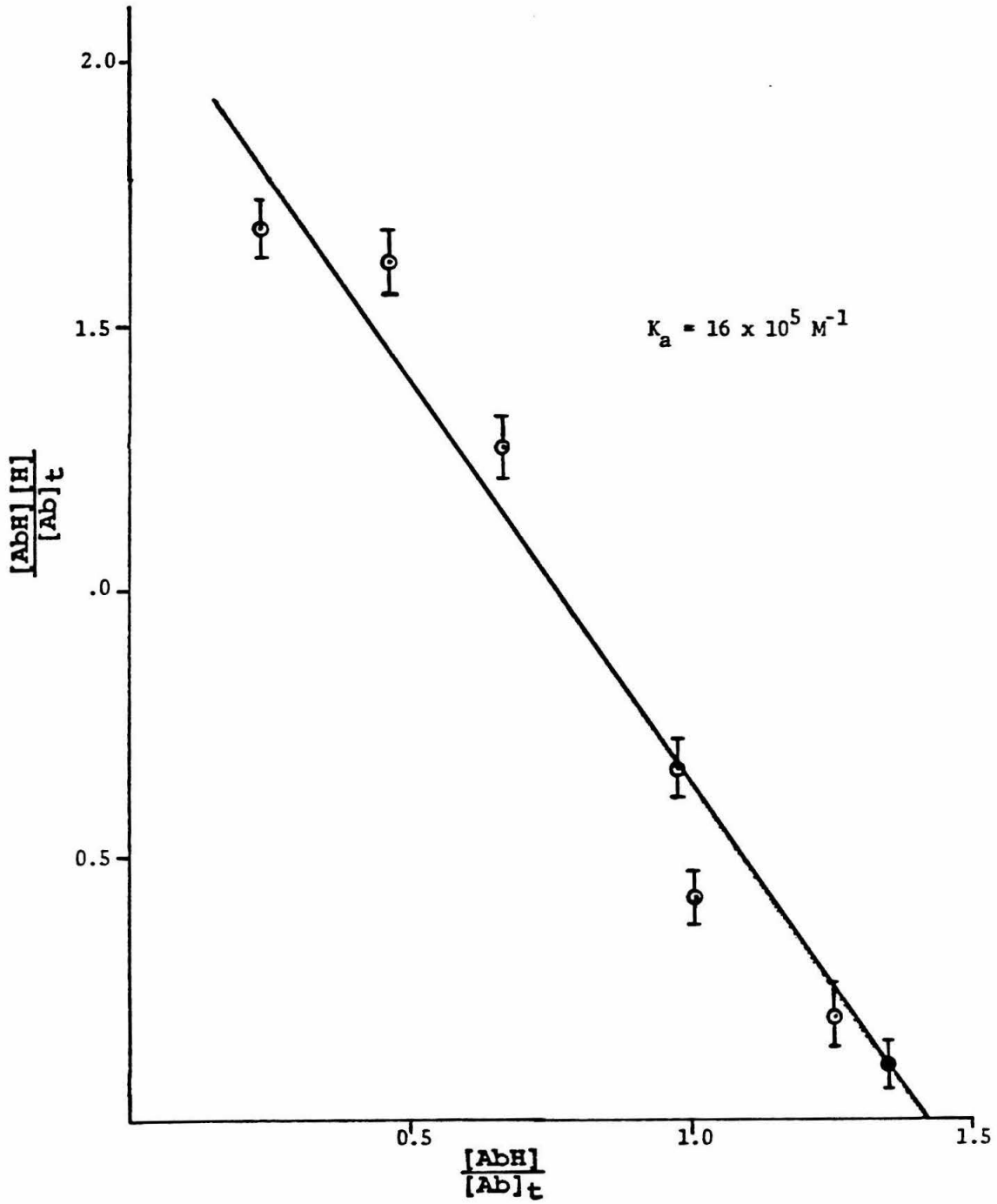
2.0
1.5
.0
0.5
$\frac{[AbH][H]}{[Ab]_t}$
$K_a = 16 \times 10^5\ M^{-1}$
0.5
1.0
1.5
$\frac{[AbH]}{[Ab]_t}$

FIGURE 4

Scatchard plot of the equilibrium dialysis data for binding of PC to M167 at 25°C, pH 7.4

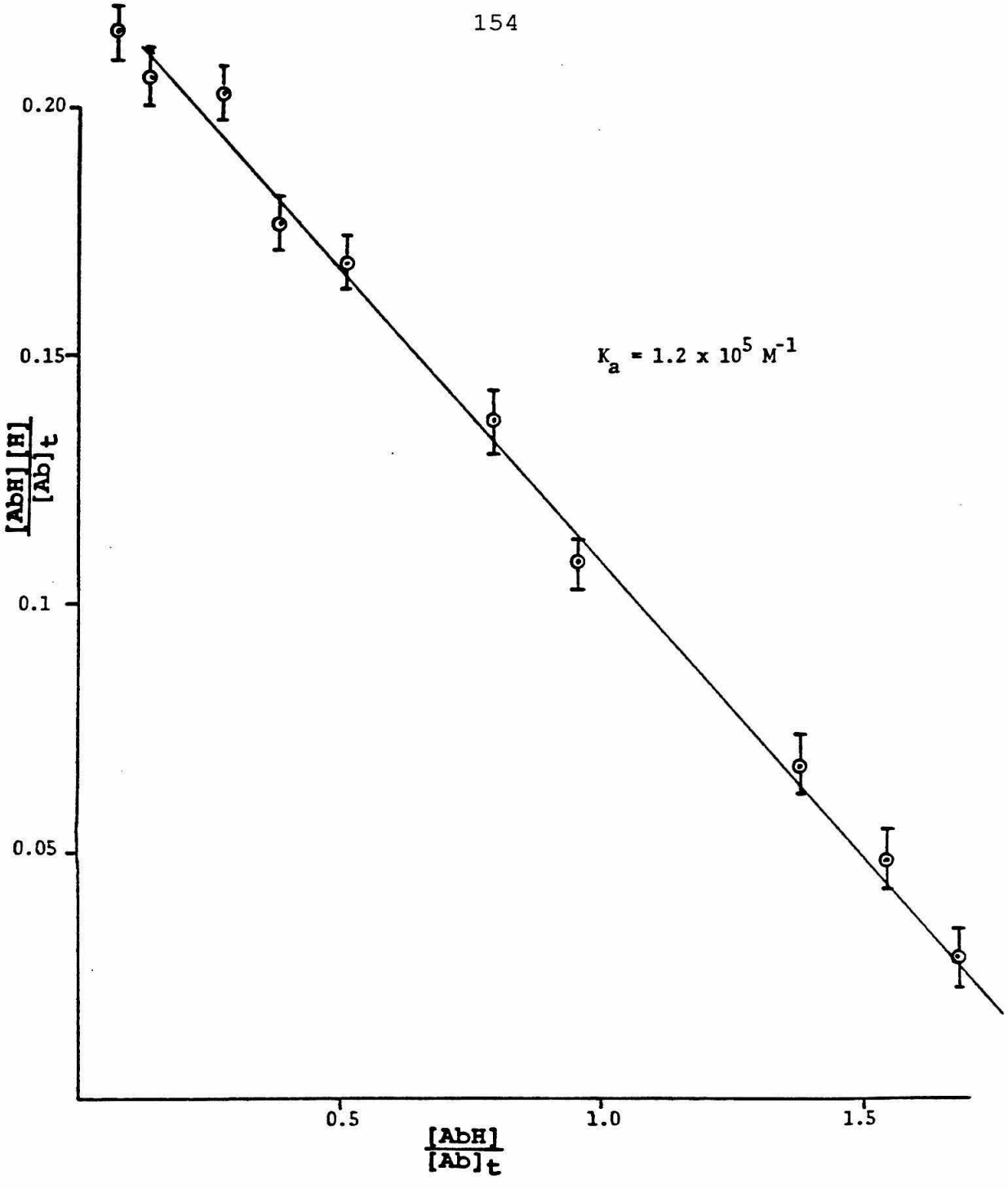
0.20
0.15
0.1
0.05
$\frac{[AbH][H]}{[Ab]_t}$
$K_a = 1.2 \times 10^5\ M^{-1}$
0.5
1.0
1.5
$\frac{[AbH]}{[Ab]_t}$

FIGURE 5

Scatchard plot of the equilibrium dialysis data for binding of PC to M603 at 25°C, pH 7.4

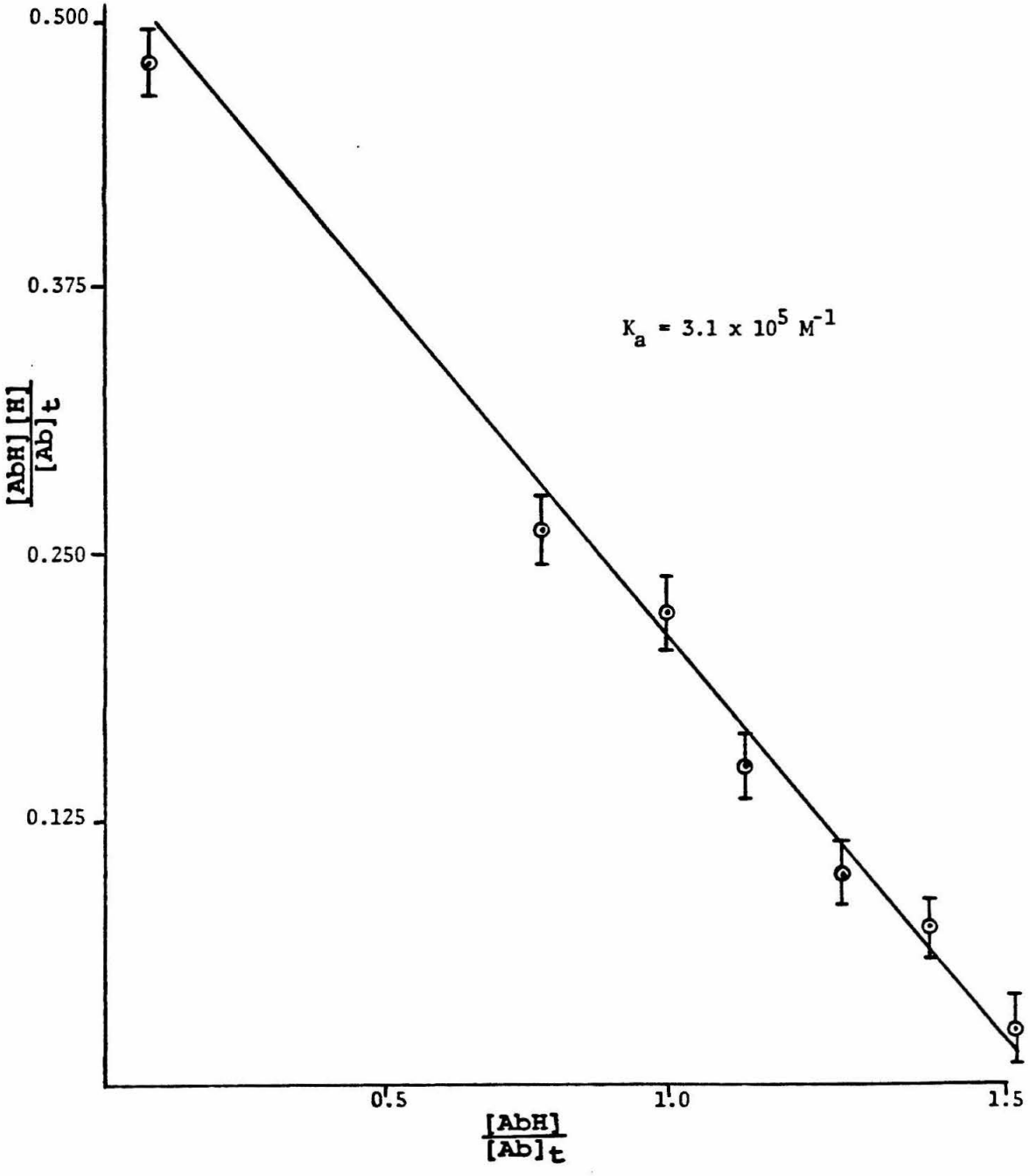
0.500
0.375
0.250
0.125
$\frac{[AbH][H]}{[Ab]_t}$
$K_a = 3.1 \times 10^5\ M^{-1}$
0.5
1.0
1.5
$\frac{[AbH]}{[Ab]_t}$

FIGURE 6

The inhibition of PC binding to T-15 by PPC at 25°C, pH 7.4

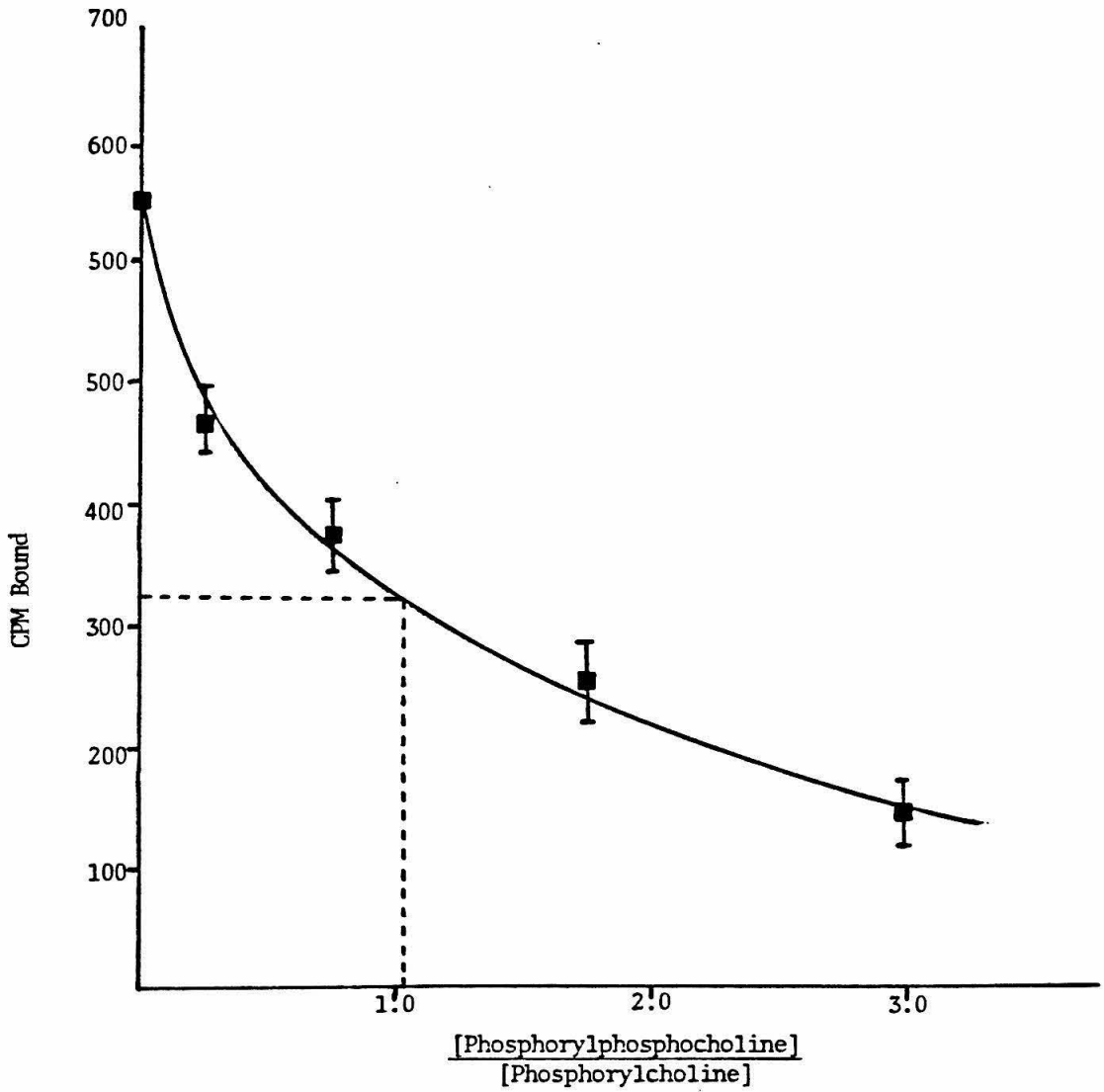
700
600
500
500
400
300
200
100
CPM Bound
1.0
2.0
3.0
[Phosphorylphosphocholine]
[Phosphorylcholine]

FIGURE 7

The pH dependence of the K_a of M603 for PC and PPC

The data are from equilibrium dialysis experiments at the pH indicated, in HBS at 25°C.

● PC at 4°C

□ PPC at 25°C

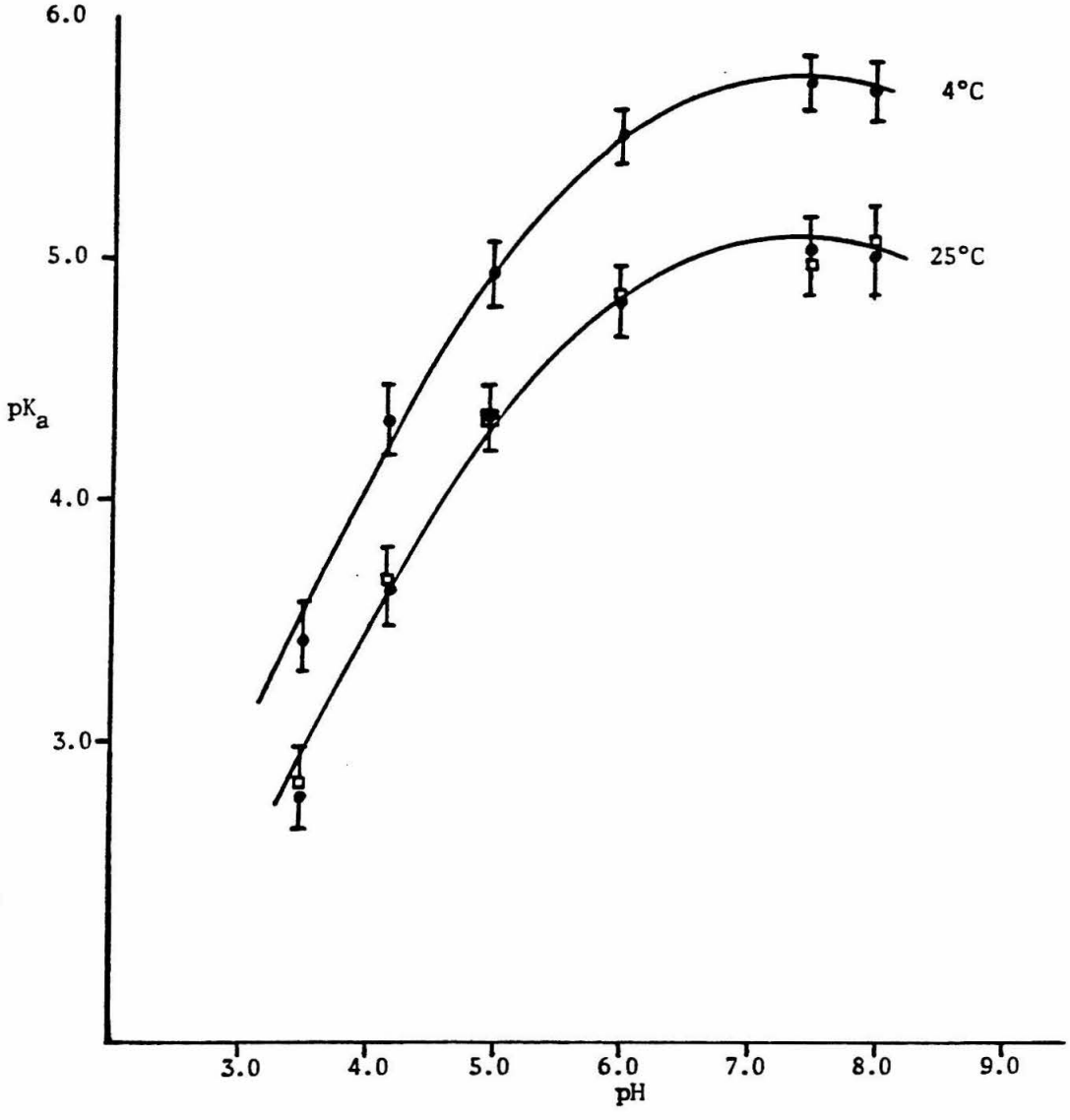
6.0
5.0
4.0
3.0
pK$_a$
4°C
25°C
3.0
4.0
5.0
6.0
7.0
8.0
9.0
pH

FIGURE 8

^{31}P NMR Titration Curve of PC and PPC

○ PC

□ PPC

Note that the phosphonium peak of PPC is pH independent over the range 3 to 9.

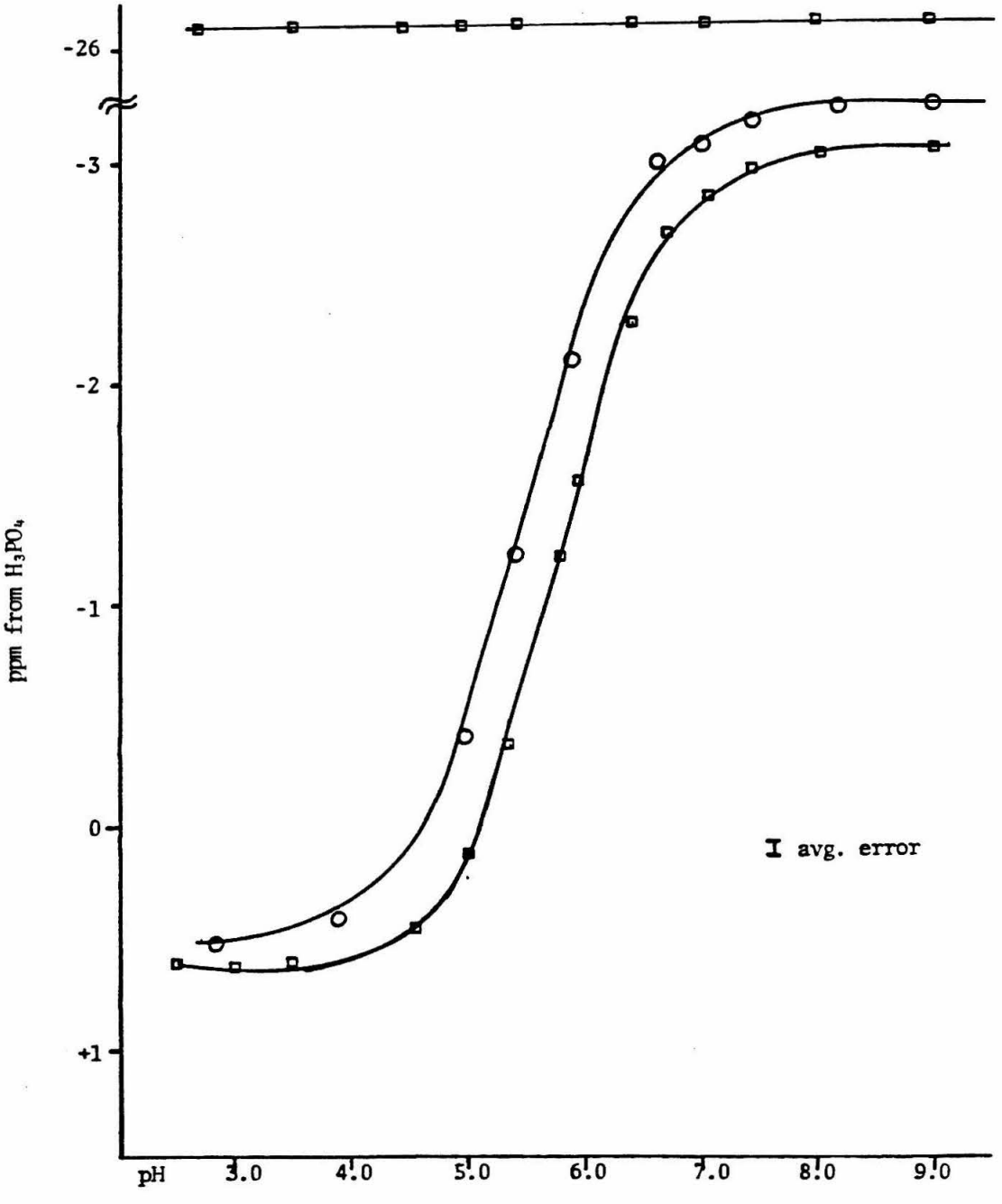
-26
-3
-2
-1
0
+1
ppm from H_3PO_4
pH
3.0
4.0
5.0
6.0
7.0
8.0
9.0
I avg. error

FIGURE 9

^{31}P NMR spectrum of PPC. The sample is 200 mM in HBS pH 2.8

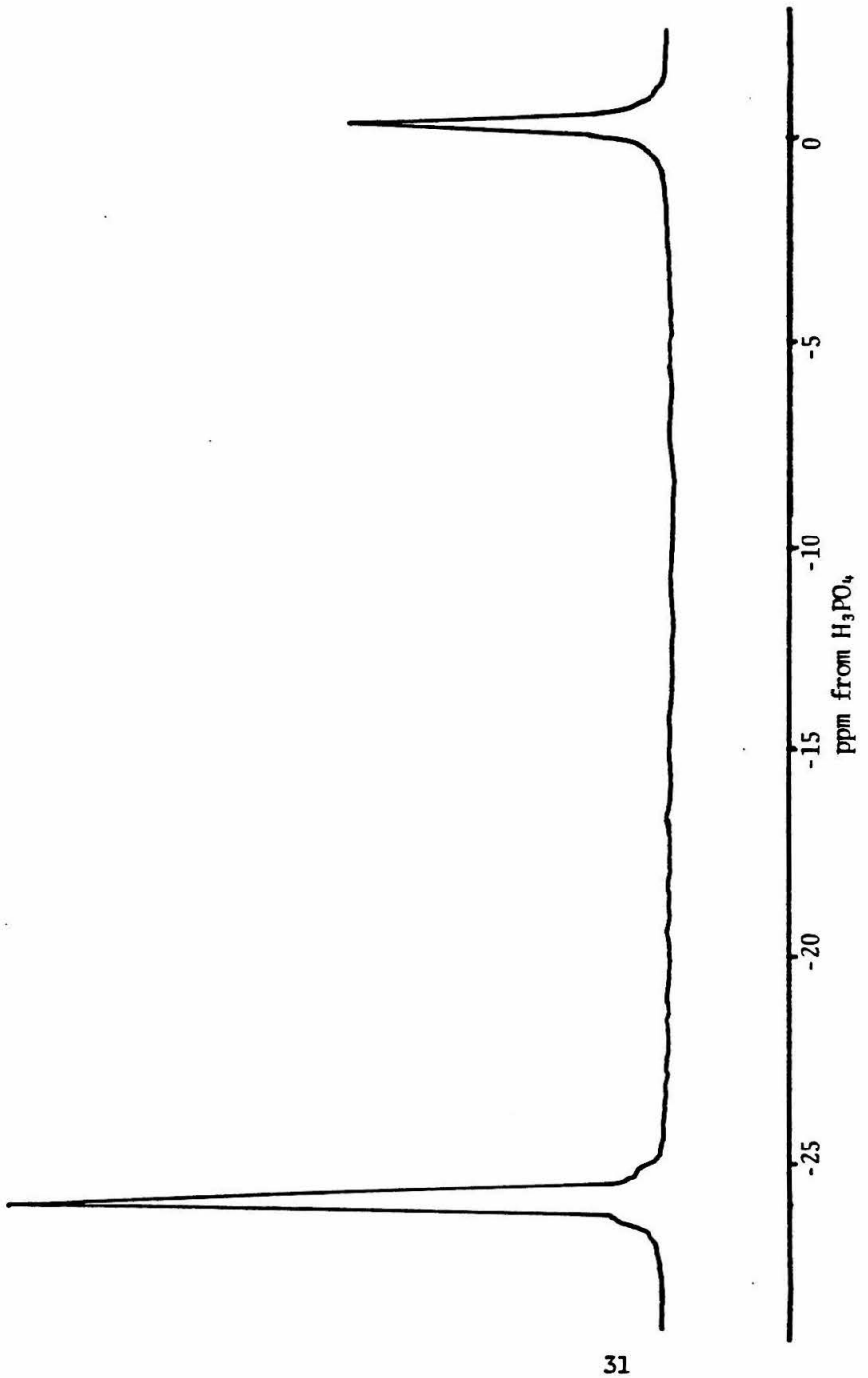
0
-5
-10
-15
-20
-25
ppm from H_3PO_4
31

FIGURE 10

T_1 Measurement of PPC bound to T-15

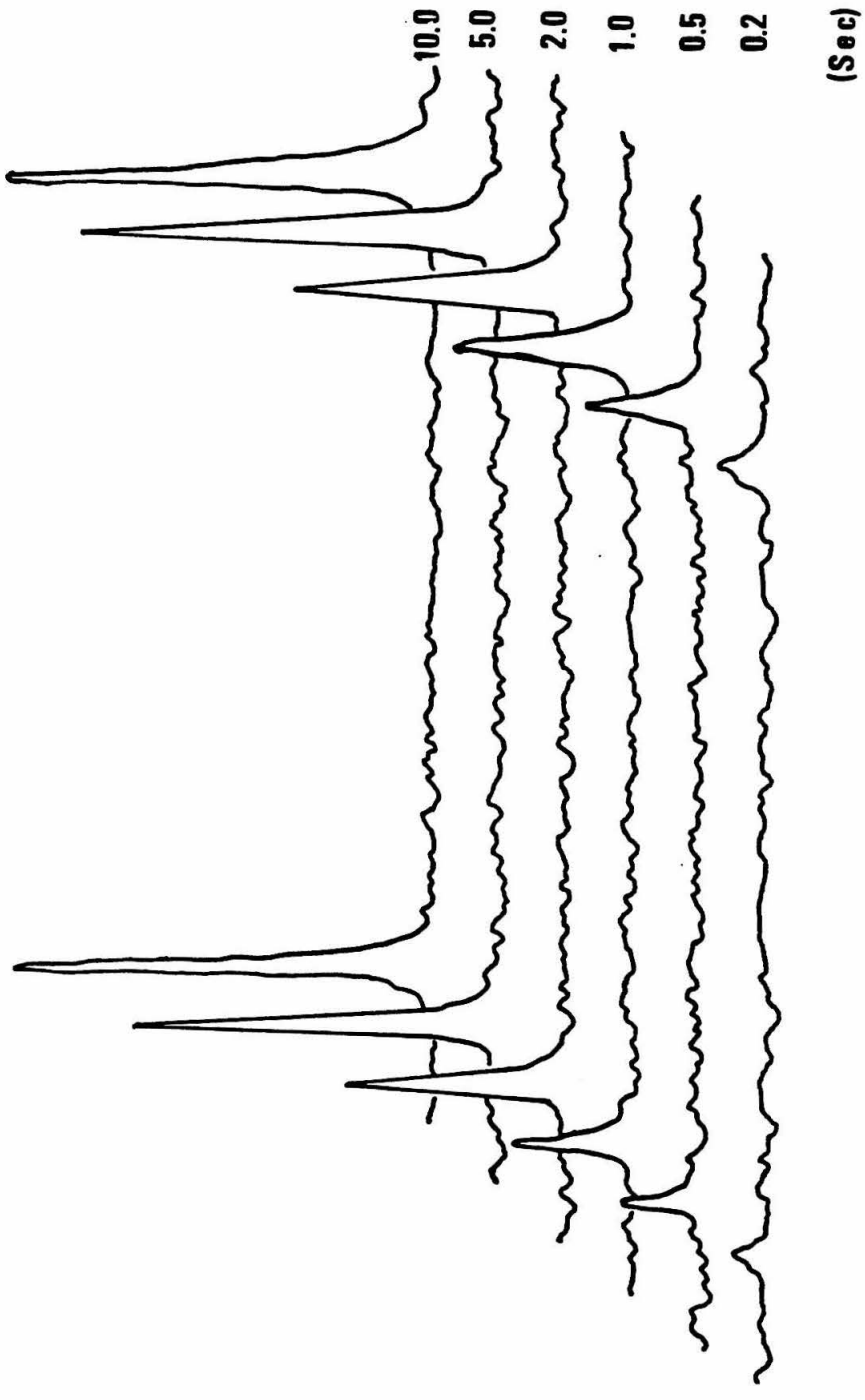
10.0
5.0
2.0
1.0
0.5
0.2
(Sec)

FIGURE 11

^{31}P pH Dependence of PC or PPC bound to T-15

○ phosphate of PC

□ phosphate of PPC

● phosphate of free PC

■ phosphonium of PPC

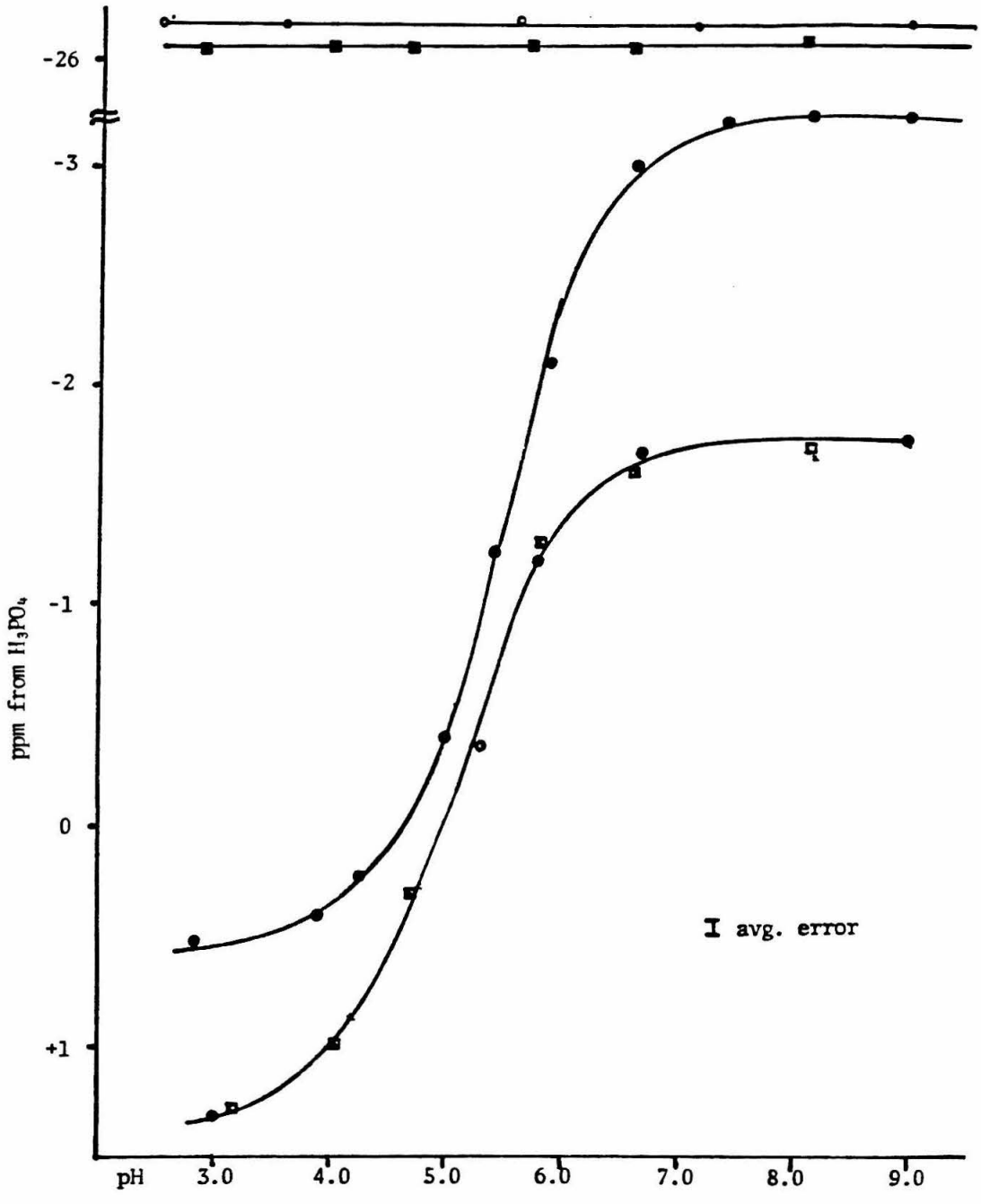
-26
-3
-2
-1
0
+1
ppm from H_3PO_4
pH
3.0
4.0
5.0
6.0
7.0
8.0
9.0
I avg. error

FIGURE 12

^{31}P pH Dependence of PC or PPC bound to M167

○ phosphate of PC

□ phosphate of PPC

● phosphate of free PC

■ phosphonium of PPC

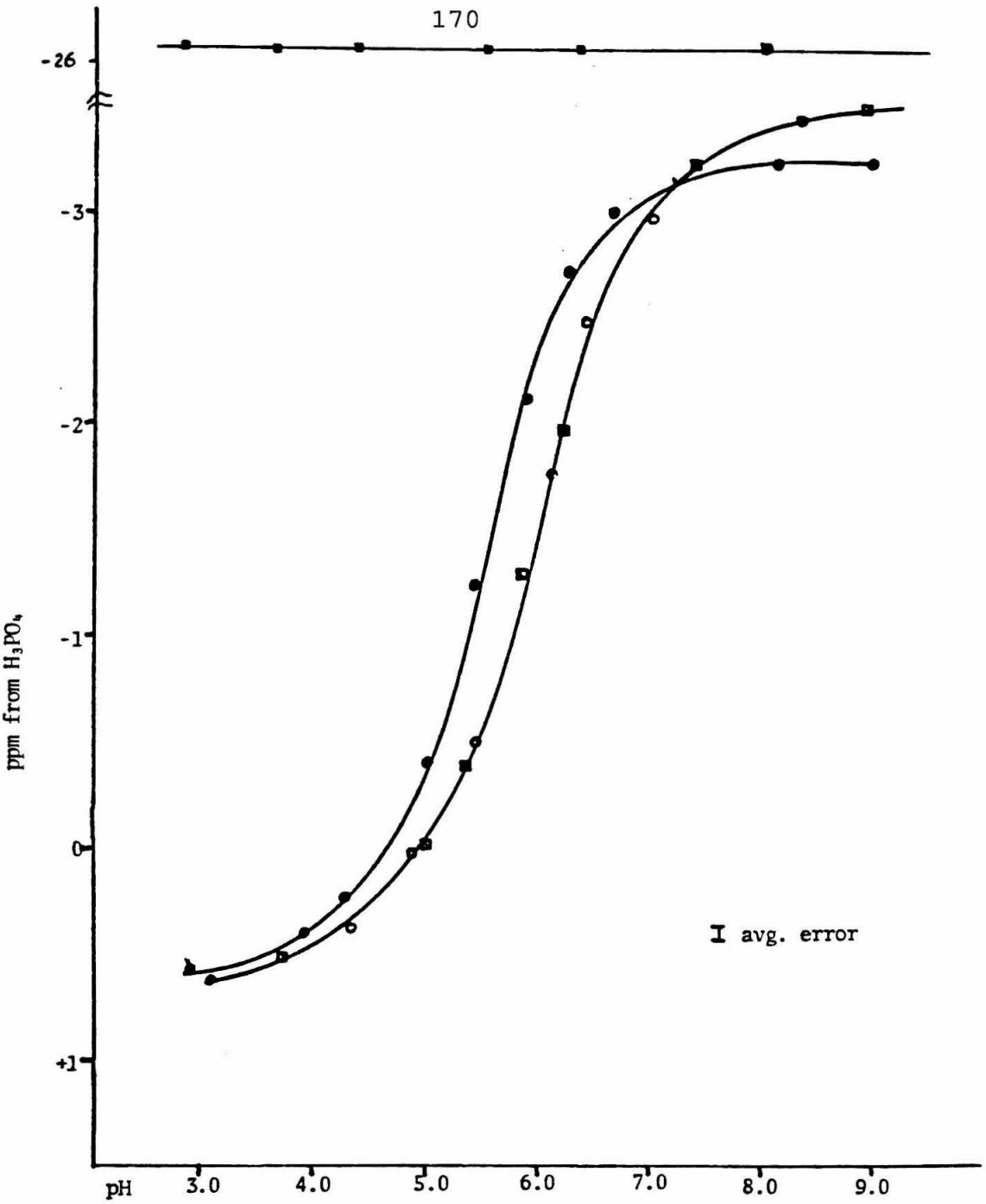
-26
-3
-2
-1
0
+1
ppm from H_3PO_4
pH
3.0
4.0
5.0
6.0
7.0
8.0
9.0
I avg. error

FIGURE 13

^{31}P pH Dependence of PC or PPC bound to M603

A) The concentration dependence of the phosphate resonance of PPC bound to M603 clearly demonstrates that PPC is in fast exchange. At equimolar concentrations, a larger chemical shift is observed compared to the chemical shift at hapten excess.

□ phosphate of PPC at equimolar concentration

△ phosphate of PPC at twofold hapten excess

● phosphate of free PPC

B) □ phosphonium of PPC at equimolar concentration

△ phosphonium of PPC at two-fold hapten excess

● phosphonium of free PPC

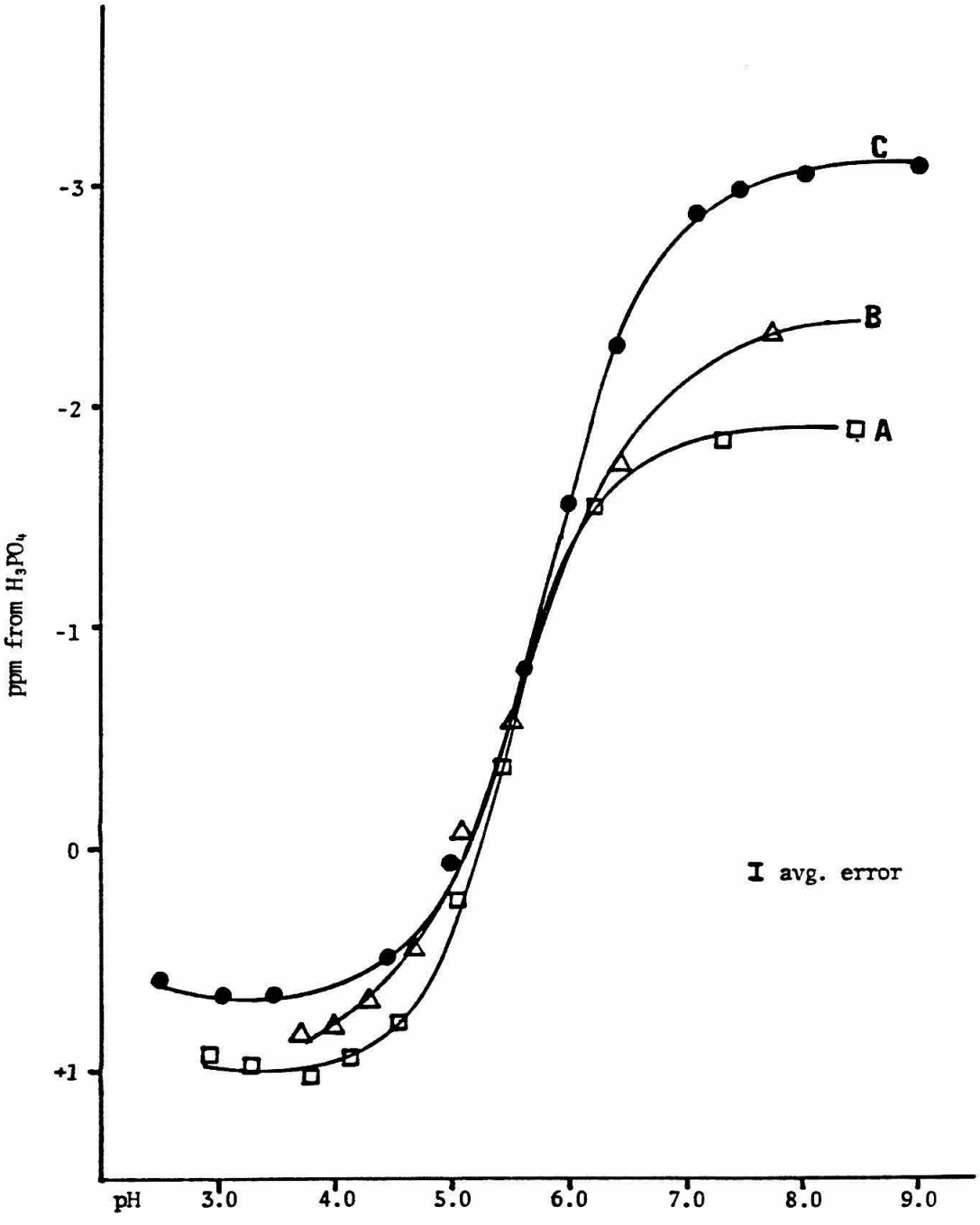
C
B
A
-3
-2
-1
0
+1
ppm from H_3PO_4
I avg. error
pH
3.0
4.0
5.0
6.0
7.0
8.0
9.0

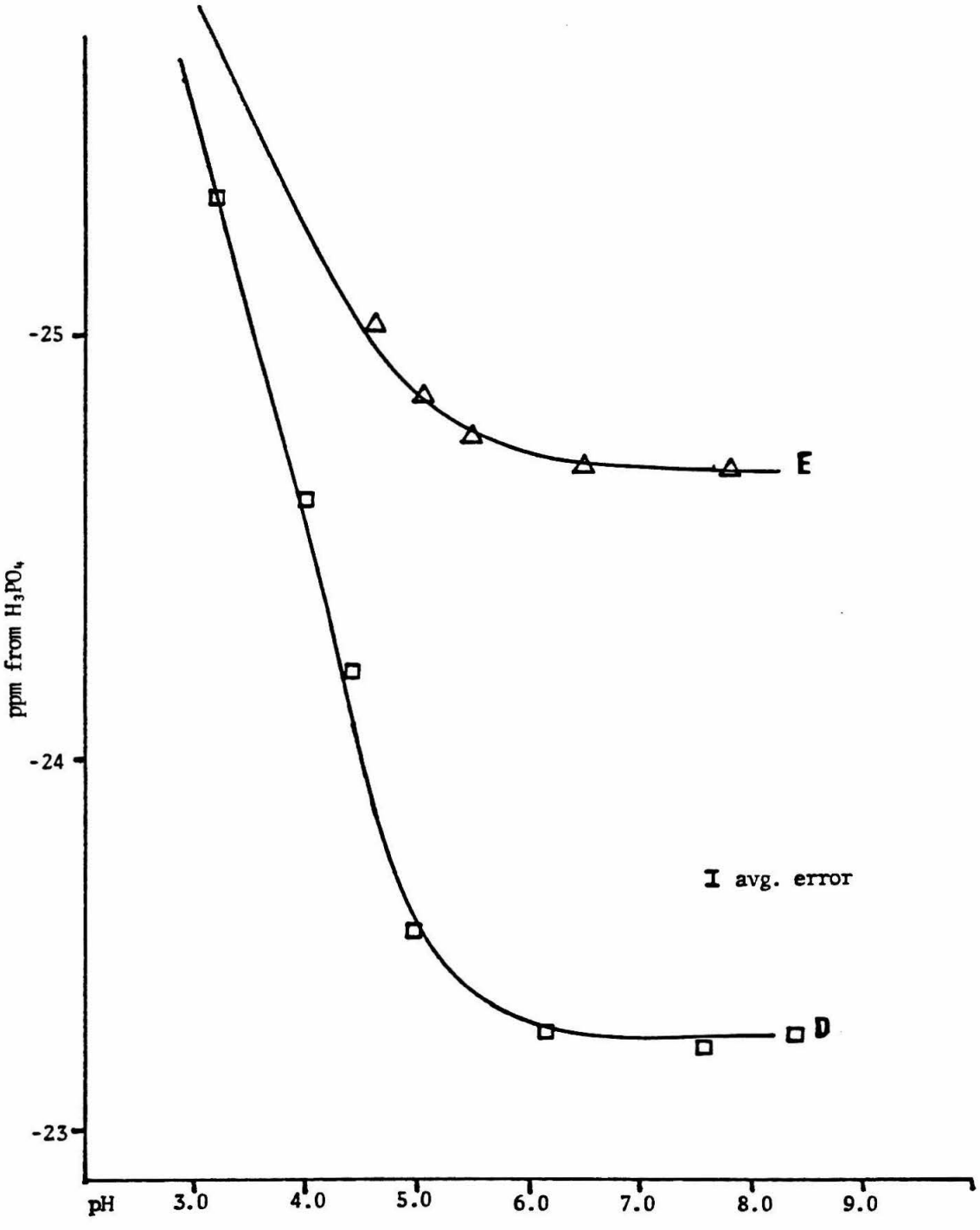
-25
-24
-23
ppm from H_3PO_4
E
D
I avg. error
pH
3.0
4.0
5.0
6.0
7.0
8.0
9.0

FIGURE 14

The Binding Site of M603 Showing the Light and Heavy Chain Hypervariable Domains

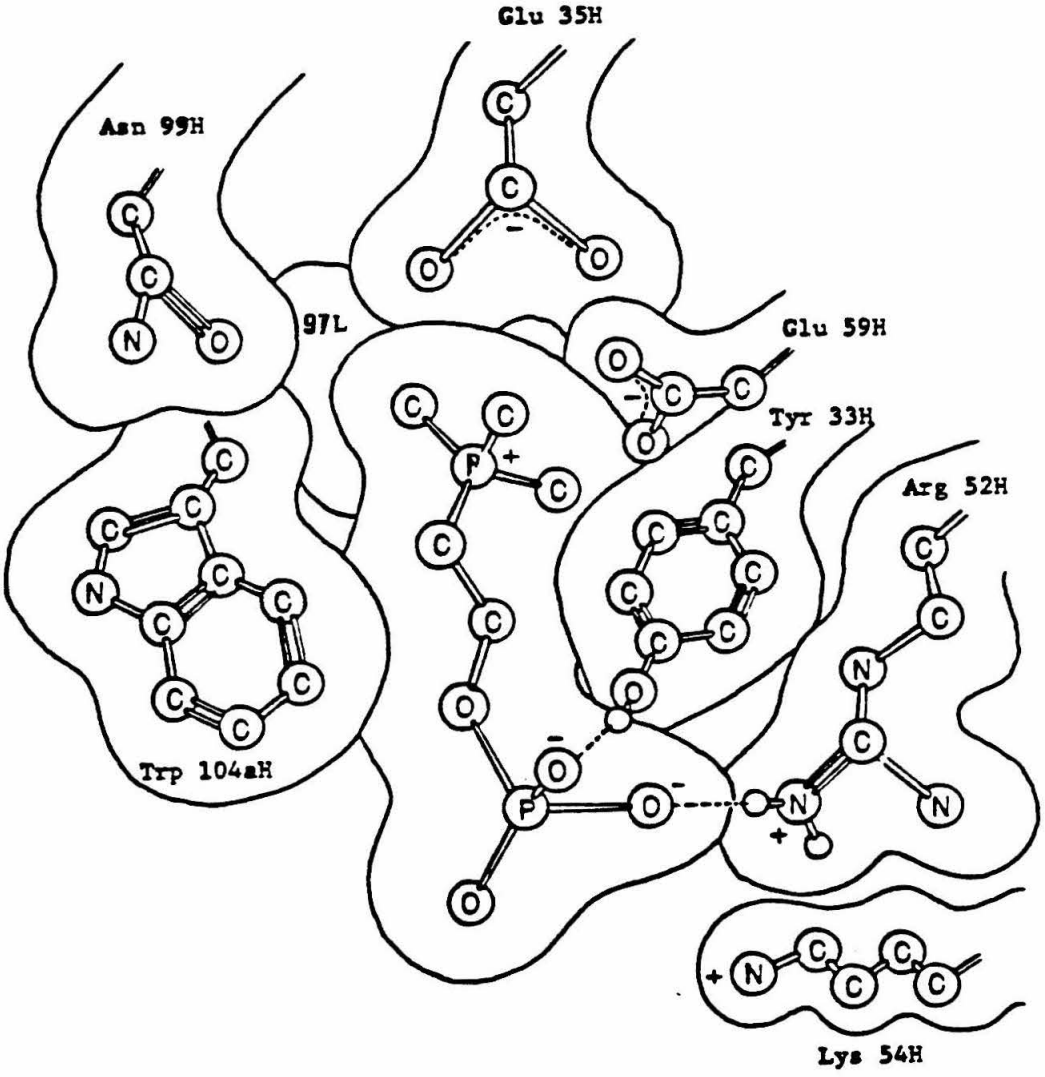
Glu 35H
Asn 99H
97L
Glu 59H
Tyr 33H
Arg 52H
Trp 104aH
Lys 54H

FIGURE 15

The Contact Residues of the M603 Binding Site

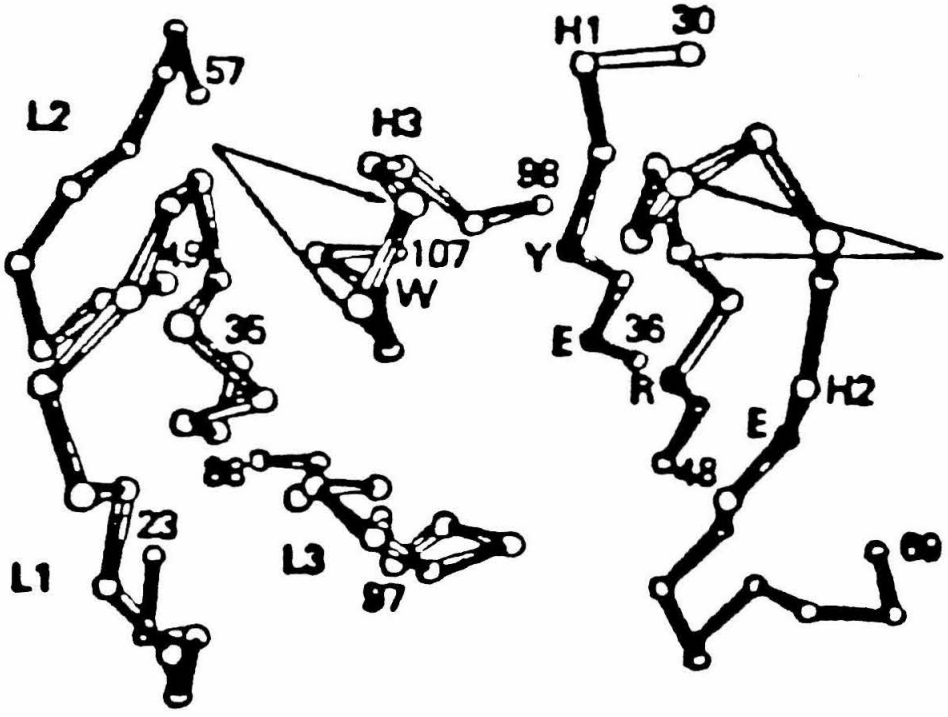
L2
57
H3
98
49
107
W
Y
H1
30
36
E
36
R
H2
E
48
88
23
L1
L3
97
89

FIGURE 16

The amino acid sequence of the variable regions of T-15, M603 and M167. The one letter amino acid code is used. Areas of the chain that are involved in binding are shown in hatched outline.

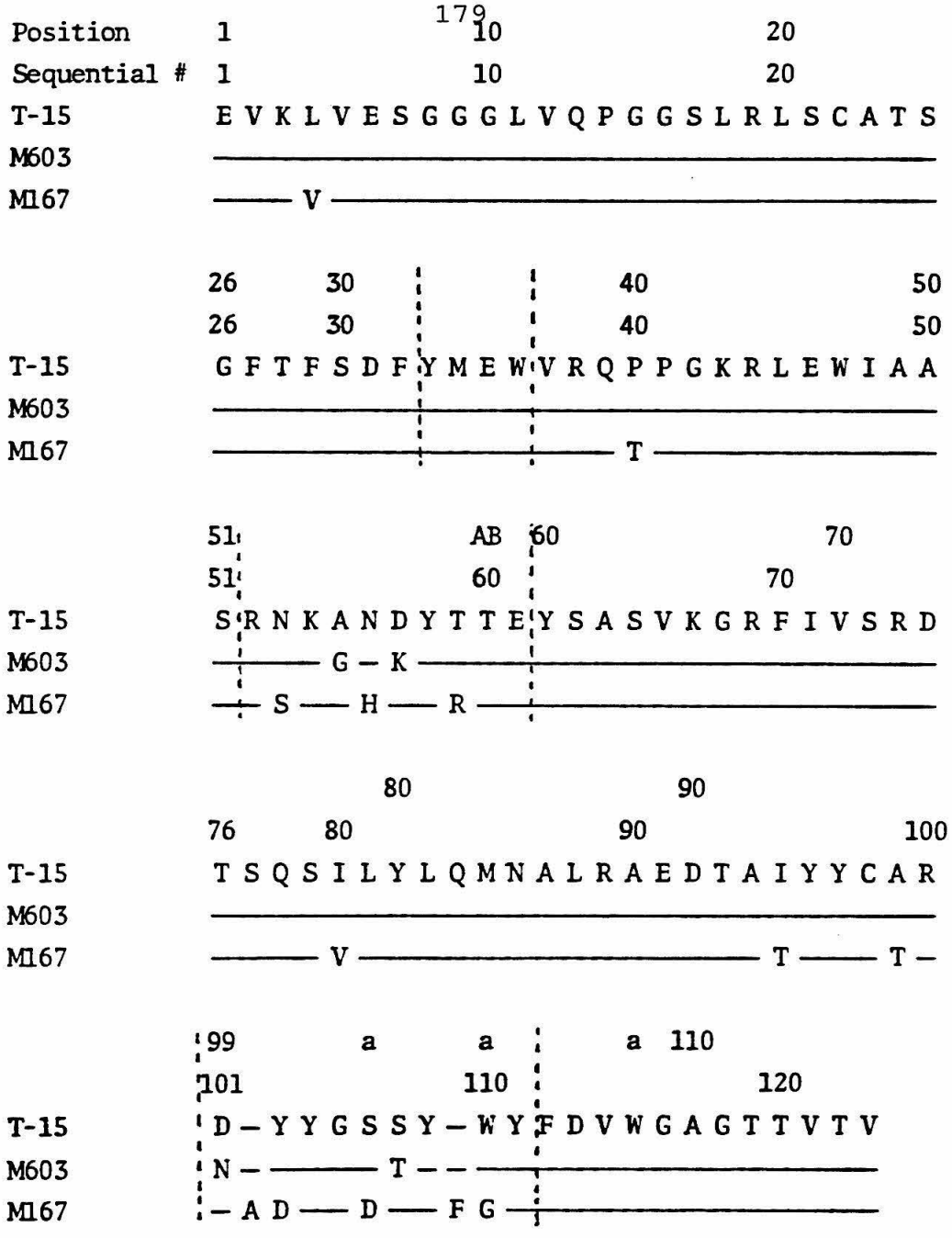
Position 1 10 20
Sequential # 1 10 20
T-15 E V K L V E S G G G L V Q P G G S L R L S C A T S
M603 ———————————————————————————————
M167 ——— V ———————————————————————————
26 30 40 50
26 30 40 50
T-15 G F T F S D F Y M E W V R Q P P G K R L E W I A A
M603 ———————————————————————————————
M167 ——————————————————————— T ———————————
51 AB 60 70
51 60 70
T-15 S R N K A N D Y T T E Y S A S V K G R F I V S R D
M603 ——— G — K ———————————————————————
M167 — S —— H —— R ———————————————————
80 90
76 80 90 100
T-15 T S Q S I L Y L Q M N A L R A E D T A I Y Y C A R
M603 ———————————————————————————————
M167 ——— V ——————————————————— T ——— T —
99 a a a 110
101 110 120
T-15 D — Y Y G S S Y — W Y F D V W G A G T T V T V
M603 N — ——— T — — ———————————————
M167 — A D —— D —— F G ———————————————

FIGURE 17

Chemical shift of the phosphonium resonance of PPC bound to M603. The effects of fast exchange have been removed by using the pH dependence of the K_a to calculate fraction bound.

□ equimolar concentration of PPC

△ 2x PPC excess

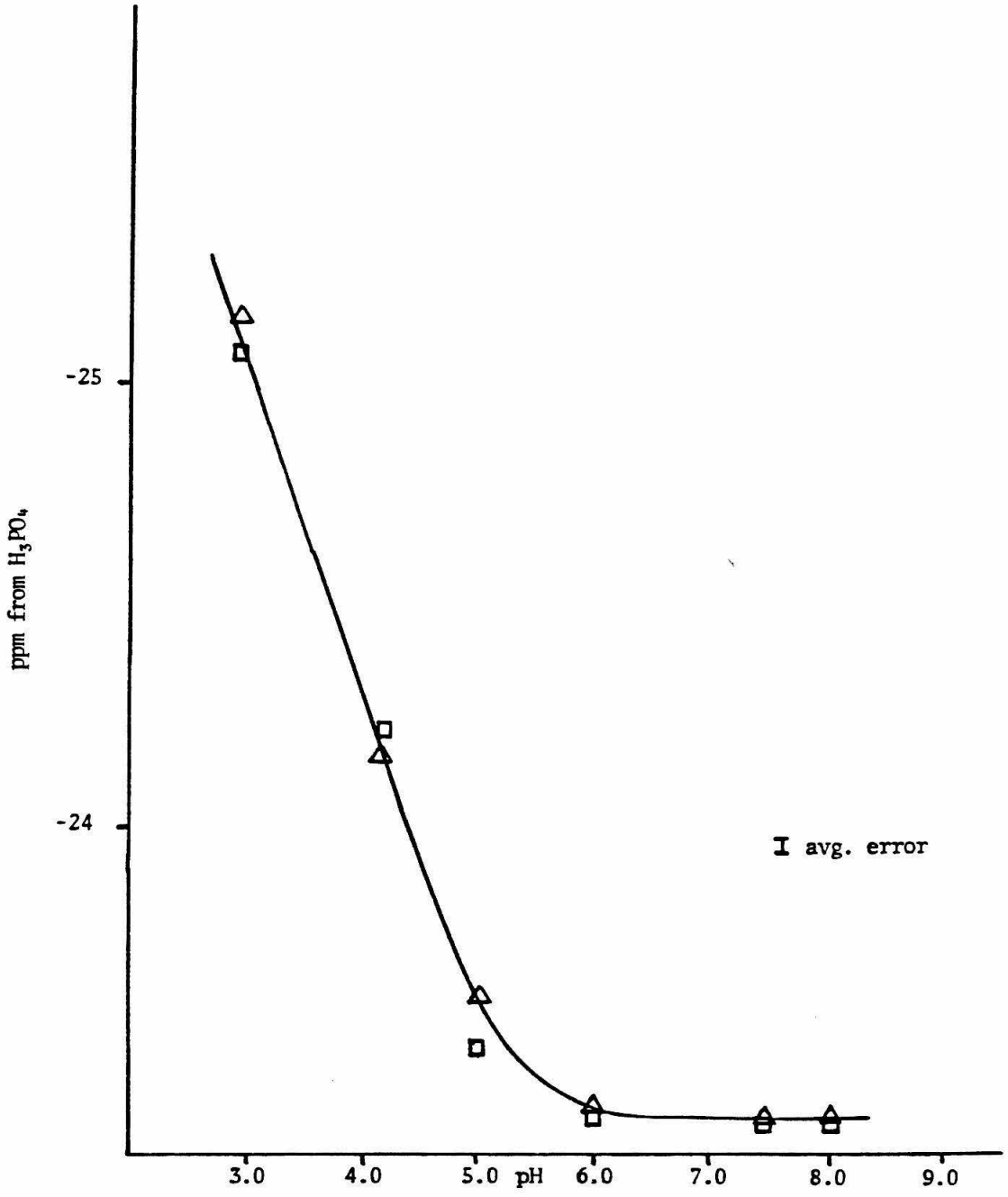
-25
-24
ppm from H_3PO_4
I avg. error
3.0
4.0
5.0 pH
6.0
7.0
8.0
9.0

FIGURE 18

The amino acid sequence of the variable regions of the light chains of T-15, M167 and M603. The one letter amino acid code is used.

Sequence #	1									10										20					25
M167	D	I	V	I	T	Q	D	E	L	S	N	P	V	T	S	G	E	S	V	S	I	J	C	R	S
T-15	—	—	—	M	—	—	S	P	T	F	L	A	—	—	A	S	K	K	–	T	—	—	—	T	A
M603	—	—	—	M	—	—	S	P	S	S	L	S	–	S	A	G	–	R	–	T	M	—	—	K	–

Sequence #	26		30							40										50
M167	S	K	S	L	L	Y	K		D	G	K	T	T	L	N	W	F	L	Q	R	P	G	Q	S	P
T-15	–	E	—	—	Y	S	S	K	N	K	V	H	Y	–	A	–									
M603	–	Z	—	—	—	B	S	G	B	Z	K	B	F	–	A	–									

Table 1

The binding constants of T-15, M167, and M603 for PC and PPC

TABLE 1

	Affinity Constant	
Protein	Phosphorylcholine	Phosphorylphosphocholine
T-15	16×10^5	17×10^5
M-603	3.1×10^5	3.0×10^5
M-167	1.2×10^5	1.2×10^5